

SHEP 95-17

OUTP-95-19P

hep-ph/9505326

Resolving the Constrained Minimal and Next-to-Minimal Supersymmetric Standard Models

S. F. King ¹*Physics Department, University of Southampton, Southampton, SO9 5NH, U.K.*P. L. White ²*Theoretical Physics, University of Oxford, 1 Keble Road, Oxford, OX1 3NP, U.K.*

Abstract

We perform a detailed analysis of the next-to-minimal supersymmetric standard model (NMSSM), imposing the constraints of two-loop gauge coupling unification, universal soft supersymmetry breaking and the correct pattern of electroweak symmetry breaking. We compare our results with those for the minimal supersymmetric standard model (MSSM) using closely related techniques and, as far as possible, a common set of input and output variables. In general, in the constrained NMSSM, there are much stronger correlations between parameters than in the constrained MSSM, and we map out the allowed parameter space. We also give a detailed discussion of how to resolve the two models experimentally, concentrating primarily on the prospects at LEP II. We find that, for top mass $\gtrsim 150\text{GeV}$, the constrained NMSSM is only viable in regions where its spectrum is in general very similar to that of the MSSM, although there are exceptions which we explore. For example, in some corners of parameter space, the lightest CP-even Higgs boson in the constrained NMSSM

¹Email king@soton.ac.uk

²Email plw@thphys.ox.ac.uk

may be detected at LEP II with singlet-diluted couplings which may allow it to be distinguished from that of the MSSM. However, if small universal gaugino mass $M_{1/2}$ is required, then we expect a standard model-like Higgs boson which may be detected at LEP II, together with a very characteristic Higgs and SUSY spectrum. We also study fine-tuning in the constrained NMSSM, which is typically a more severe constraint than in the MSSM, and give a simple analytical discussion of the potential and spectrum.

1 Introduction

Supersymmetry (SUSY) [1] is a well studied extension to the standard model which reproduces the successes of the standard model, including its radiative corrections, to the current very high level of accuracy. The existence of TeV-scale SUSY would greatly ease the naturalness problems associated with the construction of a grand unified theory (GUT) of the strong and electroweak interactions. The basic idea of GUTs is that the gauge couplings, which govern the strength of the strong and electroweak interactions at low energy, are actually equal to some unified coupling g_X at some very high scale M_X due to their renormalisation group (RG) running [2]. The original motivation for SUSY broken at a TeV was to help to stabilise the Higgs mass against GUT scale quadratic radiative corrections. The potent combination of SUSY and GUTs has recently found some indirect experimental support due to the accurate measurement of the strong and electroweak couplings on the Z pole by LEP. These measurements are inconsistent with gauge coupling unification if a standard model desert is assumed, but are consistent with unification if a SUSY desert above the TeV scale is assumed [3]. This does not of course constitute real evidence for either SUSY or GUTs, but it does provide sufficient motivation for the detailed studies which have been made since this observation.

In the first post-LEP analyses [3] the whole SUSY spectrum was either assumed to be degenerate at the scale M_{SUSY} , or smeared around this scale. In reality the SUSY partners may have a complicated spectrum, parametrised by a large number of soft SUSY-breaking parameters, which may spread over one or two orders of magnitude of masses. In order to reduce the number of independent soft SUSY-breaking parameters one may appeal to supergravity or superstring scenarios which involve the notion of SUSY breaking in a hidden sector coupled only gravitationally to our observable sector. By this means, in the minimal supersymmetric standard model (MSSM),

one ends up with just four independent soft SUSY breaking parameters: m_0 , $M_{1/2}$, A_0 and B_0 corresponding to the universal soft scalar, gaugino, trilinear and bilinear couplings, respectively. Using these four parameters together with the bilinear Higgs term μ_0 and the top quark Yukawa coupling, which plays an important role in driving electroweak symmetry breaking [4], several groups have performed an RG analysis whose goal is to predict the SUSY and Higgs spectrum and then use this spectrum as the basis of a more reliable estimate of gauge coupling unification by running the gauge couplings through the various thresholds from the Z mass M_Z up to a unification scale M_X [5, 6]. Apart from the constraints of gauge coupling unification and correct electroweak symmetry breaking, there are various other phenomenological and cosmological constraints which may be applied and recent studies have concluded that it is possible to satisfy all these constraints simultaneously [6].

In this paper we shall consider both the constrained MSSM discussed above and a slightly different low energy SUSY model, but one which is equally consistent with gauge coupling unification, namely the so-called next-to-minimal supersymmetric standard model (NMSSM) [7, 8, 9]. The basic idea of the NMSSM is to add just one extra gauge singlet superfield N to the spectrum of the MSSM, and to replace the μ -term in the MSSM superpotential with a purely cubic superpotential,

$$\mu H_1 H_2 \longrightarrow \lambda N H_1 H_2 - \frac{k}{3} N^3. \quad (1.1)$$

The motivation for this “minimal non-minimal” model is that it solves the so-called μ -problem of the MSSM [10] in the most direct way possible by eliminating the μ -term altogether, replacing its effect by the vacuum expectation value (VEV) $\langle N \rangle = x$, which may be naturally related to the usual Higgs VEVs $\langle H_i \rangle = \nu_i$. There are other solutions to the μ -problem [10]. Also, the inclusion of singlets may cause the destabilisation of the hierarchy if there are strong couplings to super-heavy particles such as Higgs colour triplets [11]. Recently similar effects have been shown to result

from non-renormalisable operators suppressed by powers of the Planck mass [12]. The dangerous non-renormalisable operators would require that gravity violate the Z_3 symmetry which is respected by the renormalisable operators of the theory. Our view is that since these effects are model-dependent the NMSSM is as well motivated as the MSSM and should be studied to the same level of approximation. Only by so doing may the two models be phenomenologically compared when (or if) Higgs bosons and SUSY particles are discovered.

The present paper is not the first to discuss the effect of unification and electroweak symmetry breaking constraints in the NMSSM. The original analysis of ref.[9], has recently been up-dated [13, 14, 15, 16]. However only one of these analyses [16] considered the effect of low-energy Higgs and SUSY particle threshold effects on gauge coupling unification. As in the MSSM, such effects play an important role in determining the unification parameters, and in constraining the parameter space of the model. In this analysis [16], and the present analysis, we input the gauge couplings $g_1(M_Z)$ and $g_2(M_Z)$ and run them up through the 24 SUSY and Higgs thresholds to find M_X and g_X , which must of course be consistent with our original input values. By iterating this procedure we obtain solutions which satisfy both the requirements of correct electroweak symmetry breaking and coupling constant unification *simultaneously*.

The result of these recent analyses [13, 14, 15, 16] is that the constrained NMSSM is always quite close to the MSSM limit. In effect the extra singlet decouples both from the Higgs sector and the neutralino sector, making the problem of resolving the NMSSM from the MSSM extremely difficult. Although there are already a large number of analyses of the constrained MSSM in the literature [6], based on different techniques, and using different input and output parameters, none of these analyses may be easily be extended to include the constrained NMSSM. In the present paper we shall introduce a set of input and output variables for the constrained MSSM which

most closely resembles those which are appropriate for our analysis of the constrained NMSSM, thereby enabling both models to be dealt with on the same footing, and enabling the results of both models to be meaningfully compared. The purpose of the present paper is therefore to analyse the constrained MSSM and NMSSM models in a unified way, which enables a comparison of the results of the two models, and hence to address the important phenomenological question of how the two models may be resolved experimentally.

The outline of the remainder of the paper is as follows. In section 2 we introduce the NMSSM and the MSSM. In section 3 we discuss our unifying approach and methods for the two models. In section 4 we apply these methods to the MSSM and discuss the basic features of this model. In section 5 we describe the results of our analysis of the NMSSM. Section 6 addresses the phenomenological question of how the two models might be resolved experimentally at forthcoming colliders, and section 7 concludes the paper. Appendices A and B supply renormalisation group equations and radiatively corrected mass matrices.

2 The MSSM and NMSSM

The MSSM has, in addition to the usual matter and gauge particle content, a Higgs sector containing two Higgs doublets H_1 and H_2 [1]. The superpotential for the MSSM is of the form

$$W_{MSSM} = h_u Q H_2 u^c + h_d Q H_1 d^c + h_e L H_1 e^c + \mu H_1 H_2, \quad (2.1)$$

and the most general soft-breaking potential with our conventions is

$$\begin{aligned} V_{MSSM}^{SOFT} = & m_Q^2 |\tilde{Q}|^2 + m_u^2 |\tilde{u}^c|^2 + m_d^2 |\tilde{d}^c|^2 + m_L^2 |\tilde{L}|^2 + m_e^2 |\tilde{e}^c|^2 + m_{H_1}^2 |H_1|^2 \\ & + m_{H_2}^2 |H_2|^2 + \frac{1}{2} (M_1 \bar{\lambda}_1 \lambda_1 + M_2 \bar{\lambda}_2 \lambda_2 + M_3 \bar{\lambda}_3 \lambda_3) \\ & - (h_u A_u \tilde{Q} H_2 \tilde{u}^c + h_d A_d \tilde{Q} H_1 \tilde{d}^c + h_e A_e \tilde{L} H_1 \tilde{e}^c - B \mu H_1 H_2 + h.c.), \quad (2.2) \end{aligned}$$

where gauge and generation indices are understood, $H_1 H_2 = H_1^0 H_2^0 - H_1^- H_2^+$, with $H_1^T = (H_1^0, H_1^-)$ and $H_2^T = (H_2^+, H_2^0)$. The chiral superfields Q contain the left-handed quark doublets; L the left-handed lepton doublets; u^c , d^c and e^c the charge conjugates of the right-handed up-type quarks, right-handed down-type quarks and right-handed electron-type leptons respectively. In the potential (rather than the superpotential) we employ the usual convention that scalar components of Higgs superfields are denoted by the same symbol as the corresponding superfield, but that the scalar components of matter superfields are tilded. λ_1 , λ_2 , λ_3 are the gauginos corresponding to the $U(1)$, $SU(2)$, $SU(3)$ gauge groups respectively, and are here Majorana fermions. The low-energy spectrum of the MSSM contains two CP-even Higgs scalars, one CP-odd Higgs scalar, and two charged Higgs scalars.

The $\mu H_1 H_2$ term and its associated $\mu B H_1 H_2$ term are necessary in order to ensure that the correct pattern of electroweak symmetry breaking occurs. Thus the VEVs of H_1 and H_2 may be taken to be of the form

$$\langle H_1 \rangle = \begin{pmatrix} \nu_1 \\ 0 \end{pmatrix}, \quad \langle H_2 \rangle = \begin{pmatrix} 0 \\ \nu_2 \end{pmatrix}, \quad (2.3)$$

where ν_1 and ν_2 are positive reals, $\sqrt{\nu_1^2 + \nu_2^2} = \nu = 174$ GeV, and we define $\tan \beta = \nu_2/\nu_1$. It might be expected that the natural scale for μ should be the Planck mass, or at least many orders of magnitude greater than the soft masses, but in fact this does not allow correct electroweak symmetry breaking. This is the μ problem. There has been extensive discussion of this problem in the literature, including attempts to solve it [10].

The introduction of a gauge singlet superfield N eliminates the necessity for a dimensionful coupling in the superpotential since its VEV plays the role of this coupling. We then obtain the NMSSM [7, 8, 9]. The superpotential for the NMSSM is

$$W_{NMSSM} = h_u Q H_2 u^c + h_d Q H_1 d^c + h_e L H_1 e^c + \lambda N H_1 H_2 - \frac{1}{3} k N^3. \quad (2.4)$$

The general soft-breaking potential in our conventions is given by

$$\begin{aligned}
V_{NMSSM}^{SOFT} &= m_Q^2 |\tilde{Q}|^2 + m_u^2 |\tilde{u}^c|^2 + m_d^2 |\tilde{d}^c|^2 + m_L^2 |\tilde{L}|^2 + m_e^2 |\tilde{e}^c|^2 \\
&+ m_{H_1}^2 |H_1|^2 + m_{H_2}^2 |H_2|^2 + m_N^2 |N|^2 + \frac{1}{2} (M_1 \bar{\lambda}_1 \lambda_1 + M_2 \bar{\lambda}_2 \lambda_2 + M_3 \bar{\lambda}_3 \lambda_3) \\
&- (h_u A_u \tilde{Q} H_2 \tilde{u}^c + h_d A_d \tilde{Q} H_1 \tilde{d}^c + h_e A_e \tilde{L} H_1 \tilde{e}^c \\
&+ \lambda A_\lambda N H_1 H_2 + \frac{1}{3} k A_k N^3 + h.c.).
\end{aligned} \tag{2.5}$$

The low-energy spectrum of the NMSSM contains three CP-even Higgs scalars, two CP-odd Higgs scalars, and two charged Higgs scalars.

The cubic term in N in the NMSSM superpotential is necessary in order to avoid a $U(1)$ Peccei-Quinn symmetry which, when the fields acquire their VEVs, would result in a phenomenologically unacceptable axion in the particle spectrum. However, there still remains a \mathbb{Z}_3 symmetry, under which all the matter and Higgs fields Φ transform as $\Phi \rightarrow \alpha \Phi$, where $\alpha^3 = 1$. This \mathbb{Z}_3 symmetry may be invoked to banish such unwanted terms in the superpotential as $H_1 H_2$, N^2 and N , all of which would have massive parameters associated with them.

It has recently been indicated that gauge singlet fields may induce a destabilisation of the gauge hierarchy in the presence of non-renormalisable operators suppressed by powers of the Planck mass [12]. These operators can only exist, however, if gravity violates the \mathbb{Z}_3 symmetry which is respected by the renormalisable operators of the theory. The coefficients of such operators, if they exist, have not yet been calculated and their size and importance is unclear. Furthermore, if the singlet couples strongly to superheavy particles, such as Higgs colour triplets, destabilisation of the gauge hierarchy may result [11]. However, this problem is strongly dependent on the structure of the GUT model, and we shall therefore not discuss it here. However we note that, after spontaneous breaking, the \mathbb{Z}_3 symmetry must result in stable domain walls at the electroweak scale [17], a cosmological catastrophe which can however be avoided by allowing explicit \mathbb{Z}_3 breaking by terms suppressed by powers of the

Planck mass which will ultimately dominate the wall evolution [18] without affecting the phenomenology of the model. The important question of whether such a cosmic catastrophe can be avoided without destabilising the hierarchy is one which we shall not address here.

The NMSSM thus has its own particular problems, so we cannot claim that it is superior to the MSSM. However, it seems to us that it deserves as close a scrutiny as the MSSM in order that the models may be compared with experiment.

Unlike the case in the MSSM, where it is possible to derive simple constraints which test whether correct electroweak symmetry breaking will occur (at least at tree level), the possible vacuum structure of the NMSSM is very complicated. We must always check that a particular selection of parameters in the low energy Higgs potential will not result in the VEVs breaking electromagnetism. The condition that electromagnetism is not broken simply reduces to requiring that the physical charged Higgs mass squared be non-negative [9]. It can be shown, at tree level, that spontaneous CP violation does not occur in a wide range of SUSY models including the NMSSM [19]. Given that these conditions are satisfied, we are left with a choice of VEVs for H_1 and H_2 as in Eq. (2.3) and with $\langle N \rangle = x$, where ν_2 is positive real and ν_1 and x are real [9]. We shall define $\tan \beta$ as before, and $r = x/\nu$.

In the squark and slepton sectors, there exists the possibility of VEVs breaking electromagnetism or colour (or both). Derendinger and Savoy [8] have formulated simple conditions which determine in which regions of parameter space such VEVs do not occur. The condition that we have no slepton VEVs is

$$A_e^2 < 3(m_e^2 + m_L^2 + m_{H_1}^2), \quad (2.6)$$

where the parameters are defined by the soft SUSY breaking potential in Eq. (2.5). This constraint is derived from the tree-level potential under certain approximations, and should be tested at a scale of order A_e/h_e , a typical VEV (for the slepton case).

A similar condition on squark parameters will ensure the absence of colour-breaking squark VEVs:

$$A_t^2 < 3(m_T^2 + m_Q^2 + m_{H_2}^2). \quad (2.7)$$

The reliability of the results has been discussed in the literature [9]. We take them as providing a coarse indication of when sparticle VEVs are likely to occur.

In the analysis which follows, we shall assume that gauge coupling unification *does* occur, that is, that $SU(3)_c \otimes SU(2)_L \otimes U(1)_Y$ does embed in a simple group defined by one gauge coupling constant. There are of course other models in the literature not based on a simple gauge group, in which exact gauge coupling unification does not occur.

Finally we note that there is a well defined limit of the NMSSM in which the components of the singlet decouple from the rest of the spectrum which therefore resembles that of the MSSM (assuming no degeneracies of the singlet with the other particles of similar spin and CP quantum numbers which may lead to mixing effects which will enable the NMSSM to be distinguished from the MSSM even in this limit.) This limit is simply [9]: $k \rightarrow 0, \lambda \rightarrow 0, x \rightarrow \infty$ with kx and λx fixed.

3 Methodology

3.1 Scaled Parameters

The NMSSM is defined at the GUT scale, M_X , by the Yukawa couplings h_{t0} , λ_0 and k_0 (we neglect all other Yukawa couplings since they are small compared to the third generation couplings) and by the soft parameters m_0^2 , the universal scalar mass squared, A_0 , the universal trilinear coupling, and $M_{1/2}$, the universal gaugino mass. The MSSM is similarly defined, except that λ_0 and k_0 are replaced by μ_0 , the $H_1 H_2$ superpotential coupling, and its associated soft-breaking parameter B_0 . Thus, the NMSSM is defined by the set of parameters $\mathcal{P}_{NM} = \{h_{t0}, \lambda_0, k_0, A_0, m_0^2, M_{1/2}\}$ and

the MSSM is defined by the set $\mathcal{P}_M = \{h_{t0}, \mu, B_0, A_0, m_0^2, M_{1/2}\}$. In the NMSSM, we shall often find it convenient to use the variable A_0/m_0 in our discussion, since this seems to classify the interesting regions of parameter space more easily.

Below the GUT scale, the soft parameters run away from their values at M_X . In the NMSSM the three soft parameters at M_X evolve into 32 separate couplings below M_X , and in the MSSM the four soft couplings at M_X evolve into 30 separate couplings below M_X (assuming no inter-generational mixing). However, since we retain only the third generation's Yukawa couplings, then the first and second generations' couplings will run identically. Below M_X we have soft scalar couplings m_i^2 (e.g. $m_{Q_3}^2, m_T^2$), gaugino masses M_i and soft trilinear couplings A_i (e.g. A_t); in the MSSM we also have B . The unification constraints then are

$$g_i^2(M_X) = g_X^2 \tag{3.1}$$

$$M_i(M_X) = M_{1/2} \tag{3.2}$$

$$m_i^2(M_X) = m_0^2 \tag{3.3}$$

$$A_i(M_X) = A_0 \tag{3.4}$$

In the MSSM, B_0 , being a bilinear soft mass, need not be related to $M_{1/2}, m_0^2$ or A_0 , and we note that with our choice of conventions $A_k(M_X) = -A_0$.

Our various phase and sign conventions in the NMSSM and MSSM are adapted from reference [9]. The conventions in the MSSM are fairly standard, but it is worth discussing the various conventions we use for the NMSSM. The phases of the dimensionless couplings in the superpotential are selected by appropriate field redefinitions and are chosen so that all the dimensionless couplings are real. We may then also impose that the gaugino masses are positive. We assume that A_0 is real, and we know that m_0 is real and positive. This then leads us to VEVs ν_1, ν_2, x which we may take to be real [19]. The problem has thus reduced to one of sign conventions for all these quantities. In principle λ_0, k_0 and A_0 are allowed to be positive or negative,

and the resulting VEVs ν_1, ν_2, x may each be positive or negative. However there are 3 symmetries of the one-loop effective potential which will lead to simplifications, namely:

$$\lambda_0 \rightarrow -\lambda_0, \quad k_0 \rightarrow -k_0, \quad x \rightarrow -x \quad (3.5)$$

$$\lambda_0 \rightarrow -\lambda_0, \quad \nu_1 \rightarrow -\nu_1 \quad (\text{or } \nu_2 \rightarrow -\nu_2) \quad (3.6)$$

$$\nu_1 \rightarrow -\nu_1, \quad \nu_2 \rightarrow -\nu_2 \quad (3.7)$$

These equations show that negative VEVs can be re-interpreted as negative λ_0, k_0 . In our analysis we shall take positive λ_0, k_0 , and search for global minima of the effective potential with positive ν_2 and both possible signs of ν_1 and x . We could have required all VEVs to be positive by using the invariance of the action under the above symmetries and then allowing λ_0 and k_0 to take negative values, but as explained in our discussion of the electroweak potential, this is rather inconvenient since we cannot impose such constraints on the VEVs when minimising the potential. It has been shown that we need not consider complex VEVs [19]. To summarise, all input parameters and VEVs are taken real and in the NMSSM only x, ν_1, A_0 may be negative, while in the MSSM only μ_0, B_0, A_0 may be negative.

Suppose that we have a set of parameters (\mathcal{P}_{NM} or \mathcal{P}_M) defined at M_X , together with g_X . In general, an arbitrary selection of parameters at M_X will not result in an acceptable pattern of electroweak symmetry breaking, both qualitatively and quantitatively (*i.e.* giving the correct Z mass). In order to ensure that a given set of parameters results in correct when electroweak symmetry breaking, we make the following observations.

Firstly, looking at the RG equations in appendix A, we see that to one loop ³ we

³To two loops this is no longer strictly true, but the error introduced in this is no worse than the error which we implicitly accept in calculating the soft masses to one loop.

have the relation

$$\frac{M_i(Q)}{M_{1/2}} = \frac{g_i^2(Q)}{g_X^2}. \quad (3.8)$$

where Q is the \overline{MS} renormalisation scale. This suggests the idea of recasting the RG equations for dimensionful quantities in terms of those quantities divided by suitable powers of $M_{1/2}$ [9]. The RG equations for A_i and m_i^2 (and B and μ) become equations for $A_i/M_{1/2}$ and $m_i^2/M_{1/2}^2$ (and $B/M_{1/2}$ and $\mu/M_{1/2}$), while knowledge of the gauge couplings allows us to avoid explicitly running the gaugino masses. Our GUT scale parameters may then be replaced by the same parameters made dimensionless by scaling with appropriate powers of $M_{1/2}$. We denote these scaled quantities by a tilde. The parameters defining the NMSSM are thus $\tilde{\mathcal{P}}_{NM} = \{h_{t0}, \lambda_0, k_0, \tilde{A}_0, \tilde{m}_0^2\}$ and those defining the MSSM are $\tilde{\mathcal{P}}_M = \{h_{t0}, \tilde{\mu}, \tilde{B}_0, \tilde{A}_0, \tilde{m}_0^2\}$. These scaled parameters may then be fed into the RG equations in order to extract the scaled low energy parameters.

By defining tilded scalar fields, that is, fields divided by $M_{1/2}$, the tree-level Higgs potential V_0 becomes \tilde{V}_0 , where the latter potential involves only scaled parameters. If ν_i (and x in the NMSSM) minimise the potential V_0 , then $\nu_i/M_{1/2}$ (and $x/M_{1/2}$) minimise the potential \tilde{V}_0 . Knowing the scaled VEVs $\tilde{\nu}_i$, we may then determine which value of $M_{1/2}$ is necessary to give us the correct Z mass from

$$\frac{M_Z^2}{M_{1/2}^2} = \frac{1}{2}(g_1^2 + g_2^2)(\tilde{\nu}_1^2 + \tilde{\nu}_2^2) \quad (3.9)$$

3.2 The Effective Potential

It is well known that VEVs may not be reliably calculated using the tree-level potential, so that it is necessary to employ the one loop effective potential [20, 21], given by

$$V_1 = V_0(Q) + \frac{1}{64\pi^2} Str \mathcal{M}^4 \left(\log \frac{\mathcal{M}^2}{Q^2} - \frac{3}{2} \right), \quad (3.10)$$

where Q is the \overline{MS} renormalisation scale, which should be selected so that the logarithms in the effective potential are relatively small, and so we select a value of $Q = 150$ GeV. This choice of Q is reasonable for $M_{1/2}$ and m_0 less than about 1 TeV. \mathcal{M}^2 is the field-dependent, tree-level mass-squared matrix of those fields whose radiative corrections we wish to include. By field-dependent mass matrices is meant the mass matrices calculated from the potential *prior* to setting the fields to their VEVs. We include radiative corrections from loops of top quarks and squarks. We do not include radiative corrections arising from the rest of the spectrum since in this model such an analysis would be computationally prohibitive. Of course it is well known [21] that in order to achieve Q independence it is necessary to include the entire SUSY spectrum and to work to all orders. There will therefore be a Q dependence in our results which we shall discuss later. If m_t , $m_{\tilde{t}_1}$ and $m_{\tilde{t}_2}$ are the field-dependent eigenvalues of the top quark and squark mass matrices respectively, then the contribution to the effective potential from radiative corrections due to these states is given by

$$\frac{3}{32\pi^2} \left[\sum_{i \in \{\tilde{t}_1, \tilde{t}_2\}} m_i^4 \left(\log \frac{m_i^2}{Q^2} - \frac{3}{2} \right) - 2m_t^4 \left(\log \frac{m_t^2}{Q^2} - \frac{3}{2} \right) \right]. \quad (3.11)$$

Notice that if particles and sparticles are degenerate, then their contribution to radiative corrections vanish — this is an instance of the well known non-renormalisation theorem in SUSY.

Unfortunately, the presence of the logarithm in V_1 rather complicates the scaling argument just presented. We may easily obtain \tilde{V}_0 , and therefore $\tilde{\mathcal{M}}^2$, but in order to be able to evaluate the logarithm, we need to know $M_{1/2}$. We may overcome this difficulty by noting that the scaled one loop potential may be written as

$$\tilde{V}_1 = \tilde{V}_0 + \frac{1}{64\pi^2} \text{Str} \tilde{\mathcal{M}}^4 \left[\log \left(\frac{\tilde{\mathcal{M}}^2}{Q^2} M_{1/2}^2 \right) - \frac{3}{2} \right]. \quad (3.12)$$

The problem then reduces to finding the value of $M_{1/2}$ which, when inserted in the logarithms of the scaled potential, give the same output value of $M_{1/2}$. This is calculable

numerically, although there are typically two consistent solutions for $M_{1/2}$.

There are a number of problems with the calculation of the minimum of the electroweak potential in the NMSSM which do not occur in the MSSM, and it is worth highlighting them here. Firstly, there is the trivial point that the space where we must look for solutions is simply bigger; instead of minimising a function of two variables which can be constrained to be positive, we are minimising a function of three, and only one of these has its sign constrained.

More significantly, the minimum in the MSSM is unique at tree-level (apart from the effects of the Z_2 symmetry taking $H_i \rightarrow -H_i$), and this is often true even for the one loop case. For the NMSSM there are virtually always several non-degenerate minima (up to five in some cases), and so we must reliably calculate all of them and compare their respective values of the potential to decide which one is preferred. Sometimes, but not always, some or all of these minima are unphysical in the sense that one or more of ν_1, ν_2, x is zero. ⁴

This problem of multiple minima in turn leads to some serious technical problems with reliably calculating the true deepest minimum of the potential, since there may be minima with very different VEVs but similar values of the potential. In this case we would not expect minor changes in our input parameters or approximations to greatly change the VEVs at the different minima, but we might well find that such changes could affect which of the minima were deepest, and so lead to very substantial changes in output. Fortunately, we do not find that this structure is common through most of parameter space, but we do find that there are certain regions where altering the input parameters leads to the failure of electroweak breaking, and clearly the exact place where this occurs is likely to be sensitive to minor changes. We shall

⁴Note that this means that if we had used different phase conventions such that all of the VEVs were positive, we would still have had to allow different signs of VEVs in the potential calculation to ensure that the minimum with positive VEVs was deeper than any of the minima with one or more VEVs negative, since there is no phase choice which will make *every* minimum occur at positive VEVs simultaneously.

discuss the implications of this when we come to study the parameter space of the NMSSM electroweak potential in detail later.

3.3 Calculation of the Spectrum

With knowledge of the VEVs and $M_{1/2}$ we may calculate the spectrum of states induced by our parameters. In appendix B we give all relevant scalar and fermion mass matrices. In the scalar sector, we calculate one loop radiative corrections to all tree-level mass matrices which arise from loops of top and bottom quarks and squarks, and thus are controlled by h_t and h_b . In particular, we calculate radiative corrections to all Higgs boson masses and to top and bottom squark masses.

In the fermionic sector, only the top and bottom quarks' masses are controlled by h_t and h_b . Since we take $Q = 150$ GeV, and as $m_t \sim 150 - 200$ GeV, the error induced by evaluating $m_t(Q)$ rather than $m_t(m_t)$ is small, and so this is what we do.⁵ Similarly we evaluate all SUSY masses at the scale Q , ignoring the effects of decoupling which have been calculated in the MSSM and are known to be a few percent [22] except for very heavy states.

3.4 Overall Procedure

Let us now discuss our explicit numerical techniques. In either the MSSM or the NMSSM, we start with a set of 5 input parameters \tilde{P} as discussed above. From this we must derive M_X , g_X , $M_{1/2}$, $\alpha_3(M_Z)$ and the entire low energy spectrum. We can find the other parameters for some given value of $M_{1/2}$ as follows. We first guess M_X , g_X , allowing us to calculate the full low energy spectrum in terms of scaled variables (and hence of unscaled variables, making use of $M_{1/2}$). Imposing correct unification of the low energy couplings after running up through all the thresholds allows us to iteratively refine our guess of M_X and g_X and to calculate $\alpha_3(M_Z)$. Even when this

⁵Note that the mass which we quote for the top quark is the pole mass.

has converged, however, our initial choice of $M_{1/2}$ will not in general be consistent with electroweak symmetry breaking and the correct value of M_Z . We must therefore repeat the entire process with new values of $M_{1/2}$ until we have found those values which are consistent with those derived from the Higgs potential as discussed above.

Although we do not include the effects of h_{b0} and $h_{\tau 0}$, their inclusion is in principle straightforward, and they are included in the analytical results in the Appendices. As might be expected, their effect is negligible when $\tan\beta$ is small. We have explored the effect of including such corrections for larger $\tan\beta$, but found that they tend to make our numerical calculations prohibitively slow, and so we do not include them.

This procedure is inevitably highly computationally intensive in the NMSSM, primarily because of the difficulties implicit in numerically minimising the Higgs potential, but is relatively simple for the MSSM. However, it is still less efficient for the latter than the “ambidextrous” approach used by many authors [6] where the input parameters are $\{m_0, M_{1/2}, A_0, m_t, \tan\beta\}$. Here the fact that B and μ do not appear in the RGEs for other parameters means that they can be regarded effectively as low energy parameters to be exchanged for m_t and $\tan\beta$, and there is thus no need for such repeated minimisation of the potential to achieve convergence. In the NMSSM B and μ are replaced by λ and k , and these appear in the RG equations for many of the other parameters, preventing us using this technique.

3.5 Physical Constraints

We now turn to a discussion of the physical constraints. Apart from the constraints of the correct pattern of electroweak symmetry breaking and gauge coupling unification mentioned in section 3, the particle spectrum resulting from an otherwise valid point in parameter space must be subjected to certain phenomenological and cosmological constraints. We have already mentioned that slepton VEVs and squark VEVs must

not be permitted.

Searches for pair production of sparticles coupling to the Z have been undertaken at LEP [23], with the following results:

- Charged sleptons and sneutrinos have masses exceeding 43 GeV
- Top squarks have masses exceeding 43 GeV
- Charginos have masses exceeding 47 GeV
- Charged Higgses have masses exceeding 45 GeV

Squarks other than top squarks, together with the gluino, must have masses in excess of 100 GeV. Constraints on the squark spectrum from flavour changing neutral currents are not considered [24].

In the MSSM the lightest neutralino must have a mass in excess of 18 GeV [25]. In the NMSSM this constraint may be greatly relaxed, with even neutralino masses of zero acceptable for some regions of parameter space since the lightest neutralino may contain a large singlet component [9, 26].

The only cosmological constraint which we impose is that the lightest SUSY particle (LSP) should be a neutralino. We do not impose the constraint that $\Omega \leq 1$, since the calculation of the relic density is complicated in this model, and has been considered elsewhere in the MSSM [27] and the NMSSM [28].

In the neutral Higgs sector of the MSSM the constraints on the lightest CP-even Higgs scalar, h , are complicated and depend on the suppression of its couplings to the Z relative to those in the standard model, with a bound of up to 60 GeV [29]. In the NMSSM, since this state may contain a significant proportion of the singlet field, its coupling to the Z will be diluted. This complicates the constraint and will be discussed in detail in section 7, while it has been considered without the imposition

of unification constraints in Ref. [30]. We do not consider further constraints on the Higgs sector from the decay $b \rightarrow s\gamma$, since the magnitude of these is uncertain; for a review of this topic, see for example, [31]. In any case it will turn out that in all the interesting regions of parameter space that the charged Higgs scalars are quite heavy.

In order that the spectra be heavy enough to evade all the constraints, it is generally only necessary that $M_{1/2}$ be large enough; if it falls below around 50–100 GeV then many of them start being violated simultaneously. Similarly, the experimental value of $\alpha_3(M_Z)$ is so uncertain that we virtually always find that our results are within experimental errors. More significant bounds arise from the value of the top mass, which has recently been measured to be about 180 GeV [32] with an error of order 10 GeV. We shall conservatively only require $m_t > 140$ GeV in presenting our numerical results. However we shall emphasise those regions of parameter space which can yield heavy top quark masses in the preferred range 160–200 GeV.

The only constraint on the dimensionless couplings is that of avoiding triviality, so that h_{t0} , λ_0 , k_0 are all < 3 , although, as we shall see, there are tight constraints on them for given values of the other parameters from correct electroweak symmetry breaking.

These constraints, and in particular the values of m_t and $\alpha_3(M_Z)$ will in general be discussed in the text when we come to consider the various different regions of parameter space in which they may be violated.

3.6 Naturalness Constraints

Finally, we note that there is a further constraint which is inspired by naturalness rather than phenomenology [5, 33, 34]. This is the so-called fine-tuning constraint, which is usually expressed as the requirement that the value of M_Z derived from the electroweak potential should not be too sensitive to small changes in h_{t0} . In practice,

this amounts in the MSSM to ensuring that the supersymmetric spectrum is not too heavy relative to the electroweak breaking scale. We follow [5] in defining

$$c_{h_t} = \left| \frac{\delta M_Z / M_Z}{\delta h_{t0} / h_{t0}} \right| \quad (3.13)$$

which allows us to quantify the fine-tuning inherent in any given set of parameters.

In the NMSSM we also define c_λ and c_k analogously to c_{h_t} as follows.

$$c_\lambda = \left| \frac{\delta M_Z / M_Z}{\delta \lambda_0 / \lambda_0} \right| \quad (3.14)$$

$$c_k = \left| \frac{\delta M_Z / M_Z}{\delta k_0 / k_0} \right| \quad (3.15)$$

We shall not impose any explicit restriction on these parameters because the amount of fine-tuning to be tolerated is essentially a matter of taste, particularly in the NMSSM where it is not clear to which dimensionless parameter any such constraint should be applied, and instead shall discuss the extent of fine-tuning further when we come to our results for each of the two models.

4 MSSM Results

It will be helpful to discuss the MSSM in some detail. Although a number of studies of this model have been done [6], none has recently considered it with our choice of variables, chosen entirely at the GUT scale, which are more enlightening for purposes of comparison with our analysis of the NMSSM.

4.1 The Spectrum

We begin by noting that there are a number of common themes to analyses of this sort which apply for both models. Firstly, the value of $\alpha_3(m_Z)$ which allows unification is around 0.126 (0.118) for $M_{1/2}$ of order 100GeV (1TeV) at two loops with $m_0 = M_{1/2}$; it is lower at one loop, by typically around 10%. Of course, this is rather an

oversimplification, and for values of m_0 far from $M_{1/2}$ there will be strong dependence on m_0 , together with dependence on μ and A , but the primary determinant of $\alpha_3(m_Z)$ is that of the scale of the gaugino thresholds. A detailed discussion of the dependence of the couplings on the various thresholds is given in reference [35].

To illustrate this, we display a plot of contours of constant α_3 and m_t in the $m_0 - M_{1/2}$ plane in Figure 1. Here the value of $\alpha_3(M_Z)$ decreases as we increase the effective scale of the SUSY breaking masses, as discussed before. It is noticeable here that the $m_0 - M_{1/2}$ plane is not completely covered with contours; this is because correct electroweak symmetry breaking does not occur in some regions, while only in part of the plane do we find acceptable top masses. Graphs generated by other authors often have smaller excluded regions, because they are for fixed $\tan\beta$ and m_t and variable B_0 and μ_0 , which makes correct electroweak breaking easier to arrange. This dependence of $\alpha_3(M_Z)$ on m_0 and $M_{1/2}$ is exactly the same for the NMSSM.

The typical spectrum is also fairly similar in both models. In general, all the scalar superpartners have masses of around m_0 (although for small m_0 , $M_{1/2}$ corrections can dominate). Masses are rather larger for squarks because of QCD effects, but the stop squark is in general rather lighter thanks to the corrections from large h_t . The gauginos, as already noted, have masses given by $M_i = (g_i/g_X)^2 M_{1/2}$, and so the gluino tends to have a mass of around three times $M_{1/2}$, while the lightest chargino and lightest neutralino have masses less than or order of $M_{1/2}$ and $\frac{1}{2}M_{1/2}$ respectively. The case for the neutralino and chargino is greatly complicated by the fact that these have mass eigenstates which are mixtures of gaugino and Higgsino. The Higgs masses are typically of the same order as the other scalars, except for the lightest CP-even Higgs state which is constrained to be lighter than an upper bound in both the MSSM [36] and the NMSSM [37, 38].

4.2 Electroweak Symmetry Breaking

Turning now specifically to the case of the MSSM, the main difference between this model and the NMSSM is its relatively simple Higgs structure. At tree level, ignoring the one-loop effective potential, it is possible to analytically find the minimum of the potential, and we shall simply quote some of the results here. These can be found in, for example, [1]. We define $m_1^2 = m_{H_1}^2 + \mu^2$, $m_2^2 = m_{H_2}^2 + \mu^2$ and $m_3^2 = B\mu$. Firstly, in order that the minimum of the potential not be at the origin, we have $m_1^2 m_2^2 < m_3^4$, while to prevent the potential being unbounded from below $m_1^2 + m_2^2 + 2m_3^2 > 0$. We must avoid breaking electromagnetism which implies $m_3^2 < 0$. These results tend to favour the case where only one of m_1^2 and m_2^2 is negative or where both are positive but one is rather less than the other. Of course, this is the reason why radiative electroweak symmetry breaking via h_t works [4], as it drives m_2^2 to be smaller (possibly negative), while m_3^2 can easily be set negative.

We now note that, from the minimisation conditions of the potential,

$$\sin 2\beta = \frac{-2m_3^2}{m_1^2 + m_2^2}, \quad (4.1)$$

and so we see that large $\tan\beta$ will occur in the region where m_3^2 is small, at least relative to $m_1^2 + m_2^2$. The second minimisation condition, expressed in terms of M_Z^2 , is

$$M_Z^2 = \frac{2m_1^2 - 2m_2^2 \tan^2 \beta}{\tan^2 \beta - 1} = \frac{2m_{H_1}^2 - 2m_{H_2}^2 \tan^2 \beta}{\tan^2 \beta - 1} - \mu^2 \quad (4.2)$$

which suggests that in general M_Z^2 will be of order $-m_2^2$ for reasonably large values of $\tan\beta$.

In numerical studies including the one-loop effective potential, we find that electroweak symmetry breaking works perfectly well for reasonably large h_t (to drive m_2^2 small enough) so long as B_0 and μ_0 are of opposite sign (in fact $B_0 \sim 0$ also works because of radiative corrections which drive B negative by the electroweak scale).

Furthermore, selecting smaller B allows us to make $\tan\beta$ as large as we like, so long as h_b is neglected. When h_b is included [39], it becomes large for large $\tan\beta$, driving $\tan\beta$ down and thus making it difficult to obtain very large $\tan\beta$ without fine-tuning the parameters.

The dependence on μ_0 is rather more complicated; although it might appear from Eq. (4.1) that small μ_0 gives larger $\tan\beta$, in fact the dependence of m_1^2 and m_2^2 on μ means that the effect of varying it is much more complicated and depends on which region of parameter space we study. Since large m_0^2 means large m_1^2 , we see that pushing up m_0 beyond a few times $M_{1/2}$ tends to increase $\tan\beta$.

In drastic contrast to the case in the NMSSM, A_0 seems to be relatively unimportant to electroweak symmetry breaking. It can be picked as small as we wish, or as large as is consistent with avoiding the constraints on slepton vevs discussed earlier.

4.3 Fine-Tuning

Finally we turn to the dependence on h_t . This is crucial as h_t has the dominant effect on m_2^2 , forcing it to become negative and so driving electroweak symmetry breaking [4]. The behaviour of $M_{1/2}$ as h_{t0} is varied is complicated, since changes in $M_{1/2}$ affect the potential in several ways: by directly changing the values of the soft masses (for fixed scaled values of the other dimensionful quantities); by affecting the logarithms in the one loop potential; and by changing the range over which we run and the couplings (since altering $M_{1/2}$ will significantly change M_X and g_X). We show a typical graph of the dependence of $M_{1/2}$ on h_{t0} in Fig.2. This kind of structure often occurs in the NMSSM too, although there the behaviour can be more complicated.

A simpler dependence on h_{t0} , and one which has been studied by a number of authors interested in the fine-tuning behaviour, is that of M_Z on h_{t0} for fixed values of the soft masses (and hence of $M_{1/2}$ in our notation) [33, 34]. From the RG equations

in Appendix A and the tree-level analysis of the last sub-section, it can be seen that if h_t is too large $-m_2^2$ will fall too rapidly ultimately becoming too negative, leading the tree-level potential to have very large VEVs. For small h_t , m_2^2 will not be driven negative, and electroweak symmetry breaking will not occur. We are thus reduced to an intermediate zone of h_t , and the behaviour of M_Z as h_t is increased is to rise rapidly from zero to a very large value (often infinity at tree level) driven by the large value of $-m_2^2$.

A crude understanding of the fine-tuning problem may be given as follows. The RG equation for m_2^2 shows that, assuming h_t^2 terms dominate, the value of m_2^2 approaches a fixed point of order minus a few times a typical squark mass squared, resulting in M_Z of order a typical squark mass (unless this large negative m_2^2 makes the potential unbounded from below). For large squark masses, the value of M_Z can only be reduced by carefully reducing h_t so that this fixed point is not approached too closely. This is the fine-tuning problem.

It should be noted that, although this discussion has been at tree-level, the behaviour at the one loop level is qualitatively similar, although the one loop contributions reduce the fine-tuning [34]. This is simply because they introduce into Eq.(4.2) extra terms of opposite sign to those which are present at tree level, and which also grow with increasing values of the squark masses.

In order to illustrate the level of fine-tuning in the MSSM, in Fig.3 we show the effect on the Z mass of changing h_{t0} with $\tilde{m}_0 = \tilde{\mu}_0 = -\tilde{B}_0 = 1$ and $A_0 = 0$, with $M_{1/2} = 50, 100, 300, 500, 1000\text{GeV}$. For the curve shown in Fig.3, the value of c_{h_t} is 2.3,4.5,25,49,83 for $M_{1/2} = 50, 100, 300, 500, 1000\text{GeV}$ at $M_Z=91.2\text{GeV}$. These very large values of c_{h_t} typically lead authors to restrict their values of the soft masses to less than 1TeV or so. The fine-tuning becomes severe only as the squark masses becomes significantly larger than M_Z ; for example, if M_Z were 200GeV then $c_{h_t} = 50$

would not be reached until $M_{1/2}$ were 1300GeV, instead of 500GeV. Lastly we remark that for very large $M_{1/2}$, we find a cutting out of the data in the curves, caused by the transition between two minima, one at the origin and one at non-zero VEVs.

5 NMSSM Results

In order to study the NMSSM parameter space, we first selected a grid of points with $h_{t0} = 0.5, 1, 2, 5$, $\lambda_0 = 0.01 - 2.0$, $k_0 = 0.01 - 2.0$, $\tilde{m}_0 = 0.2 - 5.0$, and $A_0/m_0 = -4$ to 4 (as we shall see later it is convenient to scale A_0 by m_0). Within this parameter range we can classify the successful parts of parameter space into two distinct regions:

$$(i) \quad k_0 > \lambda_0 > h_{t0}$$

$$(ii) \quad h_{t0} > \lambda_0 > k_0$$

Although the range of parameters above covers most of the parameter space it turns out that there are other phenomenologically interesting parts of parameter space outside this region. In particular there is a third region of parameter space with values of the couplings k_0 , λ_0 , \tilde{m}_0 which are significantly smaller than those considered above, and which is associated with *very* large values of r . Small λ , k and large r implies that the NMSSM is close to the MSSM limit in which the singlet completely decouples from the rest of the spectrum. Although not logically distinct from region (ii) above which also approaches the MSSM limit, this third region is so close to it that we shall refer to it as the “deep MSSM limit” of the model and discuss it separately.

The results in the case of the NMSSM are naturally more complicated than for the case of the MSSM. The primary constraint is that of correct electroweak symmetry breaking, which we shall find restricts us to only a relatively small part of parameter space. The fundamental problem with the electroweak potential in the NMSSM is that the minimum of the potential is often ruled out because, for example, it has

$\nu_1 = 0$ or $\nu_2 = 0$. This does not usually occur in the MSSM, because (at tree-level) the existence of a μ term of the correct sign guarantees that if one of ν_1 and ν_2 is non-zero, so is the other.

In order to find correct electroweak breaking in the NMSSM, we must thus ensure that N is driven to have a VEV. We find in practice that this can be done in two ways. Firstly, it is possible to force m_N^2 negative by having large Yukawa couplings in the Higgs sector. Secondly, it is possible to have electroweak breaking with $m_N^2 > 0$ by having very large trilinear terms, and hence large A_k . We shall discuss each of these two disconnected regions of correct electroweak symmetry breaking separately below, before turning to a fuller discussion of our uncertainties and approximations, and of the phenomenological implications of our findings.

5.1 $k_0 > \lambda_0 > h_{t0}$ Region

The first region which we shall discuss is that which has electroweak symmetry breaking driven by Higgs sector Yukawa couplings. Here we have λ_0, k_0 large, typically with $\lambda_0 + k_0 > 2$, thus driving the Higgs masses squared negative, and we find regions of correct electroweak symmetry breaking for values of $|A_0/m_0|$ down to zero. This is in contradiction to the results of [13, 14], although we note that this may be partially explained by the cut on the top mass used in [15].

Typically, we find that varying λ_0 and k_0 does not have a great impact in this region. Reducing either of these leads to a gradual increase in $\tan \beta$ which can thus be made to take any value from around 3 to as large as we like (until our approximations begin to break down), while they can be increased arbitrarily so long as k_0 remains rather larger than λ_0 . Varying h_{t0} , however, leads to more dramatic changes, since by tuning this we can select any value of $M_{1/2}$ we choose. Unfortunately, we generally find that in order to obtain values of $M_{1/2}$ less than many TeV it is necessary to reduce

h_{t0} until the top mass is very small, and so only very little of this data survives.

The dependence of the output on A_0/m_0 is straightforward; $M_{1/2}$ has a minimum for some value typically between 0 and -1. Electroweak breaking fails for $|A_0/m_0|$ greater than some value typically $\lesssim 2$. Dependence on \tilde{m}_0 is less crucial to correct electroweak breaking, but it seems that $\tilde{m}_0 > 1$ is preferred. As appears to occur everywhere, $|r|$ is roughly directly proportional to $M_{1/2}$ for fixed values of the other parameters, and here can be less than 1 for very small $M_{1/2}$. We note that changing the sign of A_0 has as its main effect changing the sign of r .

In Fig.4 we show a typical plot of the mass spectrum in this region. The lightest CP-even Higgs is within the reach of LEP II, and over some of the $M_{1/2}$ range the lightest chargino is also observable at LEP II. Note that the top quark mass is fairly constant at 147 GeV over the whole range, a value which is typical of the largest achievable in this region, and so future more stringent bounds on the top quark mass could exclude this region completely. For $M_{1/2} < 100\text{GeV}$ the chargino mass violates its experimental bound.

5.2 $h_{t0} > \lambda_0 > k_0$ Region

The second region of parameter space which we shall discuss is that where the VEV of N is driven to be non-zero by the effect of A_k . This region is immediately more promising than before since it allows a large top quark Yukawa coupling, and hence can have larger top quark masses. This region was also discussed in ref.[13, 15, 16] and is discussed here again for completeness. We find that here $h_{t0} > \lambda_0 > k_0$, and that we are typically in a region where $|r| \gg 1$ and $\lambda_0, k_0 \ll 1$. We find that only a restricted range of $|A_0/m_0|$ around 3 can give consistent electroweak breaking without generating slepton VEVs [13]; the reasons for this can be understood analytically and will be discussed in Section 6.

We now turn to a discussion of the behaviour of the solutions as we adjust the various input parameters. As in the $k_0 > \lambda_0 > h_{t0}$ region, we find that increasing h_t causes $M_{1/2}$ to increase arbitrarily. However, unlike in the former region, here we can avoid the constraint of small top mass by tuning λ_0 and k_0 , since in this region $M_{1/2}$ is a very sensitive function of these variables. In fact we find we find that for any given values of the other parameters, the requirements of electroweak breaking restrict us to a very small range of k_0 (or λ_0), leading to a correlation between these parameters in this region.

To illustrate the correlation between λ_0 and k_0 , in Fig.5 we show contours of h_{t0} in the $\lambda_0 - k_0$ plane with $\tilde{m}_0 = 2$, $M_{1/2} = 500$ GeV and $A_0/m_0 = -3$. Although we could have chosen other values of $M_{1/2}$, the qualitative features of Fig.5 would be unaltered, and the value of k_0 would only change by a few per cent, since in this region the value of $M_{1/2}$ is a very sensitive function of λ_0 and k_0 . The fact that for each line λ_0/k_0 is virtually constant can be understood from the electroweak potential near the MSSM limit, as discussed in Section 6. The $h_{t0} = 0.5, 1, 2, 3$ contours correspond to $m_t \sim 145, 175, 185, 190$ GeV, respectively, with $|\tan \beta|$ varying from 2-7 and $|r|$ from 100-30, from the lowest to the highest value of k_0 respectively. Values of k_0 beyond the ends of the plot are forbidden by the requirements of electroweak symmetry breaking, although the exact ranges of acceptable k_0 could be altered by varying our choice of A_0 and \tilde{m}_0 slightly. Similarly, m_t would be altered if we use a different $M_{1/2}$ primarily due to the resulting change in $\alpha_s(M_Z)$. Changing the sign of A_0 leads to qualitatively rather similar output data with a change in the sign of r .

As mentioned above, in this region we need to have $|A_0/m_0| \sim 3$. In fact we find that negative A_0 works best (because thanks to the form of the RG equations this leads to a less restrictive slepton VEVs constraint), while we can increase the maximum permitted value of $|A_0/m_0|$ somewhat by reducing \tilde{m}_0 . There is also a correlation between h_{t0} and \tilde{m}_0 ; for $h_{t0} = 1(3)$ and $A_0/m_0 = -3$ we find acceptable

solutions for $\tilde{m}_0 \approx 1 - 2(2 - 5)$.

Typically we find quite large values of $|\tan \beta|$ in this region as well, but do not in general find any obvious correlation with the other input parameters. $|r|$ is generally directly proportional to $M_{1/2}$ for fixed values of the other parameters, and as we approach the origin in the $\lambda_0 - k_0$ plane it becomes very large. This corresponds to a very close approach to the MSSM limit.

In Fig.6 we plot the spectrum as a function of $M_{1/2}$ for the case $h_{t0} = 2$, $A_0/m_0 = -3$, $\tilde{m}_0 = 5$, $\lambda_0 = 0.4$, which is a typical point in this region of parameter space. Note that the experimental constraint that the charginos are heavier than 47 GeV implies that $M_{1/2} \gtrsim 70$ GeV in this case. For $M_{1/2} \approx 100(1000)$ GeV, which is controlled by choosing $k_0 = 0.275(0.300)$, we find $|\tan \beta| \approx 6(8)$, $|r| \approx 13(120)$, $\alpha_s(M_Z) \approx 0.121(112)$, $M_X = 2.1(0.99) \times 10^{16}$ GeV, $g_X = 0.71(0.69)$. The lightest CP-even Higgs boson has standard model-like couplings ($R_{ZZh} > 0.99$ everywhere) and for $M_{1/2} \lesssim 100$ GeV is in the LEP2 range, as are the lighter chargino and neutralinos which have a much stronger $M_{1/2}$ mass dependence. The top quark mass ranges from $m_t = 193 - 184$ GeV, being smaller for larger $M_{1/2}$ due to $\alpha_s(M_Z)$ being consequently smaller. For $M_{1/2} \lesssim 100$ GeV, the lightest stop and gluino are not too much heavier than the top quark, although the remaining sparticles and Higgs bosons are significantly heavier than the top quark.

One of our most interesting results is that for choices of parameters outside a “safe” range $h_{t0} \approx 1.5 - 3$, $|A_0/m_0| \approx 3$, $\tilde{m}_0 > 3$, we find that as $M_{1/2}$ is reduced the data suddenly cuts out below some critical value of $M_{1/2}$. This corresponds to some new (often unphysical) set of VEVs becoming preferred below some $M_{1/2}$ value. The effect is somewhat Q dependent and so deserves a detailed discussion.

5.3 Uncertainties in the Electroweak Potential

We now study the effects of varying the $\overline{\text{MS}}$ scale Q . Although in principle none of our results should depend on this, in practice there are a number of inaccuracies caused by the fact that the logarithms in our potential may not be small. It is not necessarily possible to guarantee that all the logarithms are small simultaneously, since we need to investigate the relative depths of multiple minima at significantly different values of the VEVs and hence of the terms appearing in the logarithm. A Q dependence is also introduced by our neglect of all but the effects of the h_t Yukawa coupling in the effective potential, since inclusion of all the spectrum would be prohibitively computationally intensive, and by our evaluation of masses at tree-level.

We find that in practice even relatively large changes of Q (up to an order of magnitude) do not have a very large impact on the value of the VEVs, except in cases where the scaled VEVs are very small which implies very large $M_{1/2}$ and so is outside the region of greatest physical interest. However, the impact on which of the VEVs is deepest is not always negligible. We find that in regions where consistent electroweak breaking cannot be achieved below some critical value of $M_{1/2}$ this value may be reduced by a reduction of Q . However, even this sensitivity to Q is not too severe; for example, a reduction of Q to around 10GeV is necessary in order to obtain arbitrarily small values of $M_{1/2}$ for $\tilde{m}_0 = 1$. Thus we confirm that there is only a restricted safe range where arbitrarily small values of $M_{1/2}$ are possible, even allowing for changes in Q .

We illustrate the existence of the cut-out of data in Fig.7, where we plot the spectrum as a function of $M_{1/2}$ for the case $h_{t0} = 0.5$, $A_0/m_0 = -4$, $\tilde{m}_0 = 0.5$, $\lambda_0 = 0.1$. These parameters are outside the safe range $h_{t0} \approx 1.5 - 3$, $|A_0/m_0| \approx 3$, $\tilde{m}_0 \approx 3 - 5$, in which small $M_{1/2}$ can be achieved independently of the choice of the renormalisation scale Q , and so we plot the spectrum for two choices of Q . The main

effect of changing Q is to change the value of $M_{1/2}$ at which the data cuts out. For $Q = 150(25)$ GeV, we find the minimum values $M_{1/2} = 300(125)$ GeV corresponding to $m_0 = 150(62.5)$ GeV. As in Fig.6, the lightest CP-even Higgs boson has standard model-like couplings, and for a given $M_{1/2}$ is even lighter than in Fig.6. For the smaller $M_{1/2}$ values which we can obtain with $Q = 25$ GeV the lighter chargino and neutralinos may be in the LEP2 range. Compared to Fig.6, the left-handed sleptons are now much lighter (due to the smaller value $\tilde{m}_0 = 0.5$) while the lighter stop is much heavier (due to the smaller value $h_{t0} = 0.5$). The top quark mass has a maximum value of $m_t = 160$ GeV for $M_{1/2} = 300$ GeV and here $|\tan\beta| = 3.8$. The gluino in Fig.7 is now the heaviest sparticle, whereas in Fig.6 it was one of the lighter ones. In general the Higgs and sparticle masses in Fig.7 are focussed into a narrower band of masses than in Fig.6, which is a simple result of having $\tilde{m}_0 = 0.5$ rather than $\tilde{m}_0 = 5$.

5.4 The Deep MSSM Limit: $h_{t0} > \lambda_0 \gg k_0$

This region of parameter space is characterised by very small values of the parameters $\tilde{m}_0 \ll 0.2$, $k_0 \ll \lambda_0 < 0.01$, which we refer to as the deep MSSM limit of the model, since in this region we find that $|r| \gg 100$. This region is nothing more than an extreme limit of the region just discussed, but deserves a separate discussion since there is some interesting physics in this region.

We have seen that in the constrained NMSSM one of the CP-even Higgs bosons is almost pure gauge singlet. Such a decoupled Higgs boson might be expected since the constrained NMSSM is close to the MSSM limit. In the analysis of ref.[15] the decoupled Higgs boson may have a mass either less than or greater than the lighter of the other two CP-even Higgs bosons and when the would-be decoupled Higgs is close in mass to the lighter physical Higgs, strong mixing can occur, leading to two weakly coupled Higgs bosons. However, given the range of parameters considered so far, we

find that the decoupled CP-even Higgs boson is always substantially heavier than the lighter of the two physical CP-even Higgs bosons. Similarly the CP-odd Higgs bosons are much heavier than the lightest CP-even Higgs boson. The reason for this difference is simply that in ref. [15] the range of parameters considered exceeds the range discussed so far here. In order to bring down the mass of the CP-even singlet sufficiently one requires $\tilde{m}_0 \ll 0.2$, $\lambda_0 < 0.01$ and $k_0 \ll \lambda_0$, corresponding to extremely large values of $r \gg 100$. In this region of parameter space, the singlet CP-even Higgs boson does indeed become much lighter, leading to the strong mixing effect mentioned above. It is ironic that this effect only seems to take place in the deep MSSM limit of the constrained NMSSM parameter space, making the NMSSM more easily resolvable from the MSSM in the region of parameter space where the two models are formally most similar. ⁶

In order to illustrate this effect, in Fig.8 we show the spectrum as a function of $M_{1/2}$, for a point in this region. Note that the lightest CP-even Higgs bosons (dashed lines) interfere for $M_{1/2} \approx 2000$ GeV. In Fig.9 we show the amplitude of singlet N contained in the lightest two CP-even massive states, corresponding to Fig.8 (the heaviest CP-even has singlet component zero throughout). For $M_{1/2} \ll 2000$ GeV, the lightest CP-even Higgs boson is almost pure singlet, whilst for $M_{1/2} \gg 2000$ GeV the second lightest CP-even Higgs boson is almost pure singlet. Thus a simple interpretation of this effect is that as $M_{1/2}$ is steadily increased, the singlet CP-even Higgs mass rapidly rises, “crosses” the physical CP-even Higgs boson line, and continues to rapidly increase with $M_{1/2}$. In the crossing region the two CP-even states will strongly mix leading to two states with diluted couplings. We shall discuss the phenomenological implications of this in some detail in Section 7.

⁶In the unconstrained NMSSM the effect also occurs away from the MSSM limit as discussed in ref.[40].

5.5 Fine-Tuning in the NMSSM

In Table 1, we give the fine-tuning parameter c_{h_t} for a typical point in each of the three most interesting regions of parameter space and a range of values of $M_{1/2}$, together with the corresponding data for the MSSM point already discussed in Section 4.3. These points are defined below. In Tables 2,3 we also show the alternative fine-tuning parameters c_λ , c_k for the NMSSM for each of the three cases.

- NMSSM1: $h_{t0} = 2$, $\lambda_0 = 0.4$, $\tilde{m}_0 = 5$, $A_0 = -3m_0$, a point in the safe range where arbitrarily small $M_{1/2}$ can be achieved, and with the same parameters as Fig.6
- NMSSM2: $h_{t0} = 0.5$, $\lambda_0 = 0.1$, $\tilde{m}_0 = 0.5$, $A_0 = -4m_0$ a point outside the safe range, with the same parameters as Fig.7
- NMSSM3: $h_{t0} = 0.5$, $\lambda_0 = 0.005$, $\tilde{m}_0 = 0.02$, $A_0 = -5m_0$, a point in the deep MSSM limit, with the same parameters as Fig.8
- MSSM : the MSSM with $\mu_0 = -B_0 = m_0 = M_{1/2}$ for comparison, with the same parameters as Fig.3

Table 1. Fine tuning parameter c_{h_t} as a function of $M_{1/2}$ for the MSSM and the three examples of NMSSM parameter space defined in the text.

$M_{1/2}(\text{GeV})$	MSSM	NMSSM1	NMSSM2	NMSSM3
50	2.3	4.2	–	–
100	4.5	13	–	–
300	25	60	18	–
500	49	140	37	–
1000	83	390	75	59
2000	130	1200	130	110

Table 2. Fine tuning parameter c_λ as a function of $M_{1/2}$ for the three examples of the NMSSM defined in the text.

$M_{1/2}(\text{GeV})$	NMSSM1	NMSSM2	NMSSM3
50	9.9	–	–
100	30	–	–
300	160	23	–
500	360	42	–
1000	1000	70	79
2000	3300	160	130

Table 3. Fine tuning parameter c_k as a function of $M_{1/2}$ for the three examples of the NMSSM defined in the text.

$M_{1/2}(\text{GeV})$	NMSSM1	NMSSM2	NMSSM3
50	10	–	–
100	30	–	–
300	160	22	–
500	370	42	–
1000	1100	80	80
2000	3500	130	130

The main points to note from these tables are that, as usual, fine-tuning increases with increasing $M_{1/2}$ and m_0 . Many authors choose to restrict c_{h_t} to be less than a value in the range 10-100, and this would clearly be very restrictive, although would still not eliminate all of any of the different regions, despite the lack of data with small $M_{1/2}$ in some of them.

We also note that the fine-tuning in λ_0 and k_0 are the same. This can be seen to be a result of the fact that the VEVs ν_1, ν_2 depend only on λ and k only through the combination λ/k near the MSSM limit, as discussed below. Increasing \tilde{m}_0 increases c_k more than c_{h_t} , which again can be understood through the analytical discussion in Section 6.

We illustrate this behaviour with graphs of M_Z against k_0 in two of these cases. Fig.10 is for the parameters NMSSM1 above and shows the simplest behaviour. Here M_Z rises very rapidly from zero to of order m_0 and then levels off. It is clearly reasonable to suggest that the natural value of M_Z is the value in this plateau region. Fig.11 is for parameters NMSSM2 above, and shows a richer behaviour. As before,

there is a plateau region. However instead of the value of M_Z simply falling rapidly to 0 as k_0 is decreased, it changes value discontinuously. This discontinuity can occur because a change in k_0 can lead to a change in which of the various minima is deepest. This is simply the behaviour where the data cuts out in Fig.7, where it is not possible to find solutions for smaller values of $M_{1/2}$ consistent with $M_Z = 91.2\text{GeV}$.

5.6 Summary of NMSSM Results

Since this has been a lengthy and important section, we shall briefly summarise the results before continuing. Crudely speaking, the various constraints reduce the parameter space to two allowed regions (i) $k_0 > \lambda_0 > h_{t0}$, and (ii) $h_{t0} > \lambda_0 > k_0$. We found that region (i) generally involves a rather small Yukawa coupling, leading to a top quark mass smaller than about 150 GeV, which may be considered rather too small in the light of current measurements of the top quark mass [32], and so we shall not discuss it further.

Region (ii) involves an arbitrarily large top quark Yukawa coupling, leading to values of m_t up to about 200 GeV. With $h_t \gtrsim 1$, other parameters in this region are constrained to be: $\tilde{m}_0 \gtrsim 1$, $|A_0/m_0| \sim 3$, leading to large values of $r \gg 1$, with r proportional to m_0 for given k_0 . Thus this region is always close to the MSSM limit. Many of its features can be understood analytically as discussed in the next section, and it is noticeable that λ_0 and k_0 , which must always be quite small here have no great impact on the spectrum except to fix $M_{1/2}$.

One restricted subset of region (ii) can be regarded as a “safe” region, characterised by fairly restrictive parameters $h_{t0} \approx 1.5 - 3$, $|A_0/m_0| \approx 3$, $\tilde{m}_0 > 3$, where it is always possible to achieve small $M_{1/2}$. Outside this “safe” region the data suddenly cuts out below a critical $M_{1/2}$ value. The spectrum for light $M_{1/2}$ is thus always quite similar to that shown in Fig.6, and since the fine-tuning parameters for this region (NMSSM1

in Tables 1-3) tend to favour small values of $M_{1/2} < 100$ GeV, this is perhaps the most interesting region of the model/ For example, if we consider $M_{1/2} \simeq 100$ GeV, at LEP II we would expect to see a standard-model like Higgs boson with a mass of about 100 GeV. In addition there may be three SUSY particles accessible to LEP II: a chargino and two neutralinos. The heavier neutralino and the chargino become closely degenerate as $M_{1/2}$ is increased. Since the chargino has a strong $M_{1/2}$ dependence its accessibility to LEP II is not guaranteed, but the more seriously one takes the fine-tuning constraints the more likely its discovery will seem. We have varied all the parameters over the “safe” region, and the characteristic spectrum is never very different from that shown in Fig.6. The most significant differences occurs if we take larger \tilde{m}_0 , which increases all the scalar masses, but has no significant impact on the lightest states except to increase the lightest Higgs mass through radiative corrections.

If we wish to reduce \tilde{m}_0 , we must reduce h_{t0} and hence the top mass; and we must also accept that there is then a minimum value of $M_{1/2}$ below which correct electroweak symmetry breaking does not occur. The corresponding spectrum is thus less interesting phenomenologically, with a typical example shown in Fig. 7.

Another subset of region (ii) was defined as the deep MSSM limit, namely: $h_{t0} > \lambda_0 \gg k_0$. Although simply an extreme limit of region (ii), this region of parameter space involves *huge* values of $|r| \gg 100$, corresponding to quite large values of $M_{1/2}$. This deep MSSM region typically involves $\tilde{m}_0 \ll 1$, $k_0 \ll \lambda_0 < 0.01$, while the associated fine-tuning parameters corresponding to Fig.8 (NMSSM3 in Tables 1-3) all exceed 50 for the minimum $M_{1/2}$ value in this example. The reason why this rather peculiar choice of parameters is nevertheless interesting is that here we may decrease m_0 sufficiently far that the dominantly singlet state CP-even Higgs boson becomes light. Hence we may find the phenomenon of interference between the lightest two CP-even Higgs bosons (one of which is a would-be decoupled state) leading to interesting phenomenological effects which will be discussed more fully in Section 7.

6 The MSSM Limit of the NMSSM

6.1 The Electroweak Potential

Since so much of our most interesting data is in regions which have $\lambda_0, k_0 \ll 1$ and $|x| \gg \nu$, the limit where the NMSSM approaches the MSSM, it is worthwhile to discuss in some detail the potential and spectrum in this limit. We begin by looking at the full tree-level potential

$$\begin{aligned}
 V = & \frac{g_1^2 + g_2^2}{8}(\nu_1^2 - \nu_2^2)^2 + \lambda^2 x^2(\nu_1^2 + \nu_2^2) + \lambda^2 \nu_1^2 \nu_2^2 + k^2 x^4 \\
 & - 2\lambda k \nu_1 \nu_2 x^2 - 2\lambda A_\lambda \nu_1 \nu_2 x - \frac{2}{3} k A_k x^3 \\
 & + m_{H_1}^2 \nu_1^2 + m_{H_2}^2 \nu_2^2 + m_N^2 x^2
 \end{aligned} \tag{6.1}$$

In the limit, the minimisation condition for N takes the form [13]

$$x(2k^2 x^2 - k A_k x + m_N^2) = 0 \tag{6.2}$$

which implies

$$4kx = A_k \pm \sqrt{(A_k^2 - 8m_N^2)} \tag{6.3}$$

where we select the positive sign for the square root if $A_k > 0$ to ensure that we have selected a minimum and not a maximum. For simplicity we shall assume this throughout the following discussion; if $A_k < 0$ nothing is altered except this minus sign throughout. Eq. (6.3) implies that $A_k^2 > 8m_N^2$. (Note that $A_k^2 > 9m_N^2$ ensures that the minimum with non-zero x is deeper than the minimum at the origin.) The constraint of Eq.(2.6) that the sleptons should not acquire VEVs implies $A_0^2 \lesssim 3m_0^2$, with larger values of $|A_0/m_0|$ being permitted for negative A_0 and smaller \tilde{m}_0 as can be seen from the RG equations. Thus using the fact that in this limit $A_0 \sim A_k$ and $m_N \sim m_0$ we find ourselves restricted to a range of values of $|A_0/m_0|$ around 3 or slightly larger [13]. Note that Eq.(6.3) implies that for fixed \tilde{A}_0 and \tilde{m}_0 , $k\tilde{x}$ is also fixed, and so x is proportional to $M_{1/2}$. Furthermore, it is clear that reducing k will lead to an increase in x and so a very close approach to the MSSM limit.

In this region, the model mimics the MSSM, with

$$\begin{aligned}\mu &\equiv \lambda x \\ B &\equiv -A_\lambda - kx\end{aligned}\tag{6.4}$$

as can be simply read off from the lagrangian. Here the value of kx and hence effectively B is set by Eq. (6.3) for given values of the soft parameters; while λx (μ) is set by the Z mass through Eq. (4.2). We note that empirically we find that in general λx is at least a few hundred GeV in the deep MSSM limit, which leaves us close to a simple limit of the MSSM where $\mu \gg \nu$.

An interesting feature of the MSSM limit is that we may neglect all occurrences of λ and k except those of form λx and kx , and kx can be removed by use of Eq. (6.3), leaving the only dependence on λ and k that through λ/k as mentioned in Section 5.5. We may also come to understand the fine-tuning behaviour better by considering equation 4.2. Here we may consider

$$\mu^2 \equiv \lambda^2 x^2 = \left(\frac{\lambda}{k}\right)^2 (kx)^2\tag{6.5}$$

and since kx is fixed by Eq.(6.3), and ignoring the dependence of $\tan \beta$ on λ and k , we find that c_λ and c_k derived by differentiating with respect to the low energy value of λ or k is given by $c_\lambda = c_k = (\lambda x)^2/M_Z^2$. The use of λ_0 rather than λ has the effect of adding a correction factor of $\frac{\delta\lambda/\delta\lambda_0}{\lambda_0/\lambda}$ which is of order 1 (and is in fact equal to 1 if we neglect all the Yukawa terms in the running of λ , which is a reasonable approximation only for very small h_t). At low energy the three fine-tuning scenarios NMSSM1,2,3 discussed above have $\lambda x/M_{1/2}$ of around 4,1,1 respectively, which explains the relative sizes of the different parameters in NMSSM2 and 3 very well. This result is more sensitive to the closeness to the MSSM limit than others presented here, since we are neglecting the effects of changing λ , k on $m_{H_1}^2$, $m_{H_2}^2$ which is only valid for extremely small λ , k , and so we do not expect perfect agreement when we consider points such as NMSSM1 which have relatively large λ and k .

6.2 MSSM Equivalent Parameter Sets

In order to illustrate the close resemblance between the MSSM and the NMSSM near the limit, we show in Fig. 12 a plot of the spectrum versus $M_{1/2}$ in the MSSM, with all parameters the same as that in Fig. 6, and $\tilde{\mu}_0 = -7.5$, a value chosen purely in order to allow us to mimic the spectrum of Fig. 6. It is clear that the spectrum is virtually identical, with the exception that the (decoupled) singlet states are no longer present. Generating such equivalent points in the MSSM is *always* possible near the MSSM limit, since we may simply read off the low energy values of μ and B from Eq. (6.4), run them up to the GUT scale, and thus have a set of parameters which is guaranteed to give a similar spectrum. Of course, this relies on the fact that λ and k are so small that they have no impact on the other terms in the RG equations, which is clearly a good approximation even here, where λ and k are relatively large for this region.

Similarly we present Fig. 13, which is an MSSM version of Fig. 8. Here the data cuts out for some minimum value of $M_{1/2}$ just above 500GeV because $\tan\beta$ blows up, and this behaviour occurs in both the MSSM and NMSSM. Here the spectra are again extremely similar except in the region where the singlet and non-singlet Higgs are virtually degenerate. In this region, the two Higgses would have suppressed couplings to the standard model particles, and so it would be possible in principle to distinguish the two models, despite the fact that we are in a region which is extremely close to the MSSM limit. This behaviour will be discussed in detail in Section 7. Elsewhere, the extra singlet states in the NMSSM would be virtually undetectable.

By contrast, Fig. 14 shows the MSSM equivalent to Fig. 7, in which the data does not stop at $M_{1/2} < 300\text{GeV}$. This is because the data in the NMSSM version stops because of an alternate minimum which does not exist for the MSSM. This is an example of the fact that, although the MSSM can always closely mimic the NMSSM

(except where singlet and non-singlet states are nearly degenerate), the converse is not true; there are regions where the deepest minimum in the NMSSM is one of the non-physical minima which does not exist in the MSSM.

We thus conclude that ultimately the most interesting region of the NMSSM is that where there is a corresponding point in MSSM parameter space with very similar spectrum and electroweak potential. The exception is of course the spectrum of singlet states, which can sometimes mix with physical states to a detectable degree. However, because of the extremely restrictive nature of the NMSSM electroweak potential, there are some sets of MSSM which cannot be imitated in the NMSSM.

6.3 Singlet Mass Spectrum

Now we shall very briefly discuss the mass spectrum in this limit. Since this consists essentially of the usual MSSM spectrum supplemented by some almost completely decoupled singlet states we shall just present some simple results for the singlet states.

The mass of the singlet CP-even Higgs scalar is simply given by the 33 component of the Higgs mass matrix in appendix B as

$$m_{h_N}^2 = \frac{1}{4}(A_k \sqrt{(A_k^2 - 8m_N^2)} - A_k^2 + 8m_N^2) + \mathcal{O}\left(\frac{\nu^2}{x^2}\right) \quad (6.6)$$

where we have substituted for x using Eq.(6.3). Given that A_k is a few times larger than m_0 , we can immediately see that the mass of the CP-even singlet Higgs will be proportional to m_0 . Thus to get the singlet mass down to around the mass of the lighter physical CP-even Higgs or below, which is necessary if we wish to have any chance of detecting it, we must have small m_0 . Since $M_{1/2} \gtrsim 70\text{GeV}$ (to keep the chargino clear of the LEP limit), the “safe” region with $m_0 \gtrsim 3M_{1/2}$ is uninteresting, and we must consider a region with smaller \tilde{m}_0 and hence relatively large $M_{1/2}$. This is why we shall find detectable singlet states (of course, the “singlet” state has some mixing with physical states, which make it couple to the Z) only for regions with

$m_0 < 1$. We note that empirically we find that we are fairly close to the limit in which the MSSM CP-even Higgs boson approaches its mass bound, with fairly large $\tan\beta$ and μ .

Similarly, the CP-odd singlet has mass

$$m_{A_N}^2 = \frac{3}{4}A_k(A_k - \sqrt{(A_k^2 - 8m_N^2)}) + \mathcal{O}\left(\frac{\nu^2}{x^2}\right) \quad (6.7)$$

which implies that

$$\frac{m_{h_N}^2}{m_{A_N}^2} = \frac{1}{3}\sqrt{1 - 8\frac{m_N^2}{A_k^2}} \quad (6.8)$$

From this expression we see that m_{h_N}/m_{A_N} lies in the range 0.4-0.55 for $|A_0/m_0|$ between 3.5 and 6, although it can fall off to smaller values as $|A_0/m_0|$ approaches its minimum value consistent with electroweak symmetry breaking. This explains the relation between the lightest CP-even and lightest CP-odd states shown in reference [15]. The fact that the lightest CP-odd which is not primarily singlet is always heavier than around 150GeV is explained by the relatively large value of λx , since the mass of the MSSM CP-odd Higgs is given by $\mu B(\tan\beta + \cot\beta)$ at tree level.

The relationship between CP-odd and CP-even Higgs masses is clearly seen in Fig.15, where we show a simple scatter plot of the mass of the lighter CP-odd Higgs boson against the lightest and second lightest CP-even Higgses. As we would expect, there is always a physical CP-even Higgs scalar in the region of the NMSSM Higgs bound together with another CP-even which is primarily singlet. The CP-odd scalar, which is predominantly singlet everywhere in this figure, has a mass of around twice that of the singlet CP-even, leading to the diagonal line of data running through the figure, while the physical Higgs scalar has a mass in the range $\sim 110 - 140\text{GeV}$ regardless of the singlet masses, giving the vertical band of data on the figure.

Finally, we mention the singlet neutralino. This has a mass of $2kx$, which is around $2-5m_0$; given that the bino has a mass of typically around $0.5M_{1/2}$, we expect

to find that the singlet is the lightest neutralino when $\tilde{m}_0 \lesssim 0.15$, which is consistent with our numerical results.

7 Resolving the Constrained MSSM and NMSSM

Having discussed the results for both the MSSM and the NMSSM in general terms, in this section we focus on specific phenomenological aspects of the constrained NMSSM which may enable it to be distinguished from the (constrained) MSSM at future colliders. This question is far from trivial, since, as we have discovered, the constrained NMSSM is always close to the MSSM limit, and so it will present a considerable experimental challenge to resolve the two models. In particular, as we have shown above, when we are reasonably close to the MSSM limit (as we always are, except in the low top mass $k_0 > \lambda_0 > h_{t0}$ region) it is always possible to construct a set of MSSM parameters which will mimic *any* NMSSM spectrum except for the singlet states. Note that Higgs bosons do not decay into singlet Higgs bosons in regions of parameter space close to the MSSM limit.

We shall thus discuss the two possible ways in which it may be possible to resolve the constrained NMSSM from the MSSM once SUSY or Higgs bosons have been discovered. The first and most obvious of these is singlet dilution. The extra singlet degrees of freedom may mix with the physical degrees of freedom, leading to extra states with diluted production and decay couplings. This will always happen for regions of parameter space of the NMSSM away from the MSSM limit, but the effect is usually smaller and smaller as this limit is approached. An important exception is when there are degeneracies of the singlet states with physical states, leading to strong mixing effects which persist even in the deep MSSM limit. In general this effect relies on the accidental degeneracy of two states, where away from the degeneracy one of the states is essentially singlet, and the other state is physical and has the

same spin and CP quantum numbers as the singlet. This effect may be observed when the CP-even singlet becomes degenerate with a physical CP-even Higgs boson, when the CP-odd Higgs singlet becomes degenerate with the physical CP-odd Higgs bosons, or when the singlet Higgsino becomes degenerate with the physical Higgsinos (or physical neutralino states which contain a significant Higgsino component).

The second method for distinguishing the two models is by finding regions of parameter space in the MSSM where the spectrum cannot be mimicked in the NMSSM, and we shall also discuss this possibility below.

7.1 CP-even Higgs Bosons at LEP

We have already seen that the successful regions of parameter space of the constrained NMSSM mean that the model is always close to the formal MSSM limit in which the singlet components decouple. Furthermore, over much of the parameter space [15, 16] this leads to the lightest CP-even Higgs boson being in the range 70-140 GeV and having couplings which are so close to those of the standard model Higgs boson as to make it practically indistinguishable. A similar expectation arises from the MSSM in the large CP-odd mass limit where all the Higgs boson states become heavy and decoupled, apart from the lightest CP-even Higgs boson which mimics the standard model Higgs boson [41]. Thus the discovery of a standard model-like Higgs boson at LEP II is consistent with both the MSSM and the NMSSM, and would not tell us very much about supersymmetry.

However there exist regions of parameter space of the constrained NMSSM in which it may be possible to experimentally distinguish the lightest CP-even Higgs boson in the NMSSM from that of the MSSM or the standard model. For example, in the constrained NMSSM, a (would-be) decoupled singlet CP-even Higgs boson may become degenerate with a physical CP-even Higgs boson, leading to strong mixing

and hence two weakly coupled states. The purpose of this sub-section is to discuss the properties and prospects of discovery of such mixed states at LEP. Some work along these lines has already been done [15]. Specifically scatter plots of the Higgs masses against the Z couplings for the lightest CP-even Higgs boson have been made for a representative data sample. Most of the data sample was seen to lie outside of the discovery range of LEPI or LEPII. Other scatter plots were also considered including one for the second lightest CP-even Higgs [15], but not including a discussion of its Z couplings. The decay couplings of the two Higgs bosons were also not considered in ref.[15].

The CP-odd Higgs bosons play no role at LEPII since for masses less than around 150GeV the lighter one has a mass roughly equal to twice that of the lightest CP-even Higgs boson, as discussed earlier, and is in any case dominantly gauge singlet. The heavier (physical) CP-odd Higgs boson turns out to be heavier than 150 GeV [15].

The purpose of this section is try to build up a better picture of the implications which might be drawn from the discovery of non-standard Higgs bosons at LEP. After discussing the production and decay couplings of the two lightest CP-even Higgs bosons relevant for LEP, we shall discuss the effect of Higgs crossing seen in Figs.8,9 in a little more detail by plotting both Higgs masses against their respective physical couplings. We shall then discuss three different non-standard model Higgs scenarios at LEPI and LEPII, and show examples of constrained NMSSM parameter space which can yield Higgs events within experimental reach for each scenario.

We begin the discussion by summarising the production and decay couplings relevant for LEP of the two lightest CP-even Higgs bosons in the NMSSM, following closely the notation of ref.[9]. We first write down the real orthogonal matrix U_{ij} which relates the CP-even mass eigenstates (h_1, h_2, h_3) (where by definition the masses are

ordered as $m_{h_1} < m_{h_2} < m_{h_3}$) to the original CP-even states

$$(H_1, H_2, N) \equiv \sqrt{2}(\Re(H_1^0) - \nu_1, \Re(H_2^0) - \nu_2, \Re(N) - x) \quad (7.1)$$

$$\begin{pmatrix} h_1 \\ h_2 \\ h_3 \end{pmatrix} = \begin{pmatrix} U_{11} & U_{12} & U_{13} \\ U_{21} & U_{22} & U_{23} \\ U_{31} & U_{32} & U_{33} \end{pmatrix} \begin{pmatrix} H_1 \\ H_2 \\ N \end{pmatrix} \quad (7.2)$$

Following ref.[9], we now define the relative couplings R compared to the standard model couplings as: coupling = $R \times$ standard model coupling, where the relative ZZ production couplings of the lightest and second lightest CP-even Higgs bosons, and the $\bar{u}u$ and $\bar{d}d$ decay couplings of these bosons (all three generations will have their couplings suppressed by the same amount), are given below.

$$\begin{aligned} R_{ZZh_1} &= \cos \beta U_{11} + \sin \beta U_{12} \\ R_{ZZh_2} &= \cos \beta U_{21} + \sin \beta U_{22} \\ R_{\bar{u}uh_1} &= \frac{U_{12}}{\sin \beta} \\ R_{\bar{d}dh_1} &= \frac{U_{11}}{\cos \beta} \\ R_{\bar{u}uh_2} &= \frac{U_{22}}{\sin \beta} \\ R_{\bar{d}dh_2} &= \frac{U_{21}}{\cos \beta} \end{aligned} \quad (7.3)$$

These couplings should be compared to those in the MSSM:

$$\begin{pmatrix} h_1 \\ h_2 \end{pmatrix} = \begin{pmatrix} \cos \alpha & -\sin \alpha \\ \sin \alpha & \cos \alpha \end{pmatrix} \begin{pmatrix} H_1 \\ H_2 \end{pmatrix} \quad (7.4)$$

$$R_{ZZh_1} = \cos(\beta + \alpha)$$

$$R_{ZZh_2} = \sin(\beta + \alpha)$$

$$\begin{aligned}
R_{\bar{u}uh_1} &= \frac{-\sin\alpha}{\sin\beta} \\
R_{\bar{d}dh_1} &= \frac{\cos\alpha}{\cos\beta} \\
R_{\bar{u}uh_2} &= \frac{\cos\alpha}{\sin\beta} \\
R_{\bar{d}dh_2} &= \frac{\sin\alpha}{\cos\beta}
\end{aligned} \tag{7.5}$$

We have chosen to focus on the production and decay couplings of the lightest and second lightest CP-even Higgs bosons only, since the third CP-even Higgs boson expected in the NMSSM will be out of range of LEP II. We have already remarked that a likely scenario of the MSSM and NMSSM is of a single standard model-like Higgs boson in the LEP II range. Now we turn our attention to the more optimistic possibility that the lightest two CP-even Higgs have non-standard couplings. In practice this means weaker couplings than in the standard model. As seen earlier, this effect only seems to occur in the deep MSSM limit of the model, corresponding to a limited volume of parameter space of the full NMSSM, as discussed earlier.

In order to illustrate the effect, in Fig.16a we plot the lightest and second lightest CP-even Higgs boson masses m_{h_1} and m_{h_2} , against their respective R_{ZZh_1} (small crosses) and R_{ZZh_2} (large crosses). Fig.16a uses a range of parameters corresponding to those used in Figs.8,9 (*i.e.* in the deep MSSM limit of the model where the Higgs singlet may become light and mix). The correlation between the two Higgs boson masses is the obvious one: namely the lightest small crosses are associated with the lightest large crosses. The values of k_0 and $M_{1/2}$ increase from left to right, while m_t and $\tan\beta$ decrease in this direction. From left to right the data thus corresponds to the effect observed in Figs.8,9 of the singlet approaching the physical Higgs boson, mixing with it, then crossing it – although the behaviour is better described as a displacement rather than a crossing since the two states are never exactly degenerate. Also shown in Fig.16a is the region excluded by LEPI (short dashed line) [29], the discovery reach of LEP II at an energy of 175 GeV and an integrated luminosity of 500

pb⁻¹ (dashed line) and the discovery reach of LEP II at an energy of 205 GeV and an integrated luminosity of 300 pb⁻¹ (full line). The latter two lines are simply calculated from the cross-section [42] so as to give 50 events, without imposing experimental cuts. Clearly LEP II cannot reach any of these particular data points. However there do exist regions of parameter space in the singlet mixing region which are accessible to LEP, as we shall discuss.

In Fig.16b we plot the couplings $R_{\bar{d}dh_1}$ (small crosses), $R_{\bar{u}uh_1}$ (circles), $R_{\bar{d}dh_2}$ (large crosses), $R_{\bar{u}uh_2}$ (squares), against the corresponding Higgs boson mass. Note that, for a given Higgs boson mass, the relative u and d couplings are approximately equal, although often with substantially reduced couplings relative to the standard model. This effect is due to the fact that in this case the Higgs mixing effect can be regarded as taking place between a standard-model-like Higgs boson (with relative R couplings close to unity) and a singlet. The effect of mixing with the singlet is simply to dilute all the couplings equally, both here and for other parameters where we do not show the quark couplings explicitly.

We distinguish three representative scenarios for LEP:

- (i) A light very weakly coupled CP-even boson with $0 < m_{h_1} < 60$ GeV

Such a boson may be hiding in high statistics data from LEPI. If only one Higgs boson is discovered then it may be possible to exclude either the minimal standard model, or the MSSM, if the production and decay couplings of the Higgs boson are seen to be sufficiently non-standard. For example, a light very weakly coupled CP-even Higgs boson in the MSSM would correspond to $R_{ZZh_1} = \cos(\beta + \alpha) \ll 1$, but if its mass were less than about 40 GeV such a boson would necessarily be accompanied by a light CP-odd Higgs boson with $R_{ZA h} = \sin(\beta + \alpha) \approx 1$, and such a scenario is already excluded in the MSSM. Thus the discovery of such a boson at LEPI or LEP II would rule out the MSSM, and suggest the NMSSM.

An example of a light very weakly coupled Higgs boson accessible to LEPI (rather than LEP II) is shown in Fig.17. In this case the light weakly coupled Higgs boson has a mass 34-60 GeV, and is just outside the existing LEPI excluded region. Such a Higgs boson with mass around 40 GeV or less would therefore most likely be found when more Z pole data is analysed, and would be a clear signal of the NMSSM. The second lightest Higgs boson has standard model-like couplings to the Z, but has a mass of 127-130 GeV, outside the LEP II range in this example. The corresponding $R_{\bar{u}uh_1}$, $R_{\bar{d}dh_1}$, $R_{\bar{u}uh_2}$, $R_{\bar{d}dh_2}$ factors are not shown, since they are virtually identical to the R_{ZZh} , R_{ZZH} couplings in Fig.17

The remainder of the spectrum is unaccessible to any likely collider in the near future, with a singlet CP-odd Higgs in the range 70-120GeV, a singlet neutralino of 60-100GeV, and the remainder of the spectrum very heavy because of the typically large values of $M_{1/2}$ of around 1TeV. Such general comments generally apply whenever the lightest CP-even Higgs is light enough to be detectable at LEP.

(ii) A weakly coupled CP-even boson with $60 < m_{h_1} < 110$ GeV and $R_{ZZh} < 0.95$.

Such a boson may be discovered at LEP II, but since the statistics will be lower, the couplings probed must not be so weak as in the previous case. A heavier weakly coupled CP-even Higgs boson with mass $m_{h_1} > 60$ GeV is now allowed in the MSSM since for small $\tan\beta$ the CP-odd boson may be heavier than 100 GeV. In this case in order to exclude the MSSM it would be necessary to study the decay couplings $\bar{c}ch_1$, $\bar{b}bh_1$, for example. It may be difficult at LEP II to study these decays of the Higgs boson to sufficient accuracy to enable the MSSM to be excluded. Thus the discovery of such a boson at LEP II may exclude the standard model, and suggest supersymmetry, but it will be more difficult to distinguish between the MSSM and the NMSSM.

Fig.18a shows some examples of heavier weakly coupled Higgs bosons which would

be visible at LEP II. The input parameters, which are selected so that such a Higgs boson emerges in the mass range 60-110 GeV, are over quite a broad range. The corresponding $R_{\bar{u}uh_1}$, $R_{\bar{d}dh_1}$, $R_{\bar{u}uh_2}$, $R_{\bar{d}dh_2}$ factors are shown in Fig.18(b). Some of this data (for $m_{h_1} > 100$ GeV) shows relative differences between d and u type decays. The second lightest Higgs bosons are outside the range of LEP II.

(iii) Two CP-even bosons with $m_{h_{1,2}} < 110$ GeV

The situation improves dramatically if two CP-even Higgs bosons are discovered at LEP. For example, the lighter one could be discovered in high statistics data at LEPI or in the first phase of LEP II, and the heavier one could be found in the final phase of LEP II. Such twin discoveries would immediately rule out the standard model, and also the MSSM since in this model the second CP-even Higgs boson cannot be so light. In the unconstrained NMSSM this scenario is perfectly possible but this has already been discussed elsewhere[16]. In the constrained NMSSM, this possibility appears to be more unlikely than either (i) or (ii) above. The reason is clear from Figs.17, 18, where it is seen that the second lightest Higgs boson is usually outside the mass reach of LEP II.

Fig. 19 shows an example of how tantalisingly close a twin Higgs discovery might be at LEP II. The lightest Higgs bosons within the LEP II reach are associated with heavier Higgs bosons just outside the reach of the final phase of LEP II. Note that the top quark mass is below 150 GeV in this case. One reason for this is that the second Higgs boson (predominantly physical) has a mass which increases with increasing top mass due to radiative corrections, and we have required its mass to be as small as possible. We can arrange the parameters to reduce the mass of the second lightest Higgs boson to the LEP II range, and increase the top quark mass, but then we find that the lightest Higgs boson's couplings become too weak to allow it to be produced at LEP II. Thus we infer that this particular scenario, although spectacular, is very

unlikely in the constrained NMSSM. We do not show quark couplings because they are nearly equal to the Higgs couplings. Note that the lighter (heavier) values of the lightest CP-even state are correlated with the lighter (heavier) values of the second lightest CP-even state.

7.2 Neutralinos

The neutralino structure is essentially that of the MSSM supplemented by singlet, with a mass in the range around 2-5 m_0 as noted above. While it is possible for the two lightest neutralinos to be degenerate, which we find to occur for $\tilde{m}_0 \sim 0.1$, we find negligible neutralino mixing even in this region. The reason for this is that, as a look at the mass matrix (see Appendix B3) will show, there is negligible mixing between the singlet and the bino, and we always find that the lightest MSSM-like neutralino is pure gaugino (photino for small $M_{1/2}$, or Bino for large $M_{1/2}$) because we never find very small μ . Hence it is unlikely that the singlet neutralinos could ever be detected except in the case where there is mixing with a heavier higgsino-like neutralino, which would only become of phenomenological interest after the lighter states of the neutralino spectrum has been discovered.

Although over some regions of parameter space, it is kinematically possible for the lightest CP-even Higgs boson to decay to two lightest neutralinos, in fact this will not happen because the lightest neutralino is always pure gaugino except in regions where it is pure singlet and the couplings are very small. Thus invisible Higgs decays do not occur in this model.

7.3 Regions Where the NMSSM Cannot Exist

In principle, once supersymmetric particles have been discovered it would be possible to derive the values of the supersymmetric parameters $M_{1/2}$, A_0 , B_0 , m_0 , and $\tan\beta$,

although to do so would require the discovery and study of several of the supersymmetric states. The question would then arise as to whether the spectrum was the result of the MSSM, or of the NMSSM in a region where the two are indistinguishable. Here we shall review a few of the features of the constrained NMSSM which would allow it to be ruled out if the supersymmetric spectrum did not display them.

The first, and most obvious, of these features is that of large $|A_0/m_0|$. Unlike the case in the NMSSM, in the MSSM this can take any value from zero up to a maximum of around 3-5 caused by the constraint of avoiding slepton VEVs, and so if $|A_0/m_0|$ were found to take a smaller value than around 3 we could immediately rule out the constrained NMSSM. Of course, this would require a detailed enough study of the spectrum to calculate all the SUSY parameters.

The second question is that of the relation between B and A_0 given by

$$B \equiv -A_\lambda - kx = -A_\lambda - \frac{1}{4} \left(A_k - \sqrt{(A_k^2 - 8m_N^2)} \right) \quad (7.6)$$

Given that it is trivial to relate A_λ , A_k , and m_N^2 to A_0 and m_0 in the small λ_0 , k_0 limit, the MSSM limit of the NMSSM implies a relation between the effective MSSM parameters which, if violated, would allow us to rule out the constrained NMSSM.

Finally, even if the MSSM were in some region where it obeys the above relations, it would be possible to use our knowledge of μ_0 , B_0 , and A_0 together with the relation $\mu \equiv \lambda x$ and Eqs.(7.6),(6.3) to derive λ , k , x . One would then have full knowledge of all the parameters in the effective potential, and could simply test it to ensure that the minimum mimicking the MSSM were indeed the deepest. An example of such a case is that shown in Figs.7,14, where for small $M_{1/2}$ the NMSSM minimum with the correct Z mass is not the deepest, unlike the case for the MSSM.

If the MSSM were to pass all of these various tests, then we would perhaps begin to suspect that it were really the NMSSM in a limit which would be very difficult to test. However, if the NMSSM were to fail these tests, then we would either have

to rule it out altogether or consider such possibilities as non-universal soft masses to avoid these constraints, which would reduce the aesthetic appeal of the model.

8 Conclusions

In this paper we have given a comprehensive discussion of the NMSSM constrained by unification, correct electroweak symmetry breaking, and universal soft parameters, and compared the results in this model to those of the similarly constrained MSSM, where we have chosen a set of input variables most appropriate for this comparison. In particular the input parameters h_{t0} , \tilde{A}_0 and \tilde{m}_0 are common to both models, where the tilde denotes scaling by $M_{1/2}$ which is determined as an output parameter by the requirement of obtaining the correct Z mass. We have also given a short discussion of how the constraint of fine-tuning affects the model.

After briefly discussing the MSSM, which serves as a check of our methods, we have explored the parameter space of the NMSSM consistent with the above constraints. The constraint of correct electroweak symmetry breaking is much more severe in the NMSSM than the MSSM. The reason is simply that in the NMSSM there are three VEVs ν_1 , ν_2 , x to consider, and it is non-trivial to arrange for them all to be consistently non-zero. Non-physical vacua with one or more of these VEVs equal to zero litter the parameter space of the NMSSM, and often the physical vacuum is competing with several non-physical vacua. Having found a consistent physical vacuum for one choice of parameters, moving around parameter space is rather like walking through a minefield since suddenly one of the non-physical vacua can become the global minimum of the effective potential. We have mapped out the successful regions of parameter space in Section 5, and summarised the results of our survey in 5.6. Some of these results can be understood analytically as discussed in Section 6.

One important question is whether and how the constrained MSSM and NMSSM

may be resolved experimentally, and we studied this in Section 7. The main difficulty is that the allowed region of parameter space of the NMSSM which allows a large top quark mass (referred to as region (ii), which has $h_{t0} > \lambda_0 > k_0$) is always quite close to the MSSM limit of the model, while another region with $k_0 > \lambda_0 > h_{t0}$ is less interesting because it gives very small top masses. The problem was illustrated in Section 6.2 where Figs.12-14 show how the constrained MSSM can mimic the constrained NMSSM spectrum of Figs.6-8 less the (in practice almost undetectable) singlet states. The most marked difference is that between Fig.8 and Fig.13, due to the approximate degeneracy and subsequent mixing of the lightest and second lightest CP-even Higgs bosons in the constrained NMSSM. Away from the region of approximate degeneracy, one of the states is physical and one of the states corresponds to the decoupled singlet. The effect of their mixing is thus to increase the number of physical states by one, but to dilute the physical couplings of each of the two states. We refer to this phenomenon as “singlet dilution”. Paradoxically singlet dilution only appears to occur in the deep MSSM limit of the constrained NMSSM (although this is not true of the unconstrained NMSSM).

Despite the fact that the deep MSSM limit involves rather odd choices of parameters with a preference for smaller top mass, very large singlet VEV, very small $m_0/M_{1/2}$ and k_0 , and relatively large $M_{1/2}$, and also involves quite severe fine-tuning, the phenomenological consequences of singlet dilution are so important that we discussed its implications for LEP in detail in section 7. It is possible that there is a very light very weakly coupled Higgs boson which LEPI, with increased statistics could discover but which LEPII would fail to find (Fig.17). Such a discovery would be an unmistakable signal of the NMSSM, since the MSSM can never emulate this. Another possibility is that of a weakly coupled CP-even Higgs boson outside the range of LEPI but visible to LEPII (Fig.18a). Such a Higgs boson cannot exist in the standard model, but can in the MSSM. In order to differentiate between the NMSSM

and MSSM, one must study the decay couplings of the Higgs boson. As shown in Fig.18b the decay couplings in the NMSSM are diluted by a similar amount to the production couplings, which is a simple consequence of singlet dilution, and provides a clear signature of the NMSSM. The simplest and cleanest test of singlet dilution, however, would be to discover *both* the lightest two CP-even Higgs bosons at LEP, although as illustrated in Fig.19, this possibility is outside the regions of parameter space which we have explored.

We have seen that the allowed regions of parameter space of the constrained NMSSM is quite restricted. A large top mass restricts us to region (ii) (summarised in section 5.6) where $|A_0/m_0| \gtrsim 3$ is necessary. The further requirement of small $M_{1/2}$ further restricts region (ii) to a very small “safe” region of parameter space, leading to the prediction of the almost unique Higgs and SUSY spectrum, illustrated in Fig.6. However, as remarked, such a spectrum can be accurately mimicked by the MSSM, as shown in Fig.12. It would therefore not be possible to prove the existence of the NMSSM from a spectrum such as this, but it would provide circumstantial evidence for the model.

Finally it is worth emphasising that the constrained NMSSM is relatively easy to exclude. For example, once the SUSY spectrum has been studied, one may infer the value of the ratio $|A_0/m_0|$ and if it is not sufficiently large then the constrained NMSSM would be excluded. Other similar consistency checks may also be applied on the constrained NMSSM as discussed in Section 7.3, and these could also serve to rule out the model. Of course if some of the constraints are removed (for example those concerning universal soft parameters) then the NMSSM might not be excluded. Removing the constraints of unification and universal soft parameters returns us to the unconstrained NMSSM, which was recently studied in ref.[40].

Acknowledgements

We would like to thank Ulrich Ellwanger for a number of helpful discussions, and Terry Elliott for his collaboration at an early stage of this project.

Appendices

A Renormalisation Group Equations

Here we reproduce the set of one-loop Renormalisation Group Equations in the Next-to-Minimal Supersymmetric Standard Model, and in the Minimal Supersymmetric Standard Model. These may be found in Derendinger and Savoy [8] to one loop, and the derivation of the two loop extension is straightforward [43]

Retaining only h_t , h_b and h_τ (the top quark, bottom quark and tau lepton Yukawa couplings, respectively), we have the RG equations (where $t = \log \mu$, and μ is the \overline{DR} renormalisation scale) for the NMSSM are given below. The RGEs for the dimensionless couplings are given to two loops, those for the soft masses to one.

$$\begin{aligned}
16\pi^2 \frac{d}{dt} g_1 &= 11g_1^3 + \frac{g_1^3}{16\pi^2} \left(\frac{199}{9}g_1^2 + 9g_2^2 + \frac{88}{3}g_3^2 \right. \\
&\quad \left. - \frac{26}{3}h_t^2 - \frac{14}{3}h_b^2 - 6h_\tau^2 - 2\lambda^2 \right) \\
16\pi^2 \frac{d}{dt} g_2 &= g_2^3 + \frac{g_2^3}{16\pi^2} \left(3g_1^2 + 25g_2^2 + 24g_3^2 \right. \\
&\quad \left. - 6h_t^2 - 6h_b^2 - 2h_\tau^2 - 2\lambda^2 \right) \\
16\pi^2 \frac{d}{dt} g_3 &= (-3)g_3^3 + \frac{g_3^3}{16\pi^2} \left(\frac{11}{3}g_1^2 + 9g_2^2 + 14g_3^2 - 4h_t^2 - 4h_b^2 \right) \\
16\pi^2 \frac{d}{dt} h_t &= (6h_t^2 + h_b^2 + \lambda^2 - \frac{13}{9}g_1^2 - 3g_2^2 - \frac{16}{3}g_3^2)h_t \\
&\quad + \frac{h_t}{16\pi^2} \left(\frac{2743}{162}g_1^4 + \frac{15}{2}g_2^4 - \frac{16}{9}g_3^4 + \frac{5}{3}g_1^2g_2^2 + \frac{136}{27}g_1^2g_3^2 + 8g_2^2g_3^2 \right. \\
&\quad \left. + (2g_1^2 + 6g_2^2 + 16g_3^2)h_t^2 + \frac{2}{3}g_1^2h_b^2 \right. \\
&\quad \left. - 22h_t^4 - 5h_t^2h_b^2 - 5h_b^4 - h_b^2h_\tau^2 \right. \\
&\quad \left. - \lambda^2(3h_t^2 + 4h_b^2 + h_\tau^2 + 2k^2 + 3\lambda^2) \right) \\
16\pi^2 \frac{d}{dt} h_b &= (6h_b^2 + h_t^2 + h_\tau^2 + \lambda^2 - \frac{7}{9}g_1^2 - 3g_2^2 - \frac{16}{3}g_3^2)h_b \\
&\quad + \frac{h_b}{16\pi^2} \left(\frac{287}{90}g_1^4 + \frac{15}{2}g_2^4 - \frac{16}{9}g_3^4 + \frac{5}{3}g_1^2g_2^2 + \frac{40}{27}g_1^2g_3^2 + 8g_2^2g_3^2 \right. \\
&\quad \left. + (\frac{2}{3}g_1^2 + 6g_2^2 + 16g_3^2)h_b^2 + \frac{4}{3}g_1^2h_t^2 + 2g_1^2h_\tau^2 \right)
\end{aligned}$$

$$\begin{aligned}
& -22h_b^4 - 5h_t^2h_b^2 - 5h_t^4 - 3h_b^2h_\tau^2 - 3h_t^4 \\
& -\lambda^2(3h_b^2 + 4h_t^2 + 2k^2 + 3\lambda^2)) \\
16\pi^2 \frac{d}{dt} h_\tau &= (4h_\tau^2 + 3h_b^2 + \lambda^2 - 3g_1^2 - 3g_2^2)h_\tau \\
& + \frac{h_\tau}{16\pi^2} \left(\frac{27}{2}g_1^4 + \frac{15}{2}g_2^4 + 3g_1^2g_2^2 \right. \\
& \quad \left. + (2g_1^2 + 6g_2^2)h_\tau^2 + (-\frac{2}{3}g_1^2 + 16g_3^2)h_b^2 \right. \\
& \quad \left. - 10h_\tau^4 - 9h_\tau^2h_b^2 - 9h_b^4 - 3h_b^2h_t^2 \right. \\
& \quad \left. - \lambda^2(3h_\tau^2 + 3h_t^2 + 2k^2 + 3\lambda^2) \right) \\
16\pi^2 \frac{d}{dt} \lambda &= (4\lambda^2 + 2k^2 + 3h_t^2 + 3h_b^2 + h_\tau^2 - g_1^2 - 3g_2^2)\lambda \\
& + \frac{\lambda}{16\pi^2} \left(\frac{23}{2}g_1^4 + \frac{15}{2}g_2^4 + 3g_1^2g_2^2 \right. \\
& \quad \left. + 2g_1^2\lambda^2 + 2g_1^2h_\tau^2 + \frac{4}{3}g_1^2h_t^2 - \frac{2}{3}g_1h_b^2 + 6g_2^2\lambda^2 \right. \\
& \quad \left. + 16g_3^2h_t^2 + 16g_3^2h_b^2 \right. \\
& \quad \left. - 9h_t^4 - 6h_t^2h_b^2 - 9h_b^4 - 3h_\tau^4 - 10\lambda^4 - 8k^4 \right. \\
& \quad \left. - \lambda^2(9h_t^2 + 9h_b^2 + 3h_\tau^2 + 12k^2) \right) \\
16\pi^2 \frac{d}{dt} k &= 6(\lambda^2 + k^2)k + \frac{k}{16\pi^2} (6g_1^2\lambda^2 + 18g_2^2\lambda^2 \\
& - \lambda^2(12\lambda^2 - 24k^2 - 18h_t^2 - 18h_b^2 - 6h_\tau^2) - 24k^4) \\
16\pi^2 \frac{d}{dt} A_{u_a} &= 6h_t^2(1 + \delta_{a3})A_t + 2h_b^2\delta_{a3}A_b + 2\lambda^2A_\lambda \\
& - 4\left(\frac{13}{18}g_1^2M_1 + \frac{3}{2}g_2^2M_2 + \frac{8}{3}g_3^2M_3\right) \\
16\pi^2 \frac{d}{dt} A_{d_a} &= 6h_b^2(1 + \delta_{a3})A_b + 2h_t^2\delta_{a3}A_t + 2h_\tau^2\delta_{a3}A_\tau + 2\lambda^2A_\lambda \\
& - 4\left(\frac{7}{18}g_1^2M_1 + \frac{3}{2}g_2^2M_2 + \frac{8}{3}g_3^2M_3\right) \\
16\pi^2 \frac{d}{dt} A_{e_a} &= 2h_\tau^2(1 + 3\delta_{a3})A_\tau + 6h_b^2A_b + 2\lambda^2A_\lambda \\
& - 6(g_1^2M_1 + g_2^2M_2) \\
16\pi^2 \frac{d}{dt} A_\lambda &= 8\lambda^2A_\lambda - 4k^2A_k + 6h_t^2A_t + 6h_b^2A_b + 2h_\tau^2A_\tau \\
& - 2(g_1^2M_1 + 3g_2^2M_2) \\
16\pi^2 \frac{d}{dt} A_k &= 12(k^2A_k - \lambda^2A_\lambda)
\end{aligned}$$

$$\begin{aligned}
16\pi^2 \frac{d}{dt} m_{Q_a}^2 &= 2\delta_{a3} h_t^2 (m_{Q_3}^2 + m_{H_2}^2 + m_T^2 + A_t^2) + 2\delta_{a3} h_b^2 (m_{Q_3}^2 + m_{H_1}^2 + m_B^2 + A_b^2) \\
&\quad - 8\left(\frac{1}{36} g_1^2 M_1^2 + \frac{3}{4} g_2^2 M_2^2 + \frac{4}{3} g_3^2 M_3^2\right) + \frac{1}{3} g_1^2 \xi
\end{aligned} \tag{A.1}$$

$$\begin{aligned}
16\pi^2 \frac{d}{dt} m_{u_a}^2 &= 4\delta_{a3} h_t^2 (m_{Q_3}^2 + m_{H_2}^2 + m_T^2 + A_t^2) \\
&\quad - 8\left(\frac{4}{9} g_1^2 M_1^2 + \frac{4}{3} g_3^2 M_3^2\right) - \frac{4}{3} g_1^2 \xi
\end{aligned} \tag{A.2}$$

$$\begin{aligned}
16\pi^2 \frac{d}{dt} m_{d_a}^2 &= 4\delta_{a3} h_b^2 (m_{Q_3}^2 + m_{H_1}^2 + m_B^2 + A_b^2) \\
&\quad - 8\left(\frac{1}{9} g_1^2 M_1^2 + \frac{4}{3} g_3^2 M_3^2\right) + \frac{2}{3} g_1^2 \xi
\end{aligned} \tag{A.3}$$

$$\begin{aligned}
16\pi^2 \frac{d}{dt} m_{L_a}^2 &= 2\delta_{a3} h_\tau^2 (m_{L_3}^2 + m_{H_1}^2 + m_\tau^2 + A_\tau^2) \\
&\quad - 8\left(\frac{1}{4} g_1^2 M_1^2 + \frac{3}{4} g_2^2 M_2^2\right) - g_1^2 \xi
\end{aligned} \tag{A.4}$$

$$\begin{aligned}
16\pi^2 \frac{d}{dt} m_{e_a}^2 &= 4\delta_{a3} h_\tau^2 (m_{L_3}^2 + m_{H_1}^2 + m_\tau^2 + A_\tau^2) \\
&\quad - 8g_1^2 M_1^2 + 2g_1^2 \xi
\end{aligned} \tag{A.5}$$

$$\begin{aligned}
16\pi^2 \frac{d}{dt} m_{H_1}^2 &= 6h_b^2 (m_{Q_3}^2 + m_{H_1}^2 + m_B^2 + A_b^2) + 2h_\tau^2 (m_{L_3}^2 + m_{H_1}^2 + m_\tau^2 + A_\tau^2) \\
&\quad + 2\lambda^2 (m_{H_1}^2 + m_{H_2}^2 + m_N^2 + A_\lambda^2) - 8\left(\frac{1}{4} g_1^2 M_1^2 + \frac{3}{4} g_2^2 M_2^2\right) - g_1^2 \xi
\end{aligned} \tag{A.6}$$

$$\begin{aligned}
16\pi^2 \frac{d}{dt} m_{H_2}^2 &= 6h_t^2 (m_{Q_3}^2 + m_{H_2}^2 + m_T^2 + A_t^2) + 2\lambda^2 (m_{H_1}^2 + m_{H_2}^2 + m_N^2 + A_\lambda^2) \\
&\quad - 8\left(\frac{1}{4} g_1^2 M_1^2 + \frac{3}{4} g_2^2 M_2^2\right) + g_1^2 \xi
\end{aligned} \tag{A.7}$$

$$16\pi^2 \frac{d}{dt} m_N^2 = 4\lambda^2 (m_{H_1}^2 + m_{H_2}^2 m_N^2 + A_\lambda^2) + 4k^2 (3m_N^2 + A_k^2) \tag{A.8}$$

Here the subscript $a \in \{1, 2, 3\}$ is a generation index. We have assumed no inter-generational mixing. ξ is the hypercharge-weighted sum of all soft masses-squared

$$\xi = \sum_i Y_i m_i^2, \tag{A.9}$$

where i runs over all scalar particles. Notice that if we impose the constraint $m_i^2(Q) = m_0^2$ for some value of Q , typically the unification scale M_X , then $\xi(Q) = 0$. If ξ is 0 at one scale, then it is 0 at all scales.

It is well known that the gaugino masses M_i evolve identically to α_i at one loop,

so that we have the result

$$\frac{M_i(Q)}{M_{\frac{1}{2}}} = \frac{g_i^2(Q)}{g_X^2} \quad (\text{A.10})$$

The RG equations for the MSSM are identical to those for the NMSSM with λ and k set to 0, supplemented with the following two equations for μ and B :

$$16\pi^2 \frac{d}{dt} \mu = \mu(3h_t^2 + 3h_b^2 + h_\tau^2 - g_1^2 - 3g_2^2) \quad (\text{A.11})$$

$$16\pi^2 \frac{d}{dt} B = -2(3h_t^2 A_t + 3h_b^2 A_b + h_\tau^2 A_\tau - g_1^2 M_1 - 3g_2^2 M_2) \quad (\text{A.12})$$

B Scalar and Fermion Mass Matrices

In this appendix we give all relevant scalar and fermion mass matrices, including one-loop radiative corrections to the Higgs and squarks mass matrices. We neglect radiative corrections due to loops of tau leptons and sleptons since, at low energy, the tau lepton Yukawa coupling is approximately 3 times smaller than the bottom quark Yukawa coupling, and, furthermore, loops of leptons and sleptons have no colour factor associated with them. The corrections to the Higgs masses have been calculated elsewhere [36, 44, 38, 40], and are given in the notation of [44].

First we briefly review the use of the one-loop effective potential for the calculation of radiative corrections to scalar masses. The one-loop effective potential is given by Eq. (3.10). The term V_0 is the tree-level scalar potential, and the remaining contribution to the right-hand-side of Eq. (3.10) comes from radiative corrections to the scalar potential, and we denote it by ΔV_1 :

$$\Delta V_1 = \frac{1}{64\pi^2} \text{Str} \mathcal{M}^4 \left(\log \frac{\mathcal{M}^2}{Q^2} - \frac{3}{2} \right). \quad (\text{B.1})$$

The supertrace is a trace over the eigenvalues of the field-dependent mass-squared matrix weighted by spin factors $(2j+1)(-1)^{2j}$ for particles of spin j going around the loops. Thus, a scalar loop contributes +1, whereas a (2-spinor) fermion loop contributes -2.

The tree-level mass-squared matrix M^2 of general scalar particles ϕ_i is given by

$$M_{ij}^2 = \frac{\partial^2 V_0}{\partial \phi_i \partial \phi_j} \Big|_{VEVs}, \quad (\text{B.2})$$

and the one-loop corrections δM^2 are given by

$$\delta M_{ij}^2 = \frac{\partial^2 \Delta V_1}{\partial \phi_i \partial \phi_j} \Big|_{VEVs}. \quad (\text{B.3})$$

Naturally, we must insert the correct VEVs: for one-loop calculations we must minimise the full one-loop effective potential in order to extract the VEVs to one-loop. Actually, Eq. (B.3) neglects scalar self-energy contributions, but these are expected to be small for the lighter scalar states.

B.1 Higgs Mass Matrices

The CP-even mass-squared matrix in the NMSSM, in the basis $\{H_1, H_2, N\}$ is given by $M^2 + \delta M^2$, where M^2 and δM^2 are given by

$$\begin{aligned} M^2 &= \begin{pmatrix} M_Z^2 \cos^2 \beta & (\lambda^2 \nu^2 - \frac{1}{2} M_Z^2) \sin 2\beta & 2\lambda^2 x \nu \cos \beta \\ (\lambda^2 \nu^2 - \frac{1}{2} M_Z^2) \sin 2\beta & M_Z^2 \sin^2 \beta & 2\lambda^2 x \nu \sin \beta \\ 2\lambda^2 x \nu \cos \beta & 2\lambda^2 x \nu \sin \beta & kx(4kx - A_k) \end{pmatrix} \\ &+ \lambda x \begin{pmatrix} \tan \beta [A_\lambda + kx] & -[A_\lambda + kx] & -\frac{\nu_2}{x} [A_\lambda + 2kx] \\ -[A_\lambda + kx] & \cot \beta [A_\lambda + kx] & -\frac{\nu_1}{x} [A_\lambda + 2kx] \\ -\frac{\nu_2}{x} [A_\lambda + 2kx] & -\frac{\nu_1}{x} [A_\lambda + 2kx] & \frac{\nu_1 \nu_2}{x^2} [A_\lambda] \end{pmatrix} \end{aligned} \quad (\text{B.4})$$

and

$$\delta M^2 = \begin{pmatrix} \Delta_{11}^2 & \Delta_{12}^2 & \Delta_{13}^2 \\ \Delta_{12}^2 & \Delta_{22}^2 & \Delta_{23}^2 \\ \Delta_{13}^2 & \Delta_{23}^2 & \Delta_{33}^2 \end{pmatrix} + \begin{pmatrix} \tan \beta & -1 & -\frac{\nu_2}{x} \\ -1 & \cot \beta & -\frac{\nu_1}{x} \\ -\frac{\nu_2}{x} & -\frac{\nu_1}{x} & \frac{\nu_1 \nu_2}{x^2} \end{pmatrix} \Delta^2, \quad (\text{B.5})$$

where Δ^2 and the Δ_{ij}^2 are given by

$$\Delta^2 = \frac{3}{16\pi^2} (\lambda x) \left(h_t^2 A_t f(m_{\tilde{t}_1}^2, m_{\tilde{t}_2}^2) + h_b^2 A_b f(m_{\tilde{b}_1}^2, m_{\tilde{b}_2}^2) \right) \quad (\text{B.6})$$

$$\begin{aligned} \Delta_{11}^2 &= \frac{3}{8\pi^2} h_t^4 \nu_2^2 (\lambda x)^2 \left(\frac{-A_t + \lambda x \cot \beta}{m_{\tilde{t}_2}^2 - m_{\tilde{t}_1}^2} \right)^2 g(m_{\tilde{t}_1}^2, m_{\tilde{t}_2}^2) + \frac{3}{8\pi^2} h_b^4 \nu_1^2 \log \frac{m_{\tilde{b}_1}^2 m_{\tilde{b}_2}^2}{m_b^4} \\ &- \frac{3}{8\pi^2} h_b^4 \nu_1^2 \frac{A_b (-A_b + \lambda x \tan \beta)}{m_{\tilde{b}_2}^2 - m_{\tilde{b}_1}^2} \left(2 \log \frac{m_{\tilde{b}_2}^2}{m_{\tilde{b}_1}^2} - \frac{A_b (-A_b + \lambda x \tan \beta)}{m_{\tilde{b}_2}^2 - m_{\tilde{b}_1}^2} g(m_{\tilde{b}_1}^2, m_{\tilde{b}_2}^2) \right) \end{aligned} \quad (\text{B.7})$$

$$\begin{aligned}
\Delta_{12}^2 &= \frac{3}{8\pi^2} h_t^4 \nu_2^2 (\lambda x) \left(\frac{-A_t + \lambda x \cot \beta}{m_{\tilde{t}_2}^2 - m_{\tilde{t}_1}^2} \right) \left(\log \frac{m_{\tilde{t}_2}^2}{m_{\tilde{t}_1}^2} - \frac{A_t(-A_t + \lambda x \cot \beta)}{m_{\tilde{t}_2}^2 - m_{\tilde{t}_1}^2} g(m_{\tilde{t}_1}^2, m_{\tilde{t}_2}^2) \right) \\
&+ \frac{3}{8\pi^2} h_b^4 \nu_1^2 (\lambda x) \left(\frac{-A_b + \lambda x \tan \beta}{m_{\tilde{b}_2}^2 - m_{\tilde{b}_1}^2} \right) \left(\log \frac{m_{\tilde{b}_2}^2}{m_{\tilde{b}_1}^2} - \frac{A_b(-A_b + \lambda x \tan \beta)}{m_{\tilde{b}_2}^2 - m_{\tilde{b}_1}^2} g(m_{\tilde{b}_1}^2, m_{\tilde{b}_2}^2) \right)
\end{aligned} \tag{B.8}$$

$$\begin{aligned}
\Delta_{13}^2 &= \frac{3}{8\pi^2} h_t^4 \nu_2^2 (\lambda x) (\lambda \nu_1) \left(\frac{-A_t + \lambda x \cot \beta}{m_{\tilde{t}_2}^2 - m_{\tilde{t}_1}^2} \right)^2 g(m_{\tilde{t}_1}^2, m_{\tilde{t}_2}^2) + \frac{3}{8\pi^2} h_t^2 (\lambda x) (\lambda \nu_1) f(m_{\tilde{t}_1}^2, m_{\tilde{t}_2}^2) \\
&+ \frac{3}{8\pi^2} h_b^4 \nu_1^2 (\lambda \nu_2) \left(\frac{-A_b + \lambda x \tan \beta}{m_{\tilde{b}_2}^2 - m_{\tilde{b}_1}^2} \right) \left(\log \frac{m_{\tilde{b}_2}^2}{m_{\tilde{b}_1}^2} - \frac{A_b(-A_b + \lambda x \tan \beta)}{m_{\tilde{b}_2}^2 - m_{\tilde{b}_1}^2} g(m_{\tilde{b}_1}^2, m_{\tilde{b}_2}^2) \right)
\end{aligned} \tag{B.9}$$

$$\begin{aligned}
\Delta_{22}^2 &= \frac{3}{8\pi^2} h_b^4 \nu_1^2 (\lambda x)^2 \left(\frac{-A_b + \lambda x \tan \beta}{m_{\tilde{b}_2}^2 - m_{\tilde{b}_1}^2} \right)^2 g(m_{\tilde{b}_1}^2, m_{\tilde{b}_2}^2) + \frac{3}{8\pi^2} h_t^4 \nu_2^2 \log \frac{m_{\tilde{t}_1}^2 m_{\tilde{t}_2}^2}{m_t^4} \\
&- \frac{3}{8\pi^2} h_t^4 \nu_2^2 \frac{A_t(-A_t + \lambda x \cot \beta)}{m_{\tilde{t}_2}^2 - m_{\tilde{t}_1}^2} \left(2 \log \frac{m_{\tilde{t}_2}^2}{m_{\tilde{t}_1}^2} - \frac{A_t(-A_t + \lambda x \cot \beta)}{m_{\tilde{t}_2}^2 - m_{\tilde{t}_1}^2} g(m_{\tilde{t}_1}^2, m_{\tilde{t}_2}^2) \right)
\end{aligned} \tag{B.10}$$

$$\begin{aligned}
\Delta_{23}^2 &= \frac{3}{8\pi^2} h_b^4 \nu_1^2 (\lambda x) (\lambda \nu_2) \left(\frac{-A_b + \lambda x \tan \beta}{m_{\tilde{b}_2}^2 - m_{\tilde{b}_1}^2} \right)^2 g(m_{\tilde{b}_1}^2, m_{\tilde{b}_2}^2) + \frac{3}{8\pi^2} h_b^2 (\lambda x) (\lambda \nu_2) f(m_{\tilde{b}_1}^2, m_{\tilde{b}_2}^2) \\
&+ \frac{3}{8\pi^2} h_t^4 \nu_2^2 (\lambda \nu_1) \left(\frac{-A_t + \lambda x \cot \beta}{m_{\tilde{t}_2}^2 - m_{\tilde{t}_1}^2} \right) \left(\log \frac{m_{\tilde{t}_2}^2}{m_{\tilde{t}_1}^2} - \frac{A_t(-A_t + \lambda x \cot \beta)}{m_{\tilde{t}_2}^2 - m_{\tilde{t}_1}^2} g(m_{\tilde{t}_1}^2, m_{\tilde{t}_2}^2) \right)
\end{aligned} \tag{B.11}$$

$$\begin{aligned}
\Delta_{33}^2 &= \frac{3}{8\pi^2} h_t^4 \nu_2^2 (\lambda \nu_1)^2 \left(\frac{-A_t + \lambda x \cot \beta}{m_{\tilde{t}_2}^2 - m_{\tilde{t}_1}^2} \right)^2 g(m_{\tilde{t}_1}^2, m_{\tilde{t}_2}^2) \\
&+ \frac{3}{8\pi^2} h_b^4 \nu_1^2 (\lambda \nu_2)^2 \left(\frac{-A_b + \lambda x \tan \beta}{m_{\tilde{b}_2}^2 - m_{\tilde{b}_1}^2} \right)^2 g(m_{\tilde{b}_1}^2, m_{\tilde{b}_2}^2)
\end{aligned} \tag{B.12}$$

and the functions f and g are defined by

$$f(m_1^2, m_2^2) = \frac{1}{m_1^2 - m_2^2} \left(m_1^2 \log \frac{m_1^2}{Q^2} - m_2^2 \log \frac{m_2^2}{Q^2} - m_1^2 + m_2^2 \right) \tag{B.13}$$

$$g(m_1^2, m_2^2) = \frac{1}{m_1^2 - m_2^2} \left((m_1^2 + m_2^2) \log \frac{m_2^2}{m_1^2} + 2(m_1^2 - m_2^2) \right) \tag{B.14}$$

In these expressions, $m_{\tilde{t}_1}$, $m_{\tilde{t}_2}$, $m_{\tilde{b}_1}$ and $m_{\tilde{b}_2}$ denote the masses of the corresponding top and bottom squark mass eigenstates.

The CP-odd mass-squared matrix, in the basis $\{H_1, H_2, N\}$ is given by $\tilde{M}^2 + \delta\tilde{M}^2$,

where \tilde{M}^2 and $\delta\tilde{M}^2$ are given by

$$\tilde{M}^2 = \lambda x \begin{pmatrix} \tan\beta[A_\lambda + kx] & [A_\lambda + kx] & \frac{\nu_2}{x}[A_\lambda - 2kx] \\ [A_\lambda + kx] & \cot\beta[A_\lambda + kx] & \frac{\nu_1}{x}[A_\lambda - 2kx] \\ \frac{\nu_2}{x}[A_\lambda - 2kx] & \frac{\nu_1}{x}[A_\lambda - 2kx] & 3\frac{kA_k}{\lambda} + \frac{\nu_1\nu_2}{x^2}[A_\lambda + 4kx] \end{pmatrix} \quad (\text{B.15})$$

and

$$\delta\tilde{M}^2 = \begin{pmatrix} \tan\beta & 1 & \frac{\nu_2}{x} \\ 1 & \cot\beta & \frac{\nu_1}{x} \\ \frac{\nu_2}{x} & \frac{\nu_1}{x} & \frac{\nu_1\nu_2}{x^2} \end{pmatrix} \Delta^2 \quad (\text{B.16})$$

The charged Higgs mass-squared matrix, in the basis $\{H_1, H_2\}$, is given by $M_c^2 + \delta M_c^2$, where M_c^2 and δM_c^2 are given by

$$M_c^2 = \begin{pmatrix} \tan\beta & 1 \\ 1 & \cot\beta \end{pmatrix} [\lambda x(A_\lambda + kx) - (\lambda^2\nu^2 - M_W^2)\frac{1}{2}\sin 2\beta], \quad (\text{B.17})$$

and

$$\delta M_c^2 = \begin{pmatrix} \tan\beta & 1 \\ 1 & \cot\beta \end{pmatrix} (\Delta_{c_1}^2 + \Delta_{c_2}^2), \quad (\text{B.18})$$

where $\Delta_{c_1}^2$ is the correction due to loops of top and bottom quarks and is given by

$$\Delta_{c_1}^2 = -\frac{3}{8\pi^2} h_t h_b \frac{m_t m_b}{m_t^2 - m_b^2} \left[m_t^2 \left(\log \frac{m_t^2}{Q^2} - 1 \right) - m_b^2 \left(\log \frac{m_b^2}{Q^2} - 1 \right) \right], \quad (\text{B.19})$$

and $\Delta_{c_2}^2$ is the correction due to loops of top and bottom squarks and is given by

$$\Delta_{c_2}^2 = \frac{3}{16\pi^2} \sum_{i \in \{\tilde{t}_1, \tilde{t}_2, \tilde{b}_1, \tilde{b}_2\}} m_i^2 \left(\log \frac{m_i^2}{Q^2} - 1 \right) \frac{\partial^2 m_i^2}{\partial H_1^- \partial H_2^+} \Big|_{vevs}, \quad (\text{B.20})$$

where

$$\frac{\partial^2 m_a^2}{\partial H_1^- \partial H_2^+} \Big|_{vevs} = -\frac{Bm_a^4 + Cm_a^2 + D}{\Delta_a} \Big|_{vevs}, \quad (\text{B.21})$$

and

$$\Delta_a = \prod_{a' \neq a} (m_a^2 - m_{a'}^2). \quad (\text{B.22})$$

The coefficients B , C and D are messy functions of the various Yukawa couplings and soft masses which we do not reproduce here. It is possible to reduce these expressions to an elegant form in certain limits, such as $h_b \rightarrow 0$ (see [44]).

This completes the Higgs mass matrices, together with radiative corrections, in the NMSSM. To find the corresponding Higgs masses in the MSSM it is sufficient to

perform the following operations. First, strike out elements of the matrices relating to the singlet field N . Second, replace every occurrence of the term $(A_\lambda + kx)$ by $-B$. Third, replace every occurrence of the term λx by μ . Finally, any remaining dependence on λ is removed by setting λ to zero. These rules also apply to the matrices which follow.

B.2 Squark Mass Matrices

Squark contributions to radiative corrections to the squark mass-squared matrices do not appear to have been considered in the literature before. Here we present the results. The calculations are straightforward, so we do not go into the details. However, there is one subtlety in the calculation which we do mention.

If we wish to calculate radiative corrections to the squark mass-squared matrix due to loops of squarks, then we must calculate the field-dependent mass-squared matrix, in which we retain explicitly any dependence in the matrix on the squark fields. Since we shall take derivatives of this matrix with respect to the squark fields only, we may set all other fields to their VEVs. This means that the 4×4 mass-squared matrix decomposes into two 2×2 matrices when the charged Higgs fields are set to their VEVs, namely zero. In general, the field-dependent squark mass-squared matrix, \mathcal{M}^2 , has a non-trivial colour structure. If α and β are $SU(3)$ colour indices, then $\mathcal{M}_\alpha^{2\beta}$, where the colour indices are now explicit, has the form

$$\mathcal{M}_\alpha^{2\beta} = \mathcal{A}^2 \delta_\alpha^\beta + \mathcal{B}_\alpha^{2\beta}. \quad (\text{B.23})$$

This means that the two 2×2 matrices become two 6×6 matrices when the colour structure is considered. On the face of it, this implies that analytic calculation of the eigenvalues is impossible, so that we may not analytically determine the radiative corrections due to loops of squarks.

We may circumvent this problem in the following way. Since the matrix \mathcal{B}^2 trans-

forms as $3 \otimes \bar{3}$ under $SU(3)_c$, and $3 \otimes \bar{3} = 1 \oplus 8$, we may extract the singlet part of \mathcal{B}^2 by pulling out the trace. Thus \mathcal{M}^2 may be written as

$$\mathcal{M}^2 = \mathcal{M}_{singlet}^2 + \mathcal{M}_{octet}^2 \quad (\text{B.24})$$

where

$$\mathcal{M}_{singlet}^2 = (\mathcal{A}^2 + \frac{1}{3}\mathcal{B}_\gamma^{2\gamma})\delta_\alpha^\beta, \quad (\text{B.25})$$

$$\mathcal{M}_{octet}^2 = \mathcal{B}_\alpha^{2\beta} - \frac{1}{3}\mathcal{B}_\gamma^{2\gamma}\delta_\alpha^\beta. \quad (\text{B.26})$$

The octet part is a pure bilinear function of the squark fields. We know, since colour is to be left unbroken, that the radiative corrections must turn out to be have trivial colour structure. Can the octet contribute in any way? The only way to obtain a singlet is from the singlet part of $8 \otimes 8$. However, such a term would be quadrilinear in squark fields, and we need only take at most two derivatives to obtain the radiative corrections. At the end of the calculation, therefore, when the squark fields are set to their VEVs, such a contribution will vanish. Hence we may discard the octet part and retain only the singlet part in the calculations. We then regain two 2×2 matrices with trivial colour structure, and now the calculations may proceed in the usual fashion.

The top squark and bottom squark mass-squared matrices, in the basis of gauge eigenstates $\{\tilde{t}, \tilde{t}^c\}$ and $\{\tilde{b}, \tilde{b}^c\}$, are given by $M_{stop}^2 + \delta M_{stop}^2$ and $M_{sbot}^2 + \delta M_{sbot}^2$, respectively, where

$$M_{stop}^2 = \begin{pmatrix} m_Q^2 + h_t^2 \nu_2^2 & h_t(-A_t \nu_2 + \lambda x \nu_1) \\ h_t(-A_t \nu_2 + \lambda x \nu_1) & m_T^2 + h_t^2 \nu_2^2 \end{pmatrix} \quad (\text{B.27})$$

$$M_{sbot}^2 = \begin{pmatrix} m_Q^2 + h_b^2 \nu_1^2 & -h_b(-A_b \nu_1 + \lambda x \nu_2) \\ -h_b(-A_b \nu_1 + \lambda x \nu_2) & m_B^2 + h_b^2 \nu_1^2 \end{pmatrix} \quad (\text{B.28})$$

$$\delta M_{stop/sbot}^2 = \frac{3}{16\pi^2} \sum_{a \in \{\tilde{t}_1, \tilde{t}_2, \tilde{b}_1, \tilde{b}_2\}} m_a^2 \left(\log \frac{m_a^2}{Q^2} - 1 \right) M_{stop/sbot}^a \quad (\text{B.29})$$

and the $M_{stop/sbot}^a$ are given by

$$M_{stop}^{\tilde{t}_1, \tilde{t}_2} = \frac{1}{6} \begin{pmatrix} h_t^2 & 0 \\ 0 & h_t^2 \end{pmatrix} \pm \frac{1}{6} \frac{m_Q^2 - m_T^2}{m_{\tilde{t}_1}^2 - m_{\tilde{t}_2}^2} \begin{pmatrix} h_t^2 & 0 \\ 0 & -h_t^2 \end{pmatrix}$$

$$\mp \frac{h_t(-A_t\nu_2 + \lambda x\nu_1)}{m_{\tilde{t}_1}^2 - m_{\tilde{t}_2}^2} \begin{pmatrix} 0 & h_t^2 \\ h_t^2 & 0 \end{pmatrix} \quad (\text{B.30})$$

$$M_{stop}^{\tilde{b}_1, \tilde{b}_2} = \frac{1}{6} \begin{pmatrix} h_b^2 & 0 \\ 0 & h_t^2 \end{pmatrix} \pm \frac{1}{6} \frac{m_Q^2 - m_B^2}{m_{\tilde{b}_1}^2 - m_{\tilde{b}_2}^2} \begin{pmatrix} h_b^2 & 0 \\ 0 & -h_t^2 \end{pmatrix} \quad (\text{B.31})$$

$$M_{sbot}^{\tilde{t}_1, \tilde{t}_2} = \frac{1}{6} \begin{pmatrix} h_t^2 & 0 \\ 0 & h_b^2 \end{pmatrix} \pm \frac{1}{6} \frac{m_Q^2 - m_T^2}{m_{\tilde{t}_1}^2 - m_{\tilde{t}_2}^2} \begin{pmatrix} h_t^2 & 0 \\ 0 & -h_b^2 \end{pmatrix} \quad (\text{B.32})$$

$$M_{sbot}^{\tilde{b}_1, \tilde{b}_2} = \frac{1}{6} \begin{pmatrix} h_b^2 & 0 \\ 0 & h_b^2 \end{pmatrix} \pm \frac{1}{6} \frac{m_Q^2 - m_B^2}{m_{\tilde{b}_1}^2 - m_{\tilde{b}_2}^2} \begin{pmatrix} h_b^2 & 0 \\ 0 & -h_b^2 \end{pmatrix} \\ \pm \frac{h_b(-A_b\nu_1 + \lambda x\nu_2)}{m_{\tilde{b}_1}^2 - m_{\tilde{b}_2}^2} \begin{pmatrix} 0 & h_b^2 \\ h_b^2 & 0 \end{pmatrix} \quad (\text{B.33})$$

B.3 Fermionic Mass Matrices

We now turn to the fermionic sector. The neutralino mass matrix, in the basis of 2-spinors given by $\{i\tilde{B}^0, i\tilde{W}_3^0, \tilde{H}_1^0, \tilde{H}_2^0, \tilde{N}\}$ is

$$\begin{pmatrix} -M_1 & 0 & -\frac{1}{\sqrt{2}}g_1\nu_1 & \frac{1}{\sqrt{2}}g_1\nu_2 & 0 \\ 0 & -M_2 & \frac{1}{\sqrt{2}}g_2\nu_1 & -\frac{1}{\sqrt{2}}g_2\nu_2 & 0 \\ -\frac{1}{\sqrt{2}}g_1\nu_1 & \frac{1}{\sqrt{2}}g_2\nu_1 & 0 & -\lambda x & -\lambda\nu_2 \\ \frac{1}{\sqrt{2}}g_1\nu_2 & -\frac{1}{\sqrt{2}}g_2\nu_2 & -\lambda x & 0 & -\lambda\nu_1 \\ 0 & 0 & -\lambda\nu_2 & -\lambda\nu_1 & -2kx \end{pmatrix} \quad (\text{B.34})$$

The mass of the gluino, which does not mix with the other neutralinos because colour is unbroken, is simply given by M_3 .

The chargino mass matrix is given by

$$\begin{pmatrix} M_2 & g_2\nu_1 \\ -g_2\nu_2 & \lambda x \end{pmatrix} \quad (\text{B.35})$$

References

- [1] For reviews see *e.g.*
H.P. Nilles, Phys. Rep. **110** (1984) 1;
H.E. Haber, G.L. Kane, Phys. Rep. **117** (1985) 75.
- [2] H. Georgi, S. Glashow, Phys. Rev. Lett. **32** (1974) 438;
H. Georgi, H.R. Quinn, S. Weinberg, Phys. Rev. Lett. **33** (1974) 451.
- [3] U. Amaldi, W. de Boer, H. Furstenau, Phys. Lett. **260 B** (1991) 447;
J. Ellis, S. Kelley, D. V. Nanopoulos, Phys. Lett. **260 B** (1991) 131;
P. Langacker, M. Luo, Phys. Rev. **D44** (1991) 817.
- [4] L. Ibanez, G. G. Ross, Phys. Lett. **110B** (1982) 215;
H. P. Nilles, Phys. Lett. **B115** (1982) 193;
K. Inoue, A. Kakuto, H. Komatsu, S. Takashita, Prog. Theor. Phys. **68** (1982) 927;
L. Alvarez-Gaumé, J. Polchinski, M. Wise, Nucl. Phys. **B221** (1983) 495; J. Ellis, D. Nanopoulos, K. Tamvakis, Phys. Lett. **B121** (1983) 123.
- [5] G.G. Ross, R.G. Roberts, Nucl. Phys. **B 377** (1992) 571.
- [6] R. Arnowitt, P. Nath, Phys. Lett. **B 287** (1992) 89; Phys. Rev. **D69** (1992) 725;
Phys. Lett. **B 289** (1992) 368; Phys. Lett. **B 299** (1993) 58; Phys. Rev. Lett. **70** (1993) 3696;
V. Barger, M. S. Berger, P. Ohman, Phys. Rev. **D47** (1993) 1093; Phys. Rev. **D49** (1994) 4908;
W. de Boer, R. Ehret, D. I. Kazakov, IEKP-KA/94-05;
M. Carena, S. Pokorski, C.E.M. Wagner, Nucl. Phys. **B406** (1993) 59;
D.J. Castano, E.J. Piard, P. Ramond, Phys.Rev. **D49** (1994) 4882;
G. Kane, C. Kolda, L. Roszkowski and J. Wells, Phys. Rev. **D49** (1994) 6173;

- S. Kelley, J. L. Lopez, D. V. Nanopoulos, H. Pois and K. Yuan, Phys. Lett. **B273** (1991) 423; Nucl. Phys. **B 398** (1993) 3;
- J. Lopez, D.V. Nanopoulos and H. Pois, Phys. Rev. **D47** (1993) 2468;
- J. Lopez, D.V. Nanopoulos, H. Pois, X. Wang and A. Zichichi, Phys. Lett. **B306** (1993) 73;
- S. P. Martin, P. Ramond, Phys. Rev. **D48** (1993) 5365;
- M. Olechowski, S. Pokorski, Nucl. Phys. **B404** (1993) 590;
- R. G. Roberts and L. Roszkowski, Phys. Lett. **B309** (1993) 329;
- I. Jack, D.R.T. Jones and K.L. Roberts, hep-ph/9505242.
- [7] P. Fayet, Nucl. Phys. **B90** (1975) 104.
- [8] H.P. Nilles, M. Srednicki, D. Wyler, Phys. Lett. **B120** (1983) 346;
- J.M. Frere, D.R.T. Jones, S. Raby, Nucl. Phys. **B222** (1983) 11;
- J.-P. Derendinger, C.A. Savoy, Nucl. Phys. **B237** (1984) 307;
- L. Durand, J. L. Lopez, Phys. Lett. **B217** (1989) 463;
- M. Drees, Intern. J. Mod. Phys. **A4** (1989) 3645.
- [9] J. Ellis, J. Gunion, H. Haber, L. Roszkowski and F. Zwirner, Phys. Rev. **D39** (1989) 844.
- [10] L. Hall, J. Lykken, S. Weinberg, Phys. Rev. **D27** (1983) 2359;
- J.E. Kim, H.P. Nilles, Phys. Lett. **B138** (1984) 150;
- K. Inoue, A. Kakuto, T. Takano, Prog. Theor. Phys. **75** (1986) 664;
- A. A. Ansel'm, A. A. Johansen, Phys. Lett. **B200** (1988) 331;
- G. Giudice, A. Masiero, Phys. Lett. **B206** (1988) 480.
- [11] S. Ferrara, D.V. Nanopoulos, C. A. Savoy, Phys. Lett. **B123** (1983) 214;
- J. Polchinski, L. Susskind, Phys. Rev. **26** (1982) 3661;
- H.P. Nilles, M. Srednicki and D. Wyler, Phys. Lett. **B124** (1982) 337;

- A. B. Lahanas, Phys. Lett. **B124** (1982) 341;
- L. Alvarez-Gaume, J. Polchinski, M. B. Wise, Nucl. Phys. **B221** (1983) 495.
- [12] U. Ellwanger, Phys. Lett. **B133** (1983) 187;
 J. Bagger, E. Poppitz, Phys. Rev. Lett. **71** (1993) 2380;
 J. Bagger, E. Poppitz, L. Randall, preprint EFI-95-21, hep-ph/9505244.
- [13] U. Ellwanger, M. Rausch de Traubenberg, C. A. Savoy, Phys. Lett. **B315** (1993) 331.
- [14] Ph. Brax, U. Ellwanger, C. A. Savoy, Phys. Lett. **B347** (1995) 269.
- [15] U. Ellwanger, M. Rausch de Traubenberg, C. A. Savoy, LPTHE Orsay 95-04, LPT Strasbourg 95-01, SPhT Saclay T95/04, hep-ph/9502206.
- [16] T. Elliott, S. F. King, P. L. White, SHEP 93/94-19, hep-ph/9406303, Phys Lett **B** (to appear).
- [17] A. Vilenkin, Phys. Rep. **121** (1985) 263.
- [18] G. B. Gelmini, M. Gleiser, E. W. Kolb, Phys. Rev. **D39** (1989) 1558;
 W. H. Press, B. S. Ryden, D. N. Spergel, Ap. J. **357** (1990) 293;
 B. Rai, G. Senjanovic, Phys. Rev. **D49** (1994) 2729;
 S.A. Abel, P.L. White, preprint OUTP-9517P, CCL-TR-95-005, hep-ph/9505241;
 S.A. Abel, S. Sarkar, P.L. White, in preparation.
- [19] J. C. Romão, Phys Lett **B173** (1986) 309.
- [20] S. Coleman and E. Weinberg, Phys Rev **D7** (1973) 1888;
 S. Weinberg, Phys Rev **D7** (1973) 2887;
 M. Sher, Phys Rep **179** (1989) 273.
- [21] G. Gamberini, G. Ridolfi and F. Zwirner, Nucl Phys **B331** (1990) 331.

- [22] D. Pierce, A. Papadopoulos, Phys. Rev. **D50** (1994) 565; Nucl. Phys. **B430** (1994) 278.
- [23] M. Pohl, in “Proceedings of the XXVII International Conference on High Energy Physics”, eds. P. J. Bussey, I. G. Knowles, IOP Publishing (Bristol) 1994.
- [24] J. Hagelin, S. Kelley, T. Tanaka, Nucl. Phys. **B415** (1994) 293;
 J. Hagelin, S. Kelley, T. Tanaka, Mod. Phys. Lett. **A8** (1993) 2737;
 G. C. Branco, G. C. Cho, Y. Kizukuri, N. Oshimo, Phys. Lett. **B337** (1994) 316;
 F. Gabbiani, A. Masiero, Nucl. Phys. **B322** (1982) 235.
- [25] L. Roszkowski, Phys. Lett. **B252** (1990) 471.
- [26] F. Franke, H. Fraas, A. Bartl, Phys. Lett. **B336** (1994) 415.
- [27] L. Roszkowski, Phys. Lett. **B262** (1991) 59; J. L. Lopez, D. V. Nanopoulos, K. Yuan, Nucl. Phys. **B370** (1992) 445;
 S. Kelley, J. L. Lopez, D. V. Nanopoulos, H. Pois, K. Yuan, Phys. Rev. **D47** (1993) 2461.
- [28] K. Olive, D. Thomas, Nucl. Phys. **B335** (1991) 192;
 R.A. Flores, K. Olive, D. Thomas, Phys. Lett. **B263** (1991) 425;
 S.A. Abel, S. Sarkar, I.B. Whittingham, Nucl. Phys. **B392** (1993) 83.
- [29] The ALEPH collaboration, Phys. Lett. **B313** (1993) 312;
 The DELPHI collaboration, Nucl. Phys. **B373** (1992) 3;
 The OPAL collaboration, Z. Phys. **C64** (1994) 1;
 The L3 collaboration, Z. Phys. **C57** (1993) 355.
- [30] F. Franke, H. Fraas, preprint WUE-ITP-95-003, hep-ph/9504279.
- [31] J. L. Hewett, preprint SLAC-PUB-6521, hep-ph/9406302.

- [32] The CDF Collaboration, Phys. Rev. Lett. **73** (1994) 225; Phys. Rev. **D50** (1994) 2966; FERMILAB-PUB-95/022-E;
The D0 Collaboration, FERMILAB-PUB-95/028-E.
- [33] R. Barbieri, G.F. Giudice, Nucl. Phys. **B306** (1988) 63.
- [34] B. de Carlos, J.A. Casas, Phys. Lett. **B309** (1993) 320.
- [35] P. Langacker, N. Polonsky, Phys. Rev. **D47** (1993) 4028;
M. Carena, S. Pokorski, C.E.M. Wagner, Nucl. Phys. **B406** (1993) 59.
- [36] H. E. Haber and R. Hempfling, Phys Rev Lett **66** (1991) 1815;
Y. Okada, M. Yamaguchi and T. Yanagida, Prog. Theor. Phys. **85** (1991) 1.
- [37] J. Espinosa, M. Quiros, Phys. Lett. **B279** (1992) 92; Phys. Lett. **B302** (1993) 51;
G. Kane, C. Kolda, J. Wells, Phys. Rev. Lett. **70** (1993) 2686.
- [38] U. Ellwanger, M. Rausch de Traubenberg, Z Phys **C53** (1992) 521;
U. Ellwanger, M. Lindner, Phys Lett **B301** (1993) 365;
U. Ellwanger, Phys Lett **B303** (1993) 271;
P. N. Pandita, Phys Lett **B318** (1993) 338; Z Phys **C59** (1993) 575;
T. Elliott, S. F. King and P. L. White, Phys Lett **B305** (1993) 71; **B314** (1993) 56.
- [39] B. Anathanarayan, G. Lazarides and Q. Shafi, Phys. Lett. **B300** (1993) 245;
L. Hall, R. Rattazzi and U. Sarid, Phys. Rev. **D50** (1994) 7048; M. Carena,
M. Olechowski, S. Pokorski, C. Wagner, “Electroweak Symmetry Breaking and
Bottom-Top Yukawa Unification”, preprint MPI-Ph/93-103;
E.G. Floratos, G. K. Leontaris, Phys.Lett. **B336** (1994) 194; preprint IOA-320-
95, hep-ph/9503455; B. Anathanarayan and P.N. Pandita, hep-ph/9503323.

- [40] T. Elliott, S. F. King, P. L. White, Phys Rev **D49** (1994) 2435.
- [41] H. Haber, Santa Cruz preprint SCIPP 94/39, hep-ph/9501320.
- [42] J. F. Gunion, H. E. Haber, G. Kane, S. Dawson, “The Higg’s Hunter’s Guide” Addison-Wesley (1990).
- [43] D.R.T. Jones, Phys. Rev. **D25** (1982) 581;
M. E. Machacek, M. T. Vaughn, Nucl. Phys. **B236** (1984) 221;
M. E. Machacek, M. T. Vaughn, Nucl. Phys. **B222** (1983) 83;
S. P. Martin, M. T. Vaughn, Phys.Rev. **D50** (1994) 2282.
- [44] J. Ellis, G. Ridolfi, F. Zwirner, Phys Lett **B257** (1991) 83; **B262** (1991) 477;
A. Brignole, J. Ellis, G. Ridolfi, F. Zwirner, Phys Lett **B271** (1991) 123.

C Figure Captions

Figure 1 : Contours of $\alpha_3(M_Z)$ and m_t in the $M_{1/2} - m_0$ plane in the MSSM with $A_0 = 0$, $\tilde{B}_0 = -1$, $\mu_0 = m_0$, and several different values of m_0 . Ranging over h_{t0} and \tilde{m}_0 allows us to cover much of the plane, but note the regions where this is not possible (because with our choice of $\tilde{\mu}_0$, \tilde{B}_0 and \tilde{A}_0 correct electroweak symmetry breaking is not guaranteed to occur everywhere). Contours are for $\alpha_3(M_Z)=0.1125, 0.115, 0.1175, 0.120, 0.1225, 0.125$ (solid lines) and for $m_t = 100, 140, 180\text{GeV}$ (dashed).

Figure 2 : $M_{1/2}$ against h_{t0} in the MSSM, for values of the other parameters $A = 0$, $\tilde{B} = -1$, $\mu = m_0$, and $\tilde{m}_0=0.1,0.2,0.5,1,2,5,10,20$ (from left to right). This is typical behaviour in this model.

Figure 3 : M_Z against h_{t0} in the MSSM, for different choices of $M_{1/2} = 50$ (solid lines), 100 (dashed), 200 (short dashed), 500 (dotted), 1000 (dot-dashed) GeV for the fixed parameters $A_0 = 0$, $\tilde{\mu}_0 = 1$, $\tilde{B}_0 = -1$, $\tilde{m}_0 = 1$. As expected, for $M_Z = 91$ GeV, the curves corresponding to larger $M_{1/2}$ are significantly steeper than those for smaller $M_{1/2}$, indicating a higher degree of fine-tuning.

Figure 4: Masses of particles as a function of $M_{1/2}$ for the NMSSM in the region with $k_0 > \lambda_0 > h_{t0}$. The input parameters are $A_0 = 0$, $\tilde{m}_0 = 5$, $\lambda_0 = 0.8$, $k_0 = 2$, $h_{t0} = 0.37 - 0.47$. Neutralinos (solid lines), charginos (dot-dashed lines), CP-even Higgs (short dashed lines), lighter stop and top quark (both dotted lines), left-handed sleptons (long dashed lines), and gluino (quadruple dashed lines) are displayed.

Figure 5 : A contour plot showing allowed values of λ_0 and k_0 for given values of $h_{t0} = 0.5, 1, 2, 3$ in the λ_0 - k_0 plane, corresponding to $M_{1/2} = 500$ GeV, $\tilde{m}_0 = 2$ with $A_0/m_0 = -3$.

Figure 6: Masses of particles as a function of $M_{1/2}$ for the NMSSM in the region with $h_{t0} > \lambda_0 > k_0$ and for parameters lying in the “safe” region where arbitrarily

small $M_{1/2}$ can be achieved. The input parameters are $h_{t0} = 2$, $A_0/m_0 = -3$, $\tilde{m}_0 = 5$, $\lambda_0 = 0.4$, $k_0 = 0.275 - 0.3$. Neutralinos (solid lines), charginos (dot-dashed lines), CP-even Higgs (short dashed lines), lighter stop and top quark (both dotted lines), left-handed sleptons (long dashed lines), and gluino (quadruple dashed lines) are displayed. One of the CP-odd Higgs and the charged Higgs bosons (not shown) are roughly degenerate with heavier CP-even Higgs bosons. The remaining CP-odd Higgs boson (not shown) is heavier than the heaviest neutralino. The lightest CP-even Higgs (which has standard model-like couplings), lighter chargino and lightest two neutralinos are all in the LEP2 range for $M_{1/2} \lesssim 100$ GeV.

Figure 7: Masses of particles as a function of $M_{1/2}$ for the NMSSM in the region with $h_{t0} > \lambda_0 > k_0$ and for parameters lying outside the “safe” region where arbitrarily small $M_{1/2}$ can be achieved. The input parameters are $h_{t0} = 0.5$, $A_0/m_0 = -4$, $\tilde{m}_0 = 0.5$, $\lambda_0 = 0.1$, $k_0 = 0.07 - 0.13$. In addition to using $Q = 150$ GeV as usual, we also show results for $Q = 25$ GeV, corresponding to minimum values of $M_{1/2} = 300$ GeV and $M_{1/2} = 125$ GeV, respectively. Neutralinos (solid lines), charginos (dot-dashed lines), CP-even Higgs (short dashed lines), lighter stop and top quark (both dotted lines), left-handed sleptons (long dashed lines), and gluino (quadruple dashed lines) are displayed. One of the CP-odd Higgs (not shown) is roughly degenerate with the second heaviest CP-even Higgs boson. The remaining CP-odd Higgs boson (not shown) is roughly equal to the lighter stop mass. The lightest CP-even Higgs (which has standard model-like couplings as in Fig.2) has a mass $\lesssim 100$ GeV.

Figure 8: Masses of particles as a function of $M_{1/2}$ for parameters selected to lie in the deep MSSM region. The input parameters are $h_{t0} = 0.5$, $A_0/m_0 = -5$, $\tilde{m}_0 = 0.02$, $\lambda_0 = 0.005$, $k_0 = 0.0002 - 0.0004$. Neutralinos (solid lines), charginos (dot-dashed lines), CP-even Higgs (short dashed lines), lighter stop and top quark (both dotted lines), left-handed sleptons (long dashed lines), and gluino (quadruple dashed lines) are displayed.

Figure 9: Amplitude of N contained in the lightest (dashes) and second lightest (dot-dash) CP-even Higgs bosons in Fig.8. The heaviest CP-even Higgs boson has N-amplitude zero.

Figure 10: M_Z against k_0 for the NMSSM with $h_{t0} = 2$, $A_0/m_0 = -3$, $\tilde{m}_0 = 5$, $\lambda_0 = 0.4$. $M_{1/2} = 50, 100, 200, 500, 1000$ GeV

Figure 11: M_Z against k_0 for the NMSSM with $h_{t0} = 0.5$, $A_0/m_0 = -4$, $\tilde{m}_0 = 0.5$, $\lambda_0 = 0.1$. $M_{1/2} = 50, 100, 200, 500, 700, 1000$ GeV. Note the discontinuities in the lines, particularly for $M_{1/2} = 500$ and 700 GeV.

Figure 12: Masses of particles as a function of $M_{1/2}$, with parameters chosen so as to mimic Figure 6. The input parameters are $h_{t0} = 2$, $A_0/m_0 = -3$, $\tilde{m}_0 = 5$, $\tilde{\mu}_0 = -7.5$, $\tilde{B}_0 = 8.8 - 10.2$. Neutralinos (solid lines), charginos (dot-dashed lines), CP-even Higgs (short dashed lines), lighter stop and top quark (both dotted lines), left-handed sleptons (long dashed lines), and gluino (quadruple dashed lines) are displayed.

Figure 13: Masses of particles as a function of $M_{1/2}$, with parameters chosen so as to mimic Figure 8. The input parameters are $h_{t0} = 0.5$, $A_0/m_0 = -5$, $\tilde{m}_0 = 0.02$, $\tilde{\mu}_0 = 1.1$ to 0.5 , $\tilde{B}_0 = -0.015$ to -0.135 . Neutralinos (solid lines), charginos (dot-dashed lines), CP-even Higgs (short dashed lines), lighter stop and top quark (both dotted lines), left-handed sleptons (long dashed lines), and gluino (quadruple dashed lines) are displayed. Line styles are as in Figure 6.

Figure 14: Masses of particles as a function of $M_{1/2}$, with parameters chosen so as to mimic Figure 7. The input parameters are $h_{t0} = 0.5$, $A_0/m_0 = -4$, $\tilde{m}_0 = 0.5$, $\tilde{\mu}_0 = -1.3$ to -0.9 , $\tilde{B}_0 = 1.1$. Neutralinos (solid lines), charginos (dot-dashed lines), CP-even Higgs (short dashed lines), lighter stop and top quark (both dotted lines), left-handed sleptons (long dashed lines), and gluino (quadruple dashed lines) are displayed.

Figure 15: Scatter plot showing the mass of the lightest CP-odd Higgs boson against those of the lightest (+) and second lightest CP-even Higgs bosons (\times) in the NMSSM.

Figure 16a: Masses of the lightest CP-even Higgs boson in the NMSSM plotted against R_{ZZh_1} (+), and the second lightest CP-even Higgs boson, plotted against R_{ZZh_2} (\times). The input parameters are $h_{t0} = 0.5$, $A_0/m_0 = -5$, $\tilde{m}_0 = 0.02$, $\lambda_0 = 0.005$, $k_0 = 0.0002 - 0.0003$. The output parameters include $M_{1/2} \approx 600 - 2600$ GeV, $m_t \approx 161 - 152$ GeV, $\tan \beta > 10$. Also shown is the region excluded by LEPI (short-dashed line), the discovery reach of LEP II at an energy of 175 GeV and an integrated luminosity of 500 pb^{-1} (long-dashed line) and the discovery reach of LEP II at an energy of 205 GeV and an integrated luminosity of 300 pb^{-1} (full line).

Figure 16b: $R_{\bar{d}dh_1}$ (+), $R_{\bar{u}uh_1}$ (circles), $R_{\bar{d}dh_2}$ (\times), $R_{\bar{u}uh_2}$ (squares), against the corresponding Higgs boson mass, for the data shown in Fig.16a.

Figure 17: Masses of the lightest CP-even Higgs boson in the NMSSM plotted against R_{ZZh_1} (+), and the second lightest CP-even Higgs boson, plotted against R_{ZZh_2} (\times), for an example of scenario (i) defined in the text. The input parameters are $h_{t0} = 0.5$, $|A_0/m_0| = 5$, $\tilde{m}_0 = 0.01$, $\lambda_0 = 0.005$, $k_0 = 0.00012 - 0.00014$. The output parameters include $M_{1/2} \approx 1 - 2\text{TeV}$, $m_t \approx 156 - 153$ GeV, $\tan \beta \approx 10 - 20$. Also shown is the region excluded by LEPI (short-dashed line), the discovery reach of LEP II at an energy of 175 GeV and an integrated luminosity of 500 pb^{-1} (long-dashed line) and the discovery reach of LEP II at an energy of 205 GeV and an integrated luminosity of 300 pb^{-1} (full line).

Figure 18a: Masses of the lightest CP-even Higgs boson in the NMSSM plotted against R_{ZZh_1} (+), and the second lightest CP-even Higgs boson, plotted against R_{ZZh_2} (\times), for some examples of scenario (ii) defined in the text. The parameters for examples of Higgs bosons visible in the first phase of LEP II (within the dashed region) are: $h_{t0} = 0.4 - 0.5$, $A_0/m_0 = -3$ to -5 , $\tilde{m}_0 = 0.02$, $\lambda_0 = 0.01$, $k_0 = 0.0004 - 0.0006$

with output parameters including $M_{1/2} \approx 1 - 2\text{TeV}$, $m_t \approx 140 - 160 \text{ GeV}$, $|\tan \beta| \approx 9 - 18$. The parameters for examples of Higgs bosons visible in the final phase of LEP II (within the solid region) are $h_{t0} = 0.4 - 0.5$, $A_0/m_0 = -3 \text{ to } -5$, $\tilde{m}_0 = 0.02 - 0.2$, $\lambda_0 = 0.01 - 0.02$, $k_0 = 0.0005 - 0.006$. The output parameters in this case include $M_{1/2} \approx 200 - 2000 \text{ GeV}$, $m_t \approx 140 - 165 \text{ GeV}$, $|\tan \beta| \approx 6 - 12$.

Figure 18b: $R_{\bar{d}dh_1}$ (+), $R_{\bar{u}uh_1}$ (circles), $R_{\bar{d}dh_2}$ (\times), $R_{\bar{u}uh_2}$ (squares), against the corresponding Higgs boson mass, for the data shown in Fig. 18a.

Figure 19: Masses of the lightest CP-even Higgs boson in the NMSSM plotted against R_{ZZh_1} (+), and the second lightest CP-even Higgs boson, plotted against R_{ZZh_2} (\times), for a situation close to scenario (iii) defined in the text. The parameters are $h_{t0} = 0.4$, $A_0/m_0 = -5$, $\tilde{m}_0 = 0.02$, $\lambda_0 = 0.01$, $k_0 = 0.00055 - 0.00060$. The output parameters in this case include $M_{1/2} = 900 - 1200 \text{ GeV}$, $m_t \approx 143 - 145 \text{ GeV}$, $\tan \beta \approx 10$. The second Higgs bosons in this case have masses of about 120 GeV, outside the range of LEP II.

Figure 1

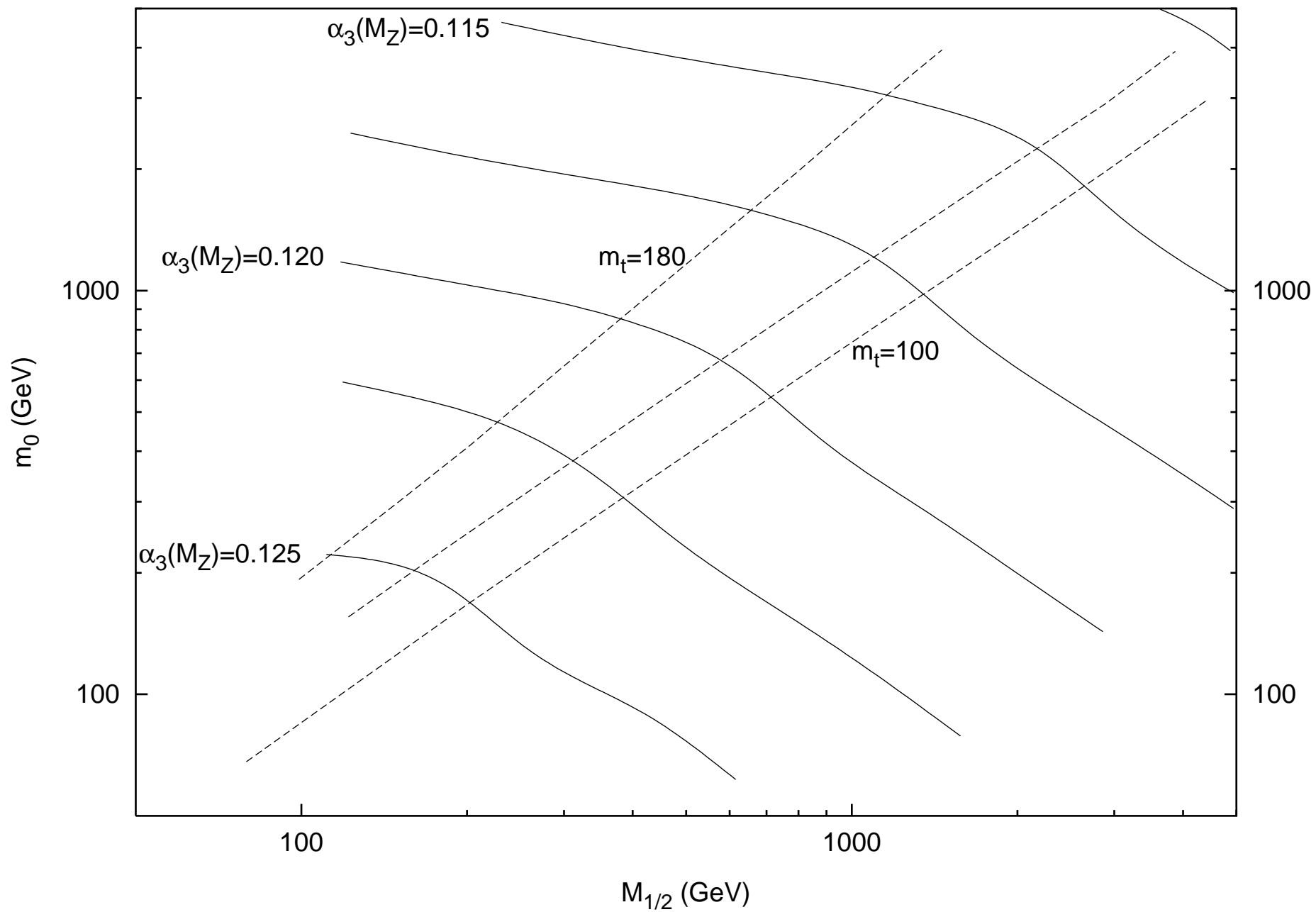


Figure 2

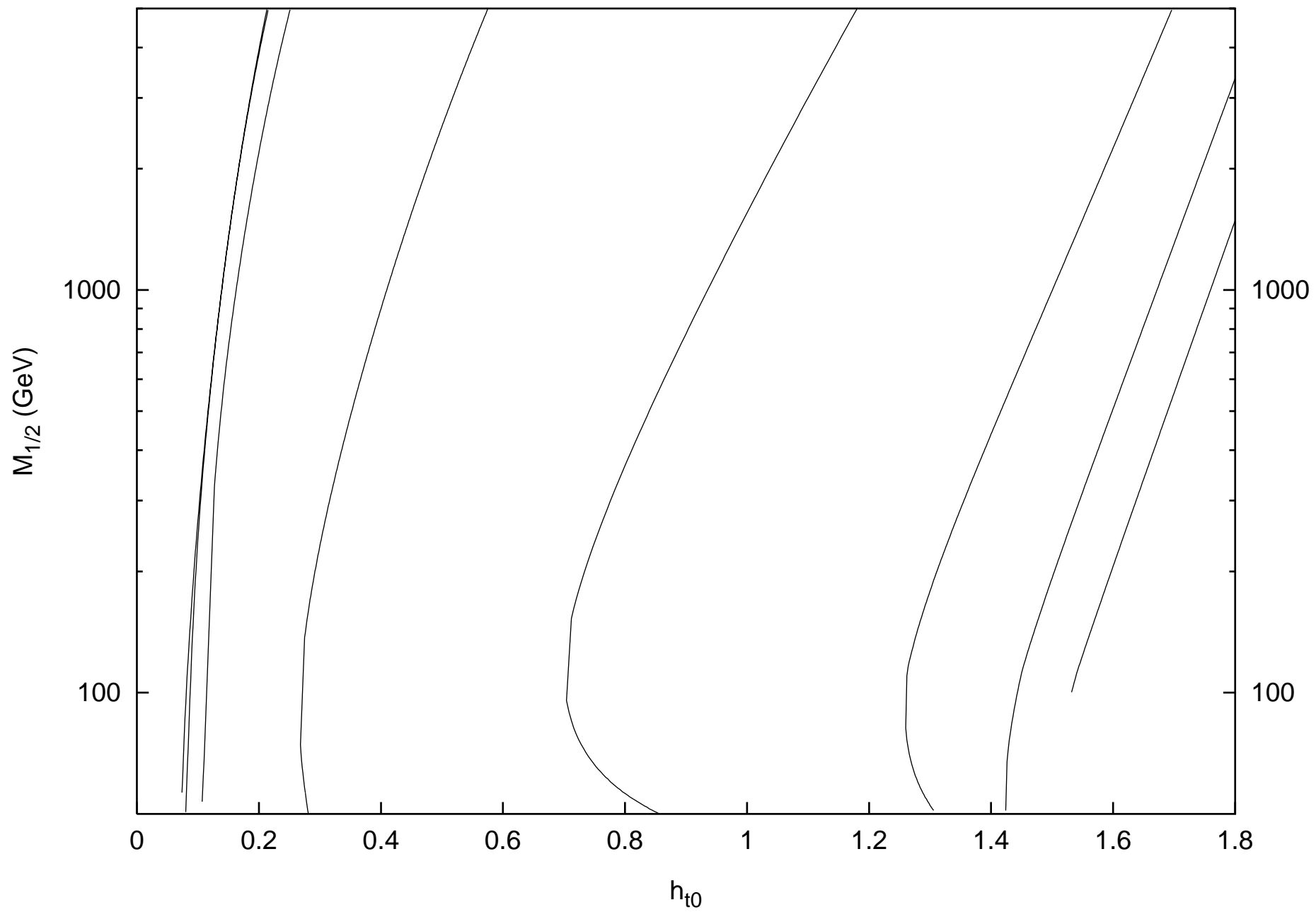


Figure 3

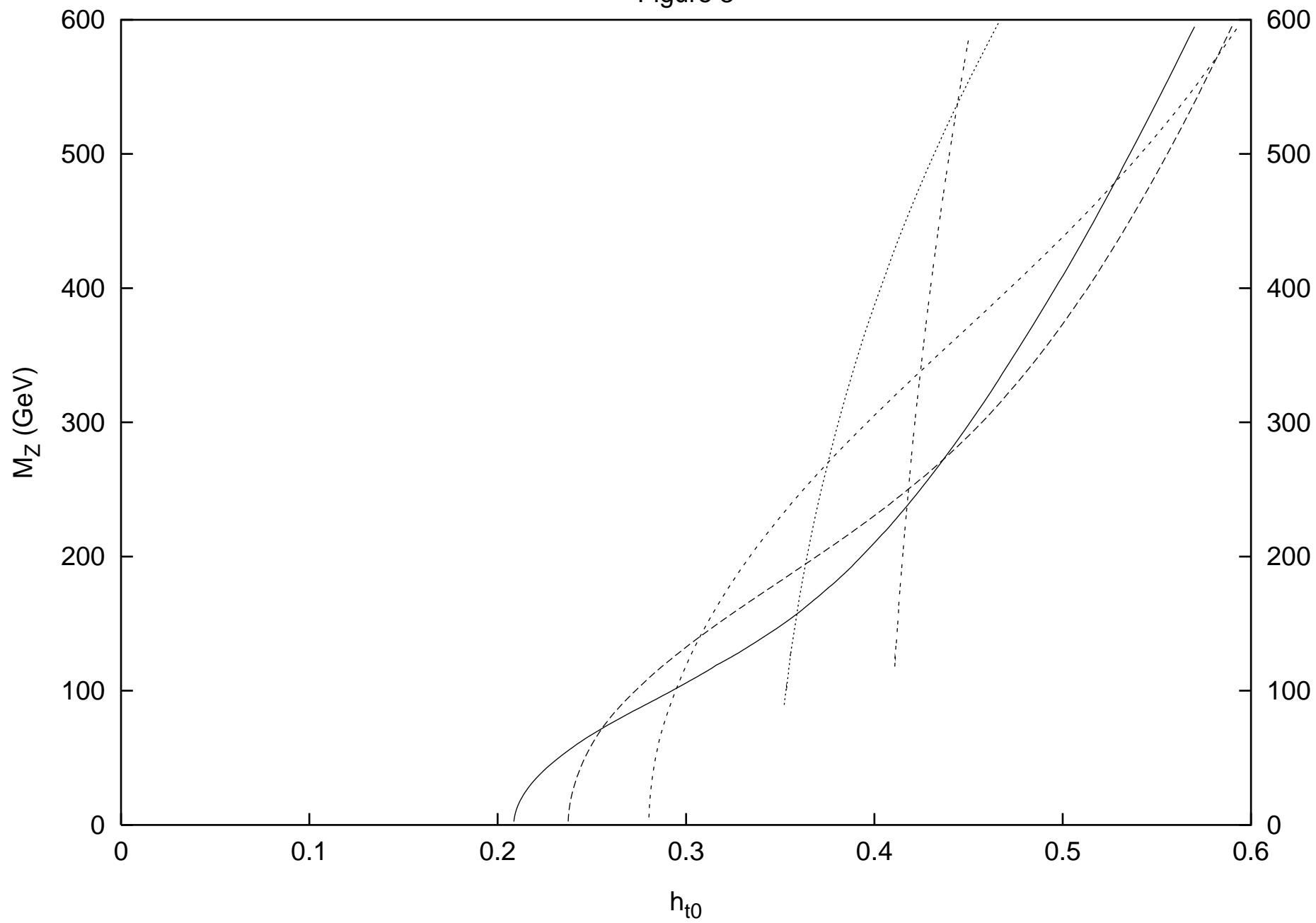


Figure 4

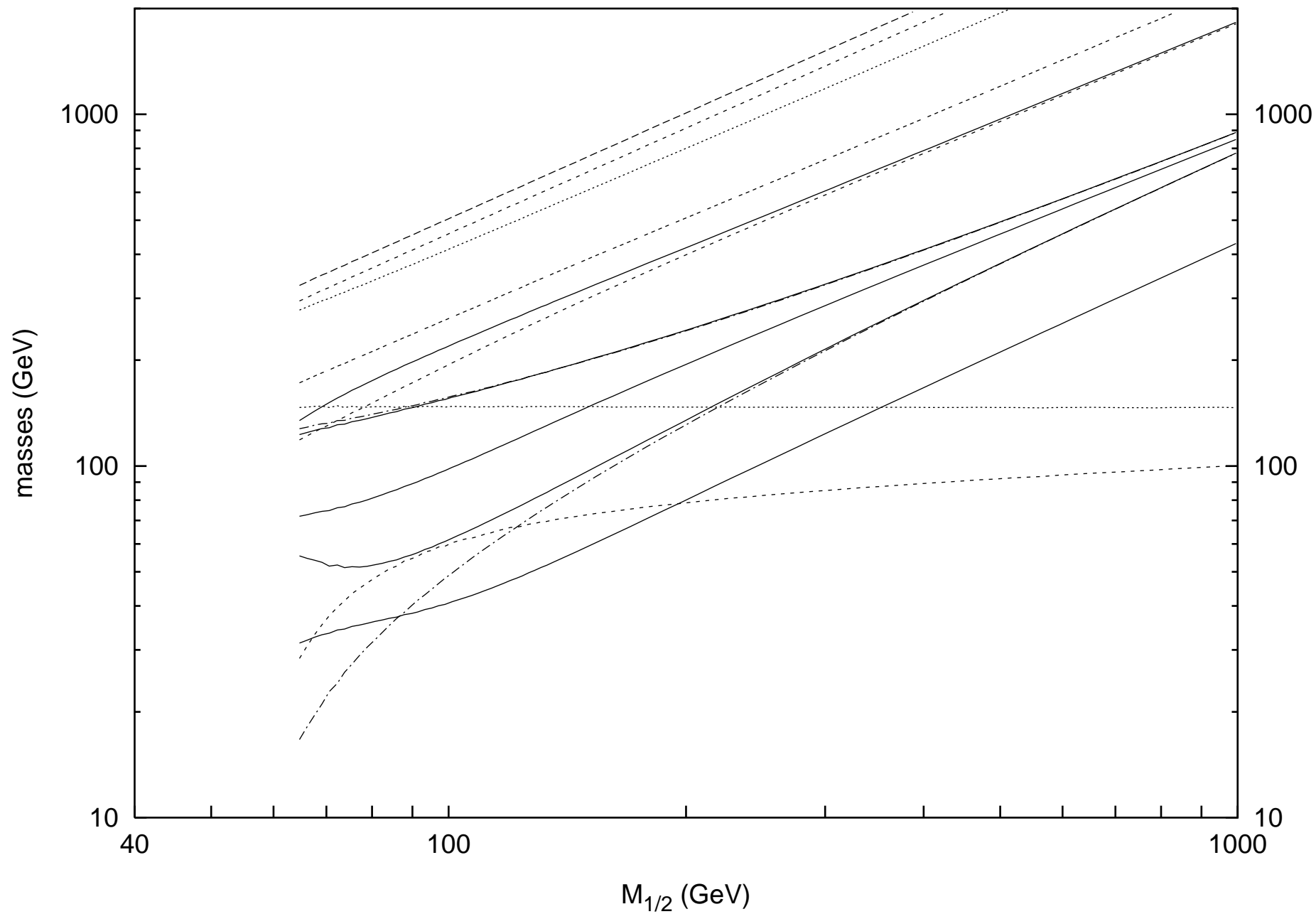


Figure 5

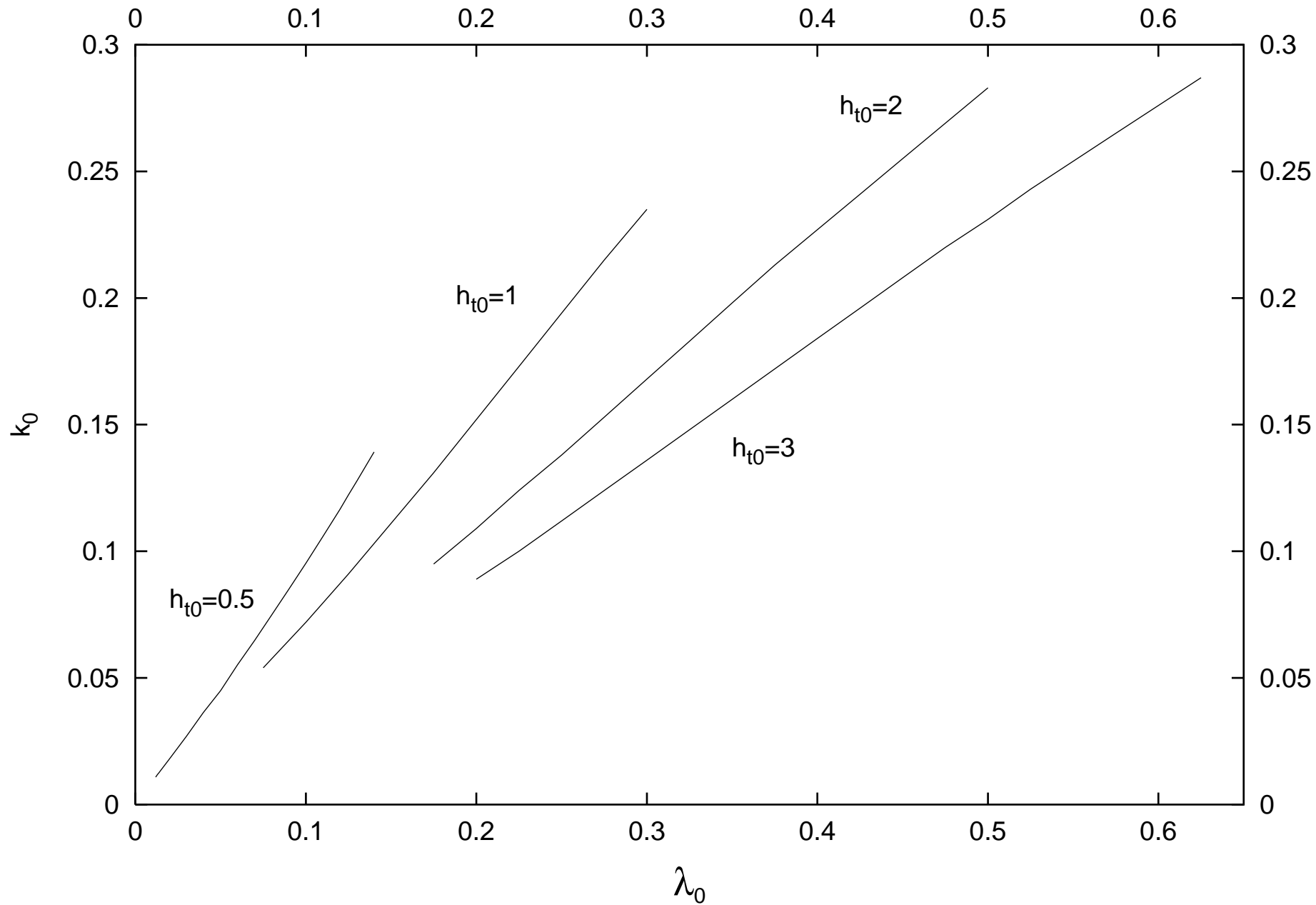


Figure 6

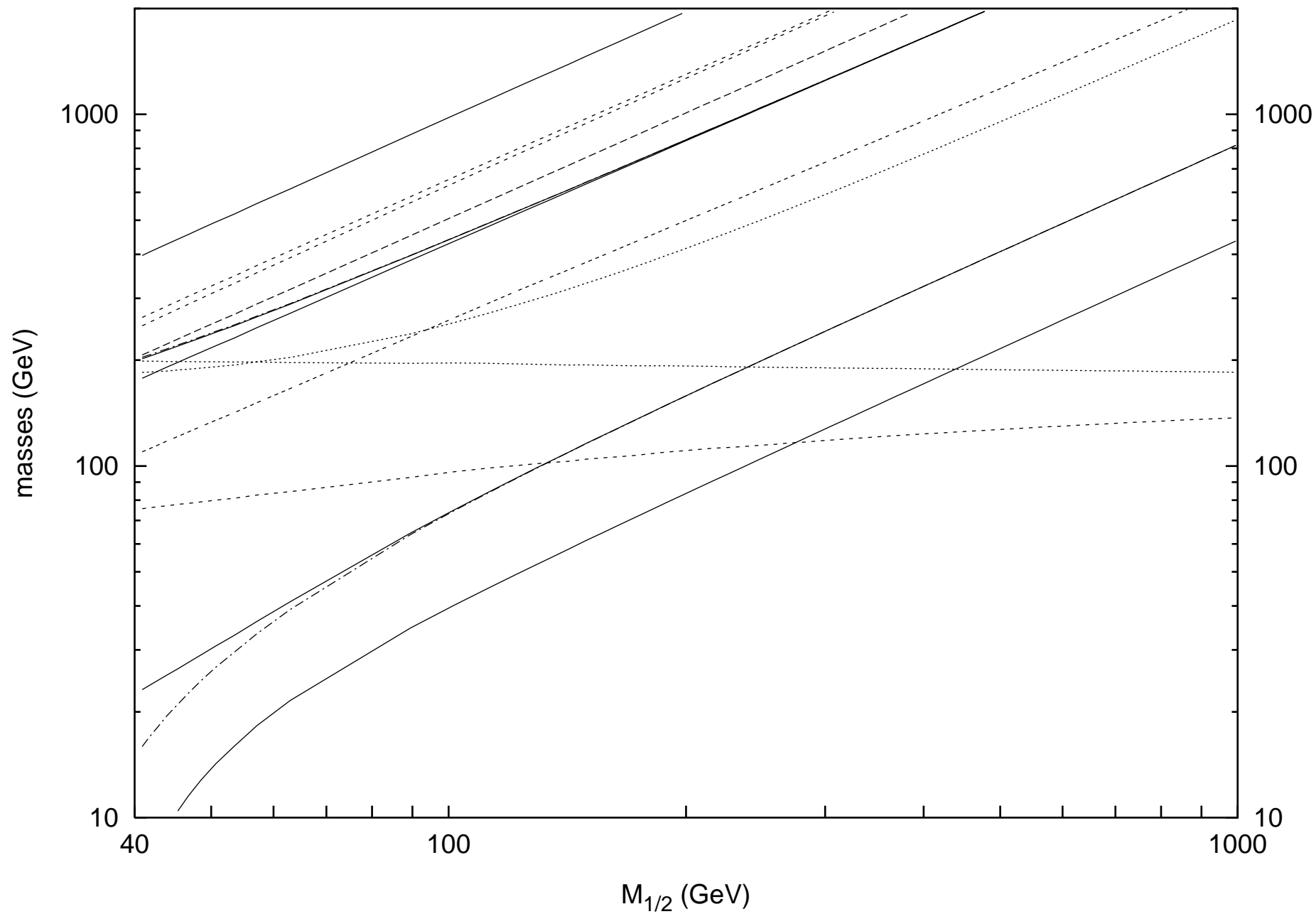


Figure 7

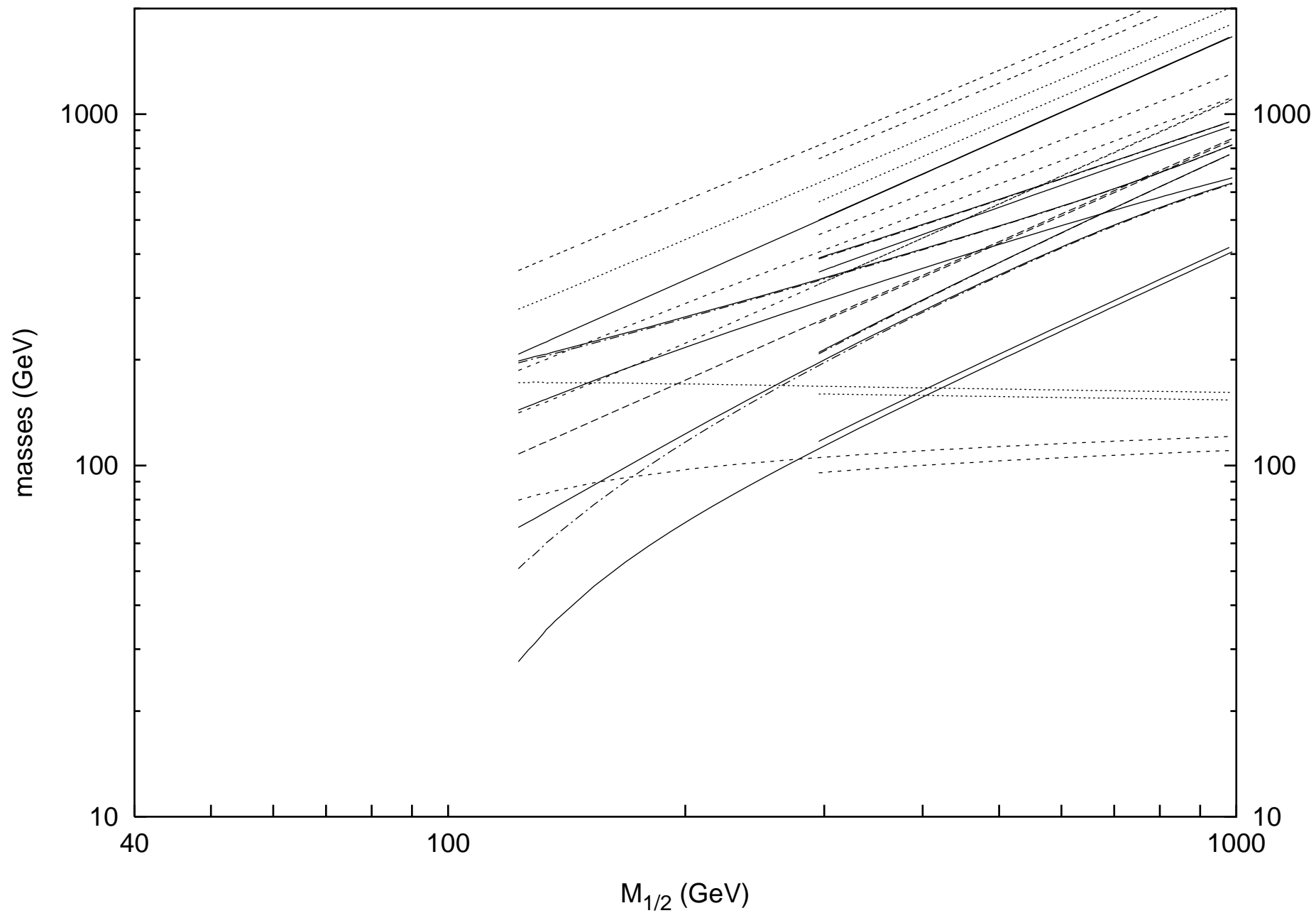


Figure 8

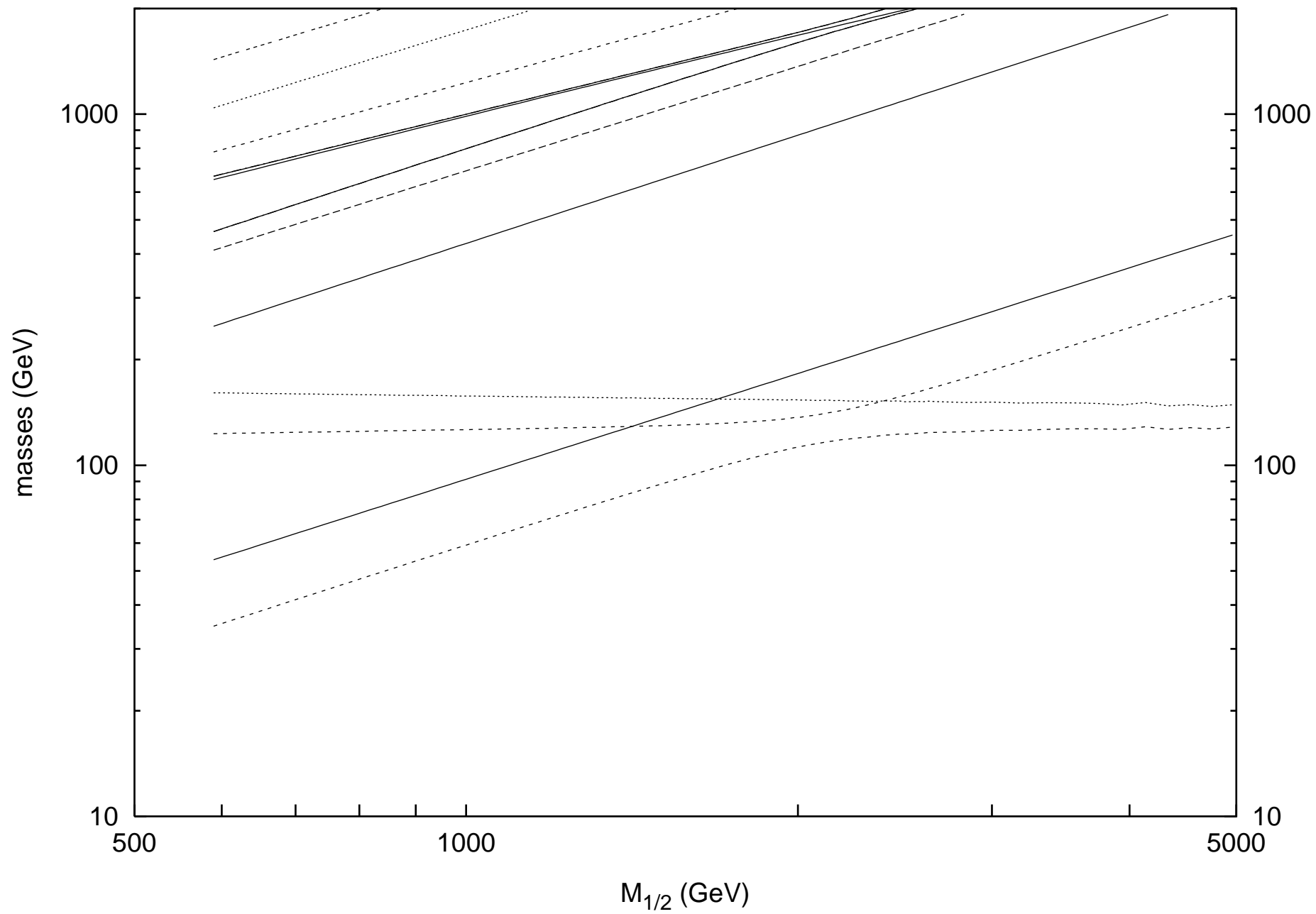


Figure 9

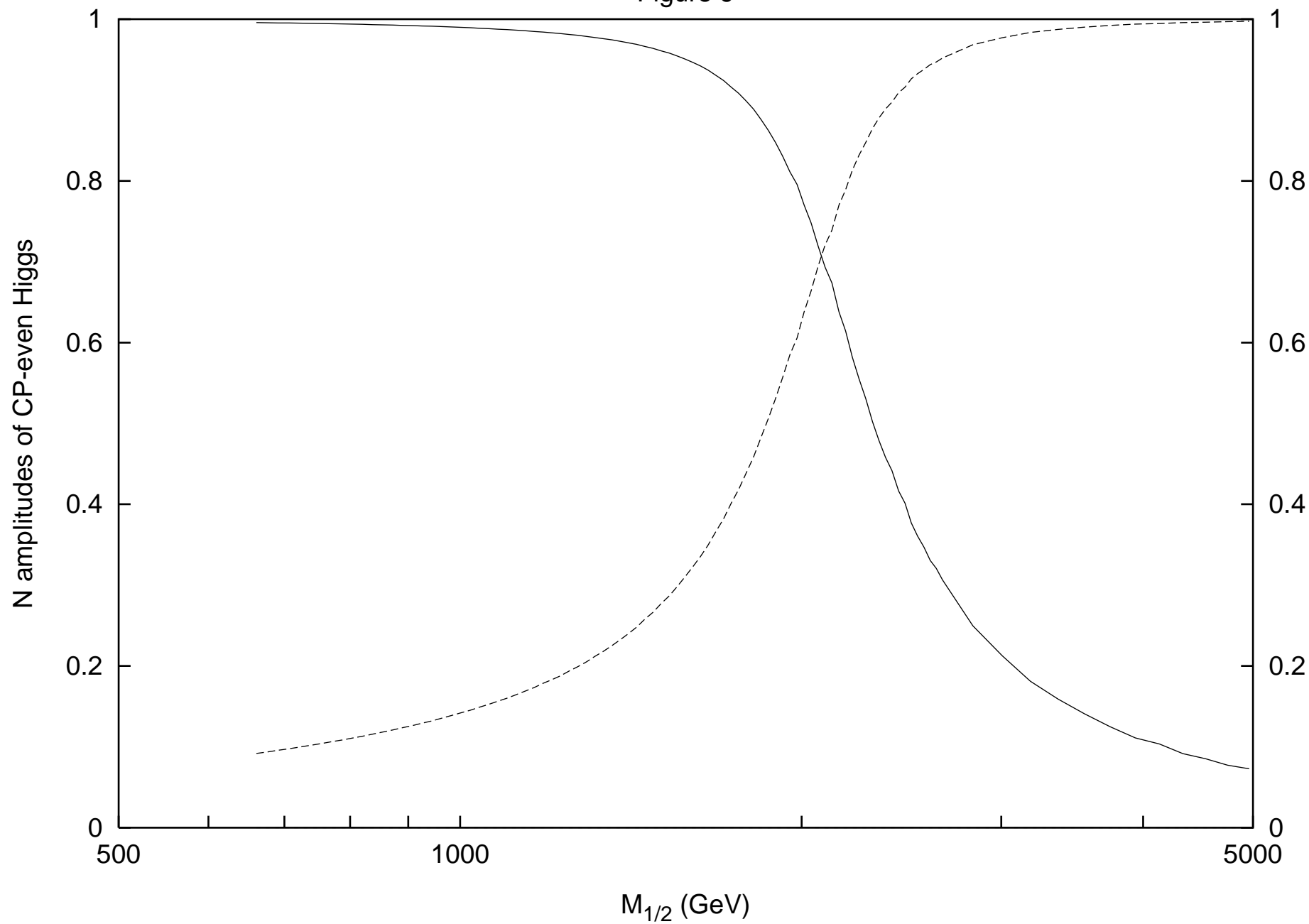


Figure 10

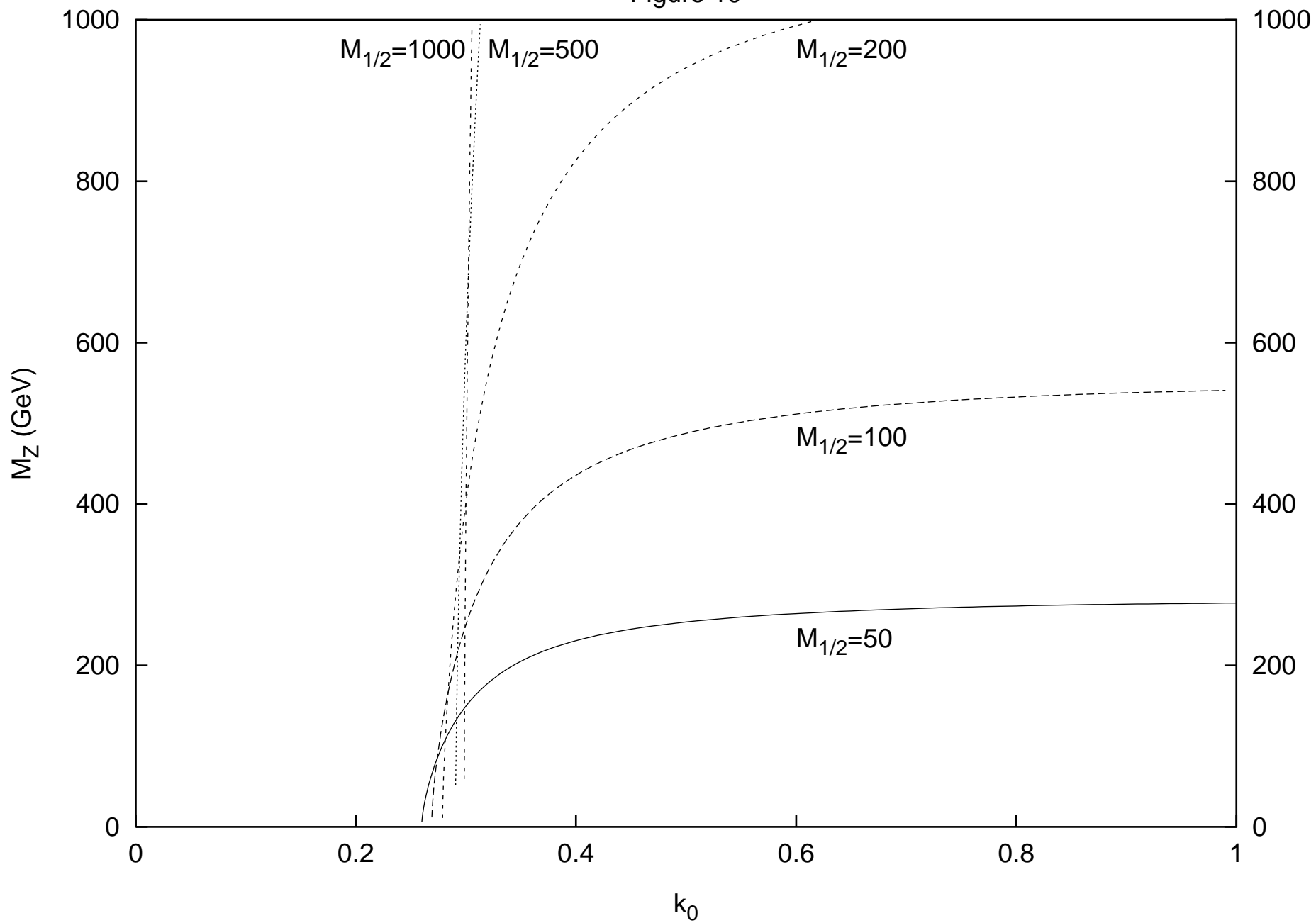


Figure 11

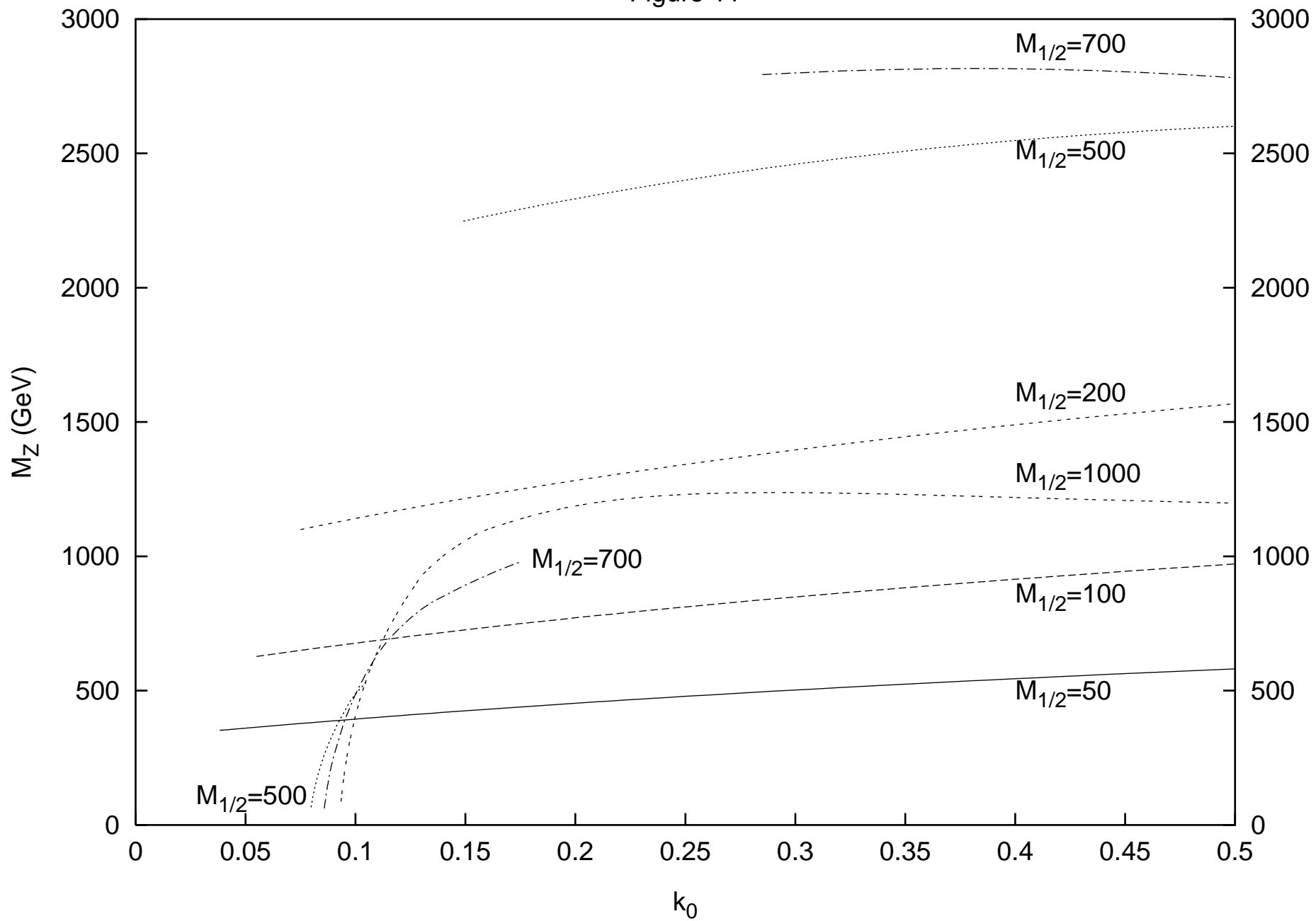


Figure 12

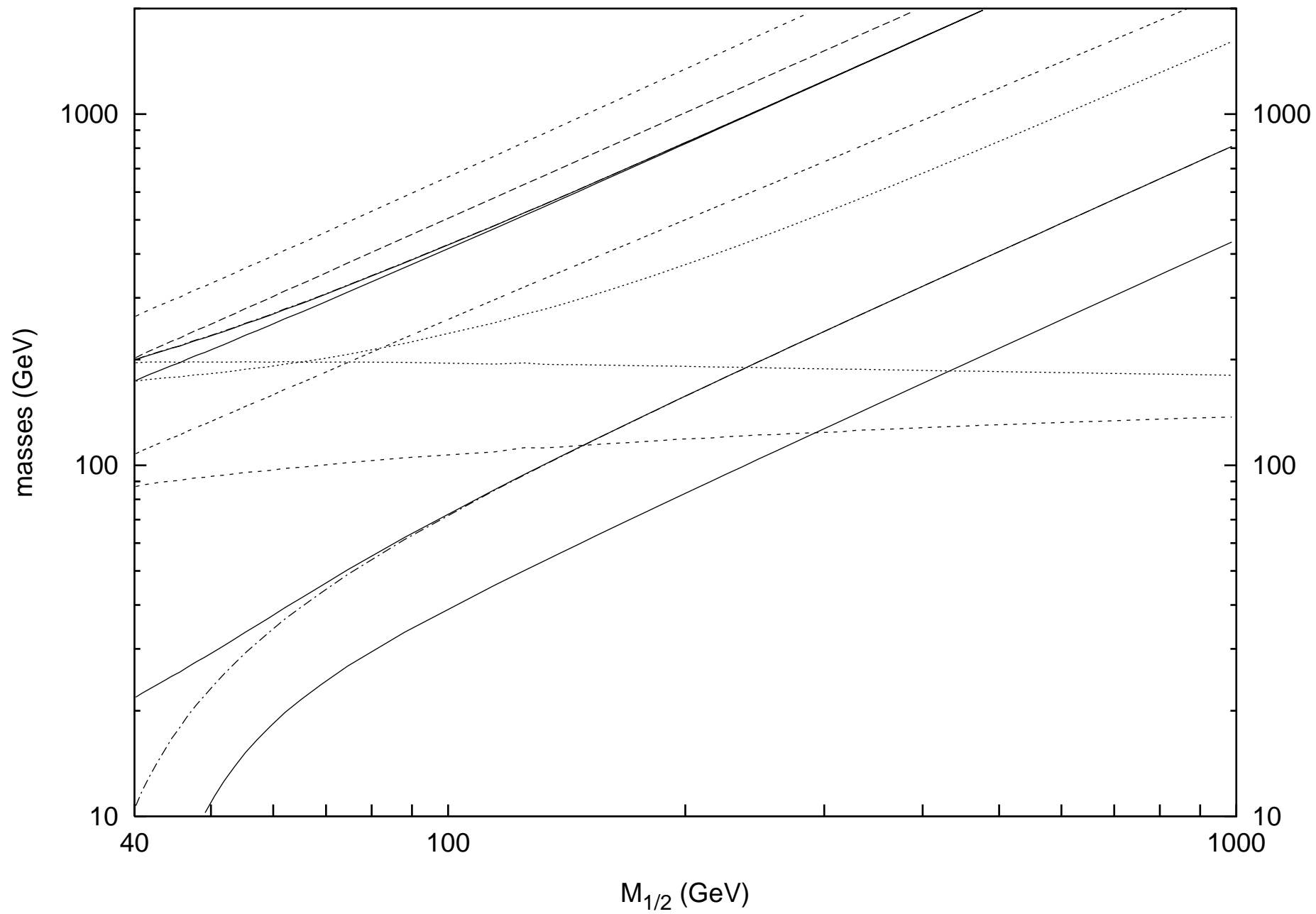


Figure 13

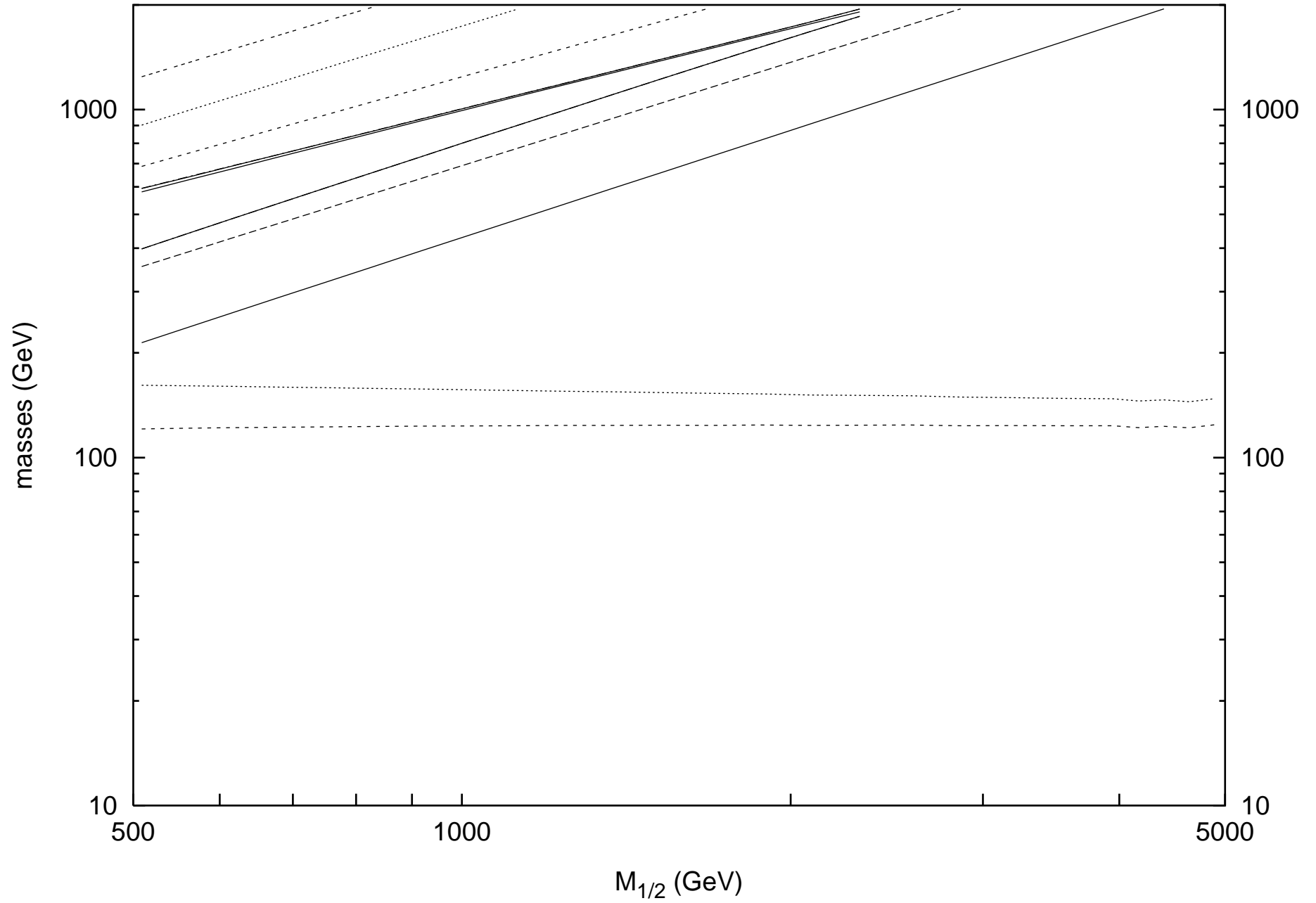


Figure 14

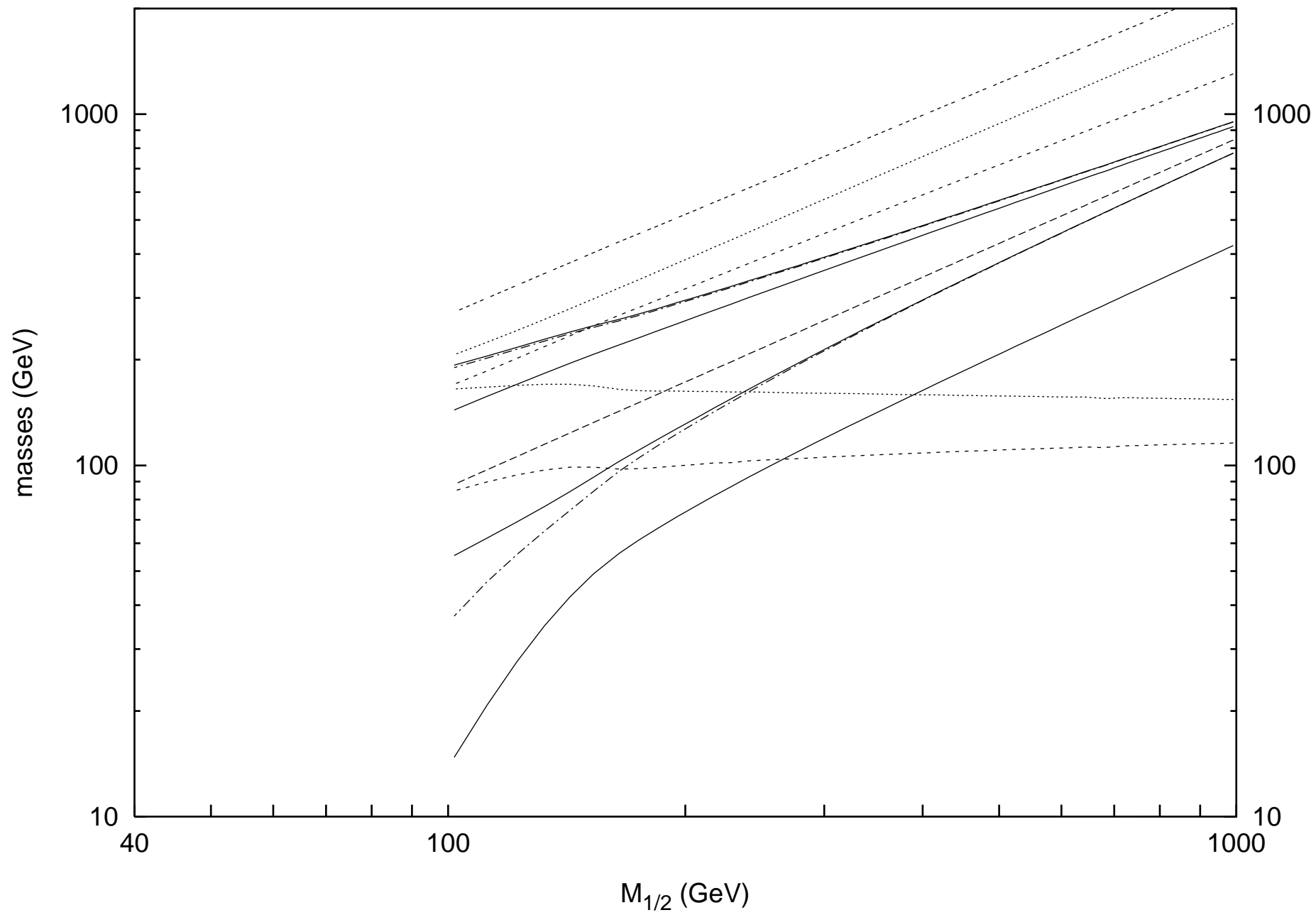


Figure 15

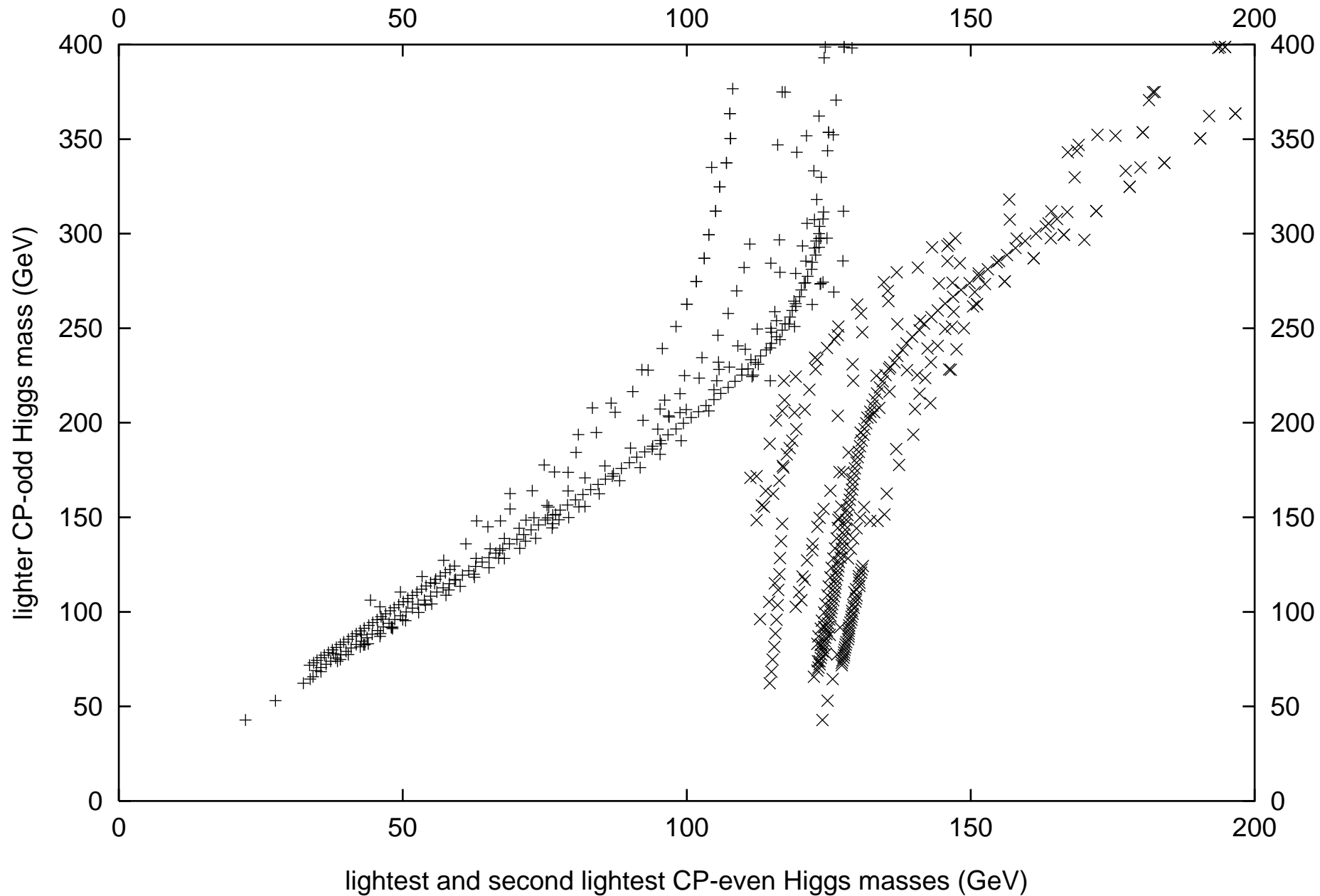


Figure 16a

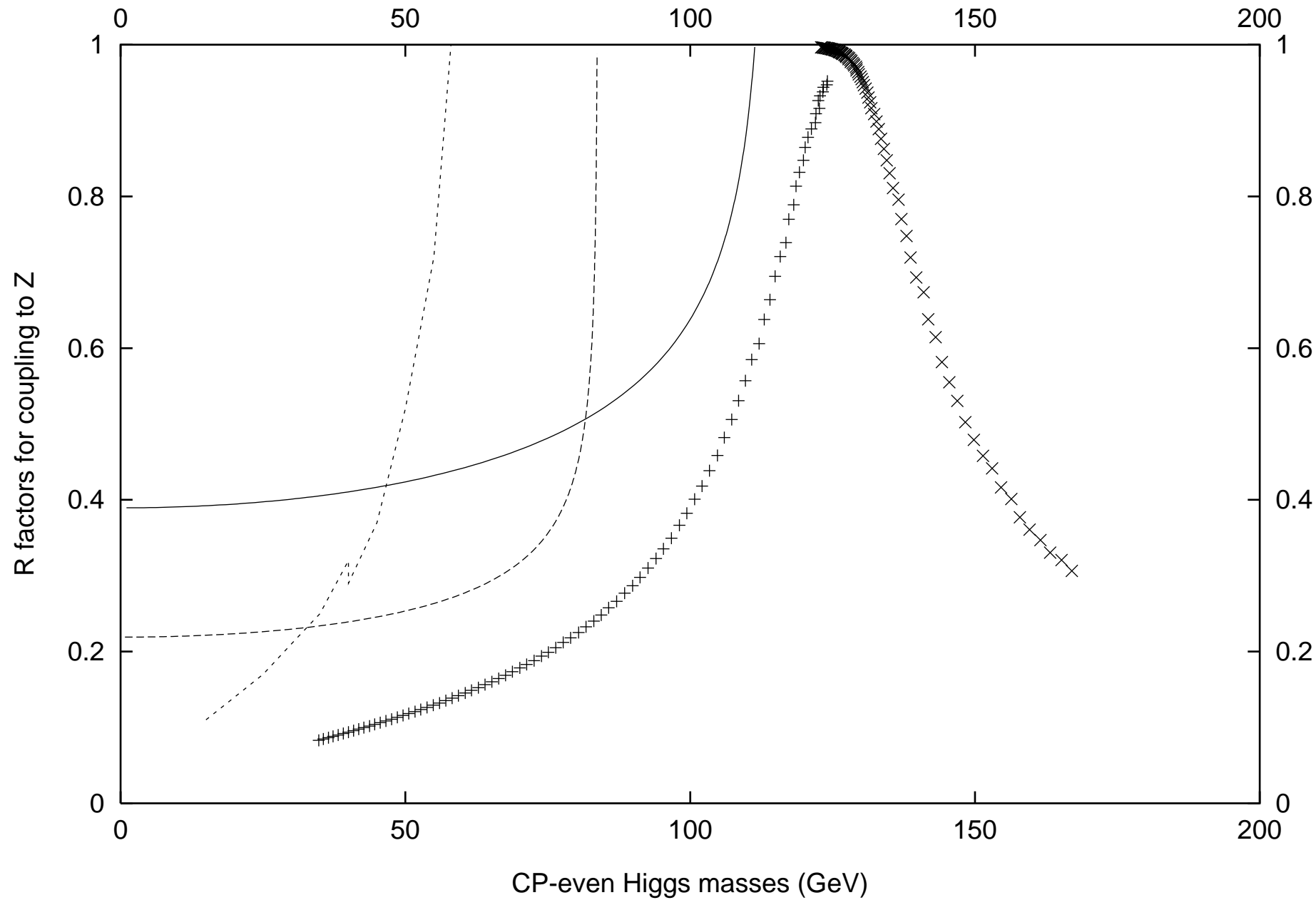


Figure 16b

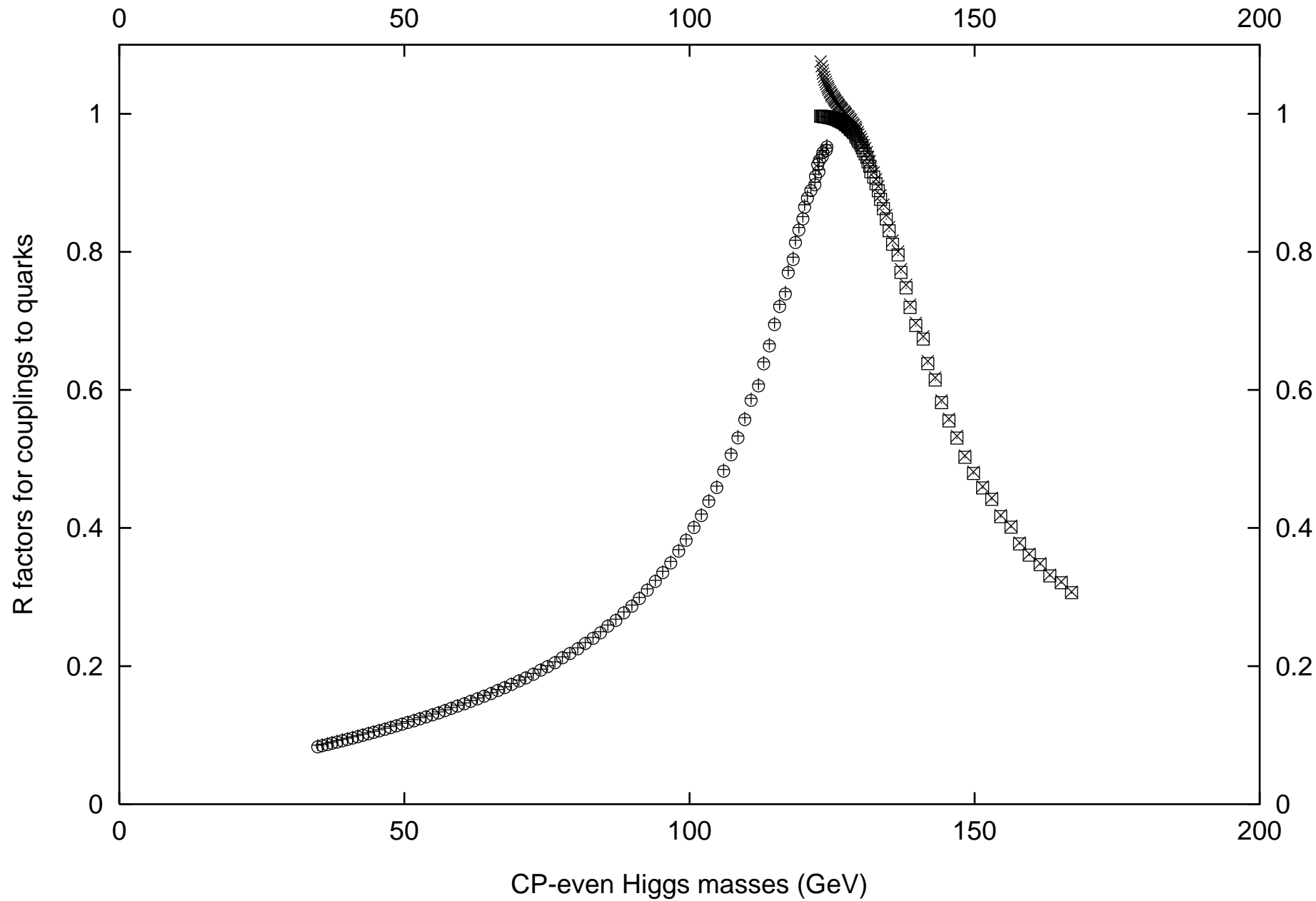


Figure 17

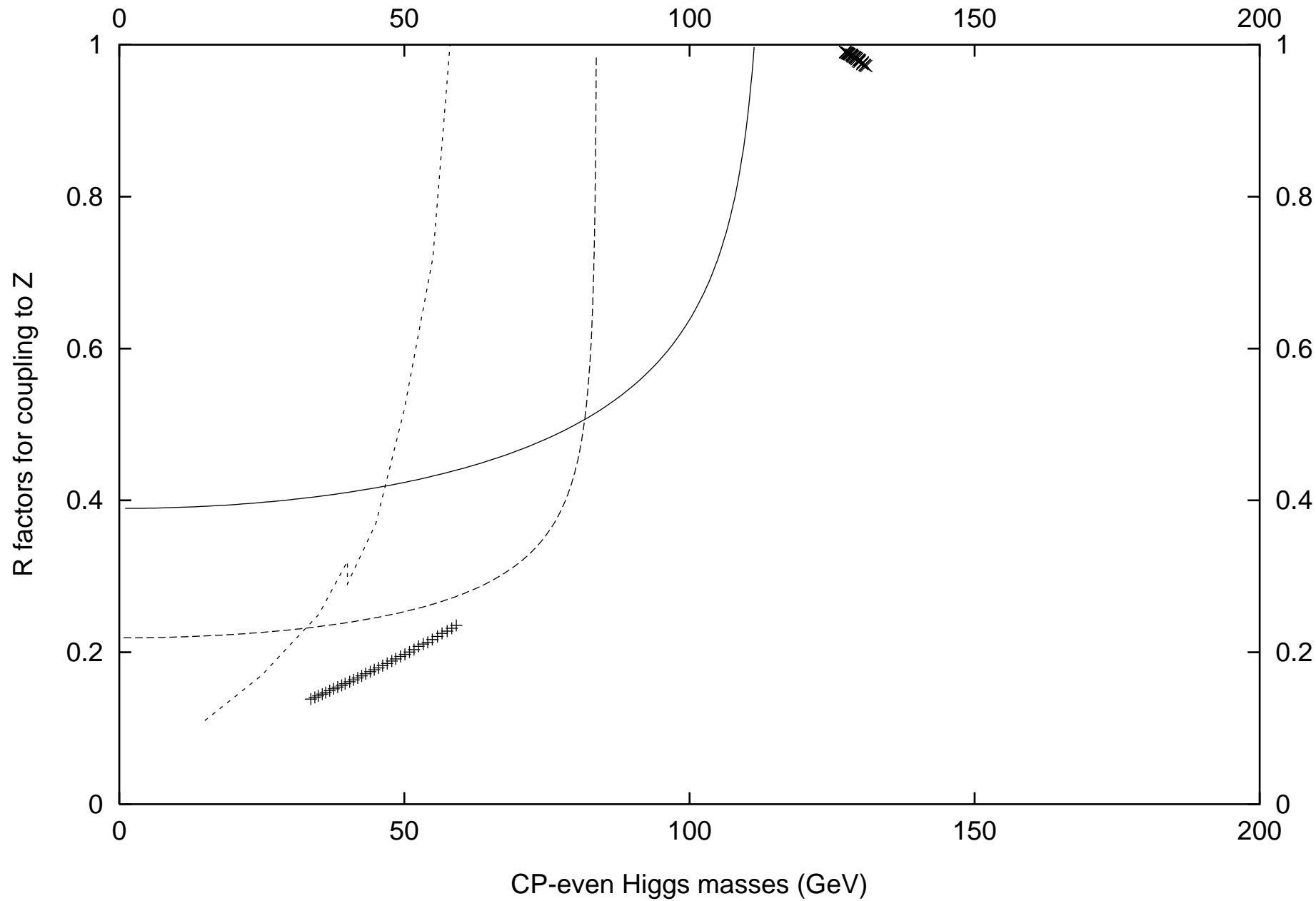


Figure 18a

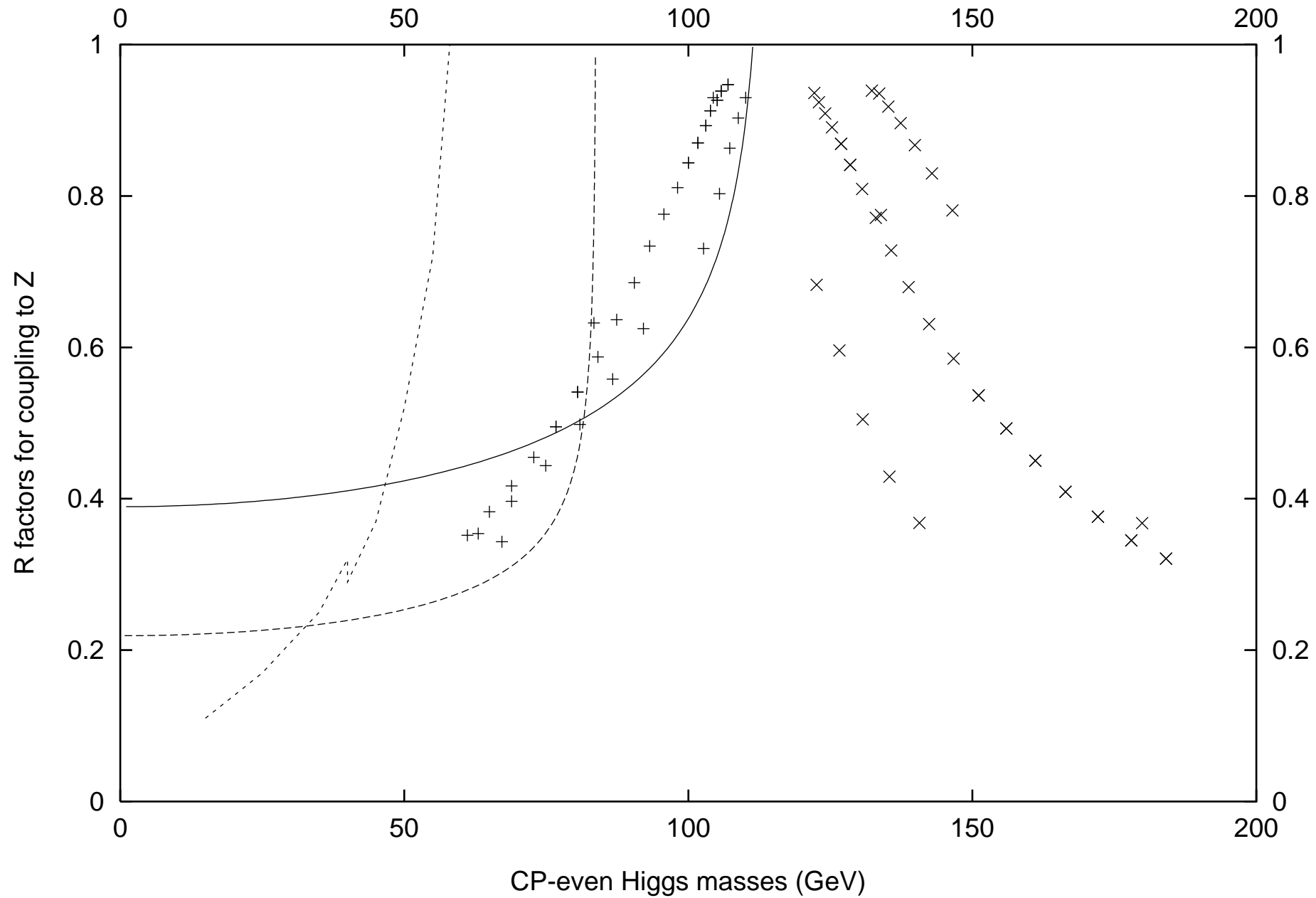


Figure 18b

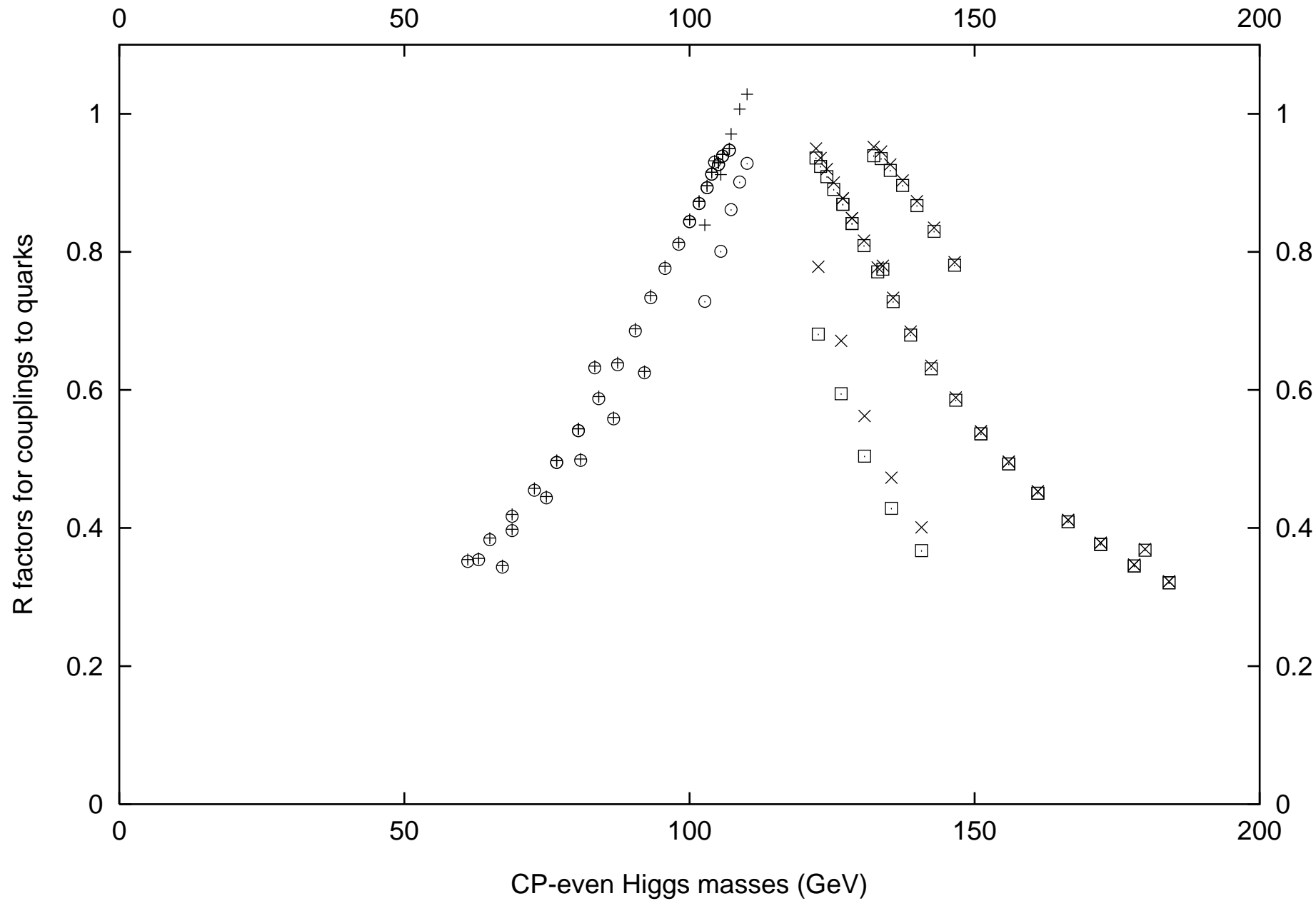


Figure 19

